POLITECNICO
MILANO 1863

SCUOLA DI INGEGNERIA INDUSTRIALE
E DELL'INFORMAZIONE

A Fourier Series-Based Semi-Analytical Model for 3D Low Thrust Collision Avoidance

Tesi di Laurea Magistrale in
Space Engineering

Author: **Alessio Bocci**

Student ID: 939743
Advisor: Prof. Juan Luis Gonzalo Gómez
Co-advisors: Camilla Colombo
Academic Year: 2021-2022

Copyright© July 2022 by Alessio Bocci.
All rights reserved.

This content is original, written by the Author, Alessio Bocci. All the non-originals information, taken from previous works, are specified and recorded in the Bibliography.

When referring to this work, full bibliographic details must be given, i.e. Bocci Alessio, "A Fourier Series-Based Semi-Analytical Model for 3D Low Thrust Collision Avoidance". 2022, Politecnico di Milano, Faculty of Industrial Engineering, Department of Aerospace Science and Technologies, Master in Space Engineering, Supervisor: Juan Luis Gonzalo Gómez, Co-supervisor: Camilla Colombo

Printed in Italy

Nella società dell'apparire occorre apparire, ma l'essere oggi rappresenta ancora un valore fondamentalmente. Ritengo che l'apparire abbia breve durata, ma l'essere sia per la vita ... L'eleganza non è farsi notare, ma farsi ricordare.

Giorgio Armani

Abstract

The number of artificial satellites is growing continuously year after year. This, coupled with the well known problem of space debris, leads to possible hazardous impacts between active satellites and resident orbiting objects. For this reason, collision avoidance manoeuvres are planned to mitigate the risk. This is just the frame where this thesis is inscribed. The increasing number of close approaches and objects makes the risk analysis more complex and operator time-demanding, thus the need of computationally efficient models for preliminary analysis. The aim of this work is to develop a semi-analytical mathematical model for the 3D low thrust collision avoidance problem capable of describing the change of orbital elements driven by a generic thrust action whose components are in all three directions. Starting from Gauss Planetary Equations in absence of any environmental perturbation, we first moved from the time-derivative formulation to a true anomaly-derivative one. Then, assuming a small variation of the Keplerian parameters after the application of the thrust action, we performed a Taylor expansion in the neighbourhood of the reference condition. From this point on, we developed two different methods. The first, denoted as *full model*, consists of a direct integration of the system obtained after the expansion. On the contrary, the second, denoted as *small thrust model*, has in addition a MacLaurin expansion of the previous equations with the aim of making explicit the dependence from the small thrust parameters. In both cases the integrations are performed by means of the Fourier Series tool. It allows, not only to carry out the integrations in an easy manner, but also to take apart the constant and oscillatory contributions of the solutions. In the case of the *small thrust model* the expressions of the Fourier Series coefficients are provided in closed form in terms of complete elliptic integrals and series expansions involving the Gauss Hypergeometric function. Finally, different simulations with various test cases are provided to assess the accuracy and the effectiveness of the method.

This thesis was part of the COMPASS project: “Control for Orbit Manoeuvring through Perturbations for Application to Space Systems" (Grant agreement No 679086). This project is a European Research Council (ERC) funded project under the European Unions Horizon 2020 research.

Keywords: 3D Low Thrust, Collision Avoidance, Collision Probability, Fourier Series, Hypergeometric Functions, Miss Distance, Semi-Analytical Model, Taylor Series

Abstract in lingua italiana

La quantità di satelliti artificiali in orbita aumenta in maniera incessante anno dopo anno. Ciò, insieme al ben noto problema dei detriti spaziali, rende assai concreta la possibilità di impatti potenzialmente fatali fra i vari oggetti orbitanti. Per questo motivo, sono previste manovre di prevenzione delle collisioni per mitigare il rischio. Questa è la cornice in cui è inscritta questa tesi. Il numero crescente di incontri ravvicinati e oggetti orbitanti di diversa natura rende l'analisi di rischio più difficile e onerosa dal punto di vista delle tempistiche. Sorge quindi la necessità di modelli computazionalmente efficienti per una analisi preliminare. Lo scopo di questa tesi è sviluppare un modello matematico semi-analitico per il problema 3D di prevenzione delle collisioni qualora il sistema propulsivo possa fornire solo una bassa spinta. Il modello deve essere in grado di descrivere il cambiamento dei parametri orbitali qualora l'azione di spinta sia un generico vettore con componenti in tutte e tre le direzioni spaziali. Partendo dalle Equazioni Planetarie di Gauss in assenza di qualsiasi perturbazione relativa all'ambiente circostante, si è in primo luogo passati dalla formulazione con la derivata temporale di suddette equazioni a quella con la derivata rispetto all'anomalia vera. Quindi, ipotizzando una variazione non eccessiva dei parametri Kepleriani dopo l'applicazione dell'azione di spinta volta a deviare il satellite dalla traiettoria per schivare l'ostacolo, si è eseguita un'espansione di Taylor nell'intorno della condizione di riferimento. Da questo punto in poi, vengono sviluppati due diversi metodi. Il primo, indicato come *full model*, consiste in una diretta integrazione del sistema ottenuto dopo l'espansione. Al contrario, il secondo, indicato come *small thrust model*, ha in aggiunta un'espansione di MacLaurin delle precedenti equazioni con lo scopo di rendere esplicita la loro dipendenza dai parametri di bassa spinta. In entrambi i casi le integrazioni vengono eseguite tramite la Serie di Fourier. Essa, infatti, ci consente, non solo di eseguire le integrazioni in modo semplice, ma anche di separare i contributi costanti delle soluzioni da quelli oscillatori. Nel caso del *small thrust model* le espressioni dei coefficienti della Serie di Fourier sono fornite in forma chiusa in termini di integrali ellittici completi ed espansioni in serie che coinvolgono la funzione ipergeometrica di Gauss. Infine, vengono fornite diverse simulazioni con vari casi test per valutare l'efficacia del metodo.

Questa tesi è parte del progetto COMPASS: "Control for Orbit Manoeuvring through

Perturbations for Application to Space Systems" (Grant agreement No 679086). Questo progetto è finanziato dall' European Research Council (ERC) sotto la European Unions Horizon 2020 research.

Parole chiave: Bassa Spinta, Manovre Anti-Collisione, Probabilità di Collisione, Serie di Fourier, Funzioni Ipergeometriche, Distanza Critica, Modello Semi-Analitico, Serie di Taylor

Contents

1 | Introduction

1.1. Background

The Sputnik 1 was the first artificial satellite placed in orbit after its successful launch, October 4th, 1957. From that time on, space exploration and utilization has been continuously growing and the number of satellites launched per year significantly increased. The Union of Concerned Scientists (UCS) created the Satellite Database [1] as a listing of more than 4852 operational satellites currently (updated January 1st, 2022) in orbit around Earth. The database is updated three times a year and holds 28 types of data for each satellite, including technical information about it (mass, power, launch date, expected lifetime) and its orbit (apogee, perigee, inclination, and period), the satellite mission and who owns, operates, and built it. One of the most relevant aspects is that around 4078 satellites are placed in Low Earth Orbits (LEO) and around 574 in Geostationary Orbits (GEO). The former are the most used in various disciplines and activities: navigation, telecommunication, agriculture, meteorology, Earth observation, wildfires, natural disasters monitoring and also ecology applications as polar caps melting, greenhouse and gases emissions.

The increasing space activities and the huge number of satellites has, year after year, led to the problem of space debris: these are different nature man-made Earth orbiting objects, not only defunct satellites but also mission related objects and fragments of collisions and explosions. On the purpose, as explained by Holger Krag [2], Head of the Space Safety Program, the biggest contributor to the space debris problem is explosion in orbit, caused by left-over energy (fuel and batteries) on board spacecraft and rocket. This problem has been increasing in time due to lack of regulations. In the last years the consciousness of the problem has risen, so that international guidelines and standards now exist. According to ESA [2], the main items are: minimize the amount of detached objects during launch, prevent explosions by *passivating*[1] spacecraft at the end of life, move defunct spacecraft to graveyard orbits and prevent crashes by means of collision avoidance manoeuvres (CAMs).

[1] prevent explosions by releasing stored energy

At international level, the mitigation measures and technical consensus are discussed at IADC (Inter-Agency Space Debris Coordination Committee) [3]. The primary objective is to connect all the member space agencies to facilitate opportunities for cooperation in space debris field. In the same context, also the NASA Orbital Debris Program Office (ODPO) [4] has a relevant role. It is a Delegated Program in the Office of Safety and Mission Assurance (OSMA) at NASA HQ (NASA Headquarters). It performs measurements of the orbital environment and develops technical consensus for adopting mitigation measures. In the website[2] it is possible to see a video showing the sudden growth of space debris starting from 1960 till 2019. The catalogued objects are all with a diameter greater than 10 cm (see also NASA [5]).

In ESA's 2022 Space Environment Report [6] a very accurate description of the space debris situation is provided. In particular, LEO orbits are considered; based on ESA models, the true number of objects larger than 1 cm in size is likely over one million. The increase in launch traffic and the long-lasting nature of space debris in LEO is causing a significant number of close encounters, known as *conjunctions*, between active satellites and other objects in heavily congested orbits. These close encounters could end up in unwanted impacts which could lead to the satellite failure or, in the worst case scenario, to the satellite crash. In ESA Space debris 2017 a journey to Earth [7] a relevant video gives a closer look at the different regions used for space flight and explains how mitigation and removal measures could preserve future usage of these orbits. It was produced by ESA for the 7th European Conference on Space Debris, 18-21 April 2017.

As already said, if a close encounter occurs the possibility of having serious damages to the spacecraft or even losing it is quite high. Therefore, the need of planning CAMs becomes strict. First, Conjunction Data Messages (CDMs) are generated. According to B. Reihs et al. [8], these messages include the time of the encounter, the predicted positions with the consequential miss distance and the covariance matrices at the time of the encounter (see R. Book *Conjunction data message* [9]). As example, in [10] it is available a collection of CDMs received by ESA from 2015 to 2019. These messages, provided by Combined Space Operations Center (CSpOC)[3], notifies satellite operators about the possible risks of collisions. Satellite operators then perform their own way of evaluating significance of the CDMs: a manoeuvre is performed only if the CDM is evaluated as risky in order to not interrupt the regular spacecraft operations. Since this procedure has to be repeated several times (hundreds of collision alerts per week for possible close encounters between two catalogued resident space objects), ESA is developing automated systems that use

[2] see https://orbitaldebris.jsc.nasa.gov/modeling/

[3] other entities (companies, etc.) are also providing this kind of service, although the main one remains the CSpOC

artificial intelligence and other technologies to help operators to carry out CAMs, see ESA *Dodging debris to keep satellites safe* [11], and reduce the number of false alarms. More informations about how CDMs work could be found in S.Dural et al. [12].

Finally, referring to Gonzalo et al. [13], nowadays many current satellites complement or substitute traditional impulsive thrusters with low thrust electric propulsion systems[4]. This choice is mainly due to the advantage of reducing the launch mass, possibly increasing the payload mass, while keeping advanced manoeuvring capabilities. The main issue coming from these low thrust technologies is that, differently from the traditional impulsive one, the CAM has to be performed sufficiently in advance of time of the closest approach (TCA).

1.2. State of the art

The main strategies to perform CAMs are two: impulsive and low thrust. The simplest way to deal with this kind of problem is to formulate it in absence of any environmental perturbation[5] with the addition of the external action[6]. Referring to the traditional literature on this topic, many formulations can be adopted, e.g. Cartesian equations of motion or Gauss Planetary Equations. This kind of problem could be faced either in a full numerical way or in an analytical/semi-analytical one. While the numerical approach allows to formulate the problem as a whole, the analytical/semi-analytical approach relies on some simplified hypothesis. This implies that these kind of solutions are approximated and they are usually obtained through some series expansions with reasonable assumptions such as small thrust parameters appearing into equations or small variation of a certain quantity over one orbital revolution. Regardless of the type of approach used, the ultimate goal is to evaluate the Miss Distance and the probability of collision (PoC) at the close approach (CA) for given uncertainties.

1.2.1. A short about numerical methods and relevant software

The aim of this thesis work is the development of a semi-analytical model for the low thrust collision avoidance problem. Therefore most of the scientific literature analysed here is about the relevant semi-analytical approaches commonly adopted to deal with such a problem. Nevertheless, the semi-analytical way is not the only path followed in the usual practice. There are plenty of operational software using numerical approaches.

[4] they provide a low thrust with a very high specific impulse.
[5] i.e. a two body problem.
[6] impulsive or constant in magnitude and with a very small value.

Without going too much into details, we will now present some relevant works.

In Aida et al. [14] is presented the collision avoidance system implemented at GSOC (German Space Operation Center) since 2008. The software detects close approaches of operational LEO satellites against more than 14000 space objects listed in the TLE catalogue provided by USSTRATCOM (US Strategic Command). In brief it works as follows. The collision risk is detected around 7 days in advance using the TLE catalogue as well as precise orbit data of the spacecraft. The PoC is then evaluated with a threshold of 10^{-4}; in case of an high collision risk, the orbit refinement using a radar tracking is foreseen as the second step. A comparison between the analytical SGP4 (Simplified General Perturbation 4) orbit propagation and the software for numerical propagation ODEM (Orbit Determination for Extended Manoeuvres) is performed. By means of the same tools (TLEs and SGP4), Abay [15] investigates the optimal impulse manoeuvre using a semi-numerical method. In this paper, TLEs are estimated using ephemerides generated by the orbit propagator of Orekit, which is an open source low-level space dynamics library. The main result of the work is an increased accuracy with less computational effort for the optimal CAM evaluation. Moreover, this calculation is shown to be possible using machine learning (ML) techniques . Without going too much into details, ML is growing in popularity in the collision avoidance field; for instance a relevant work is Sánchez et al. [16]. Here a simple calculation of an optimal CAM is performed when the Intelligent Classification System (ICS) suggests that a CAM is needed.

In Crassidis et al. [17] a different numerical approach with respect to those already discussed is presented. This indeed is a discretized space approach to conjunction analysis. It is proved that it efficiently reduces the number of computationally expensive conjunction analyses required for the PoC evaluation. After assessing the effectiveness of the method a mathematical model is investigated in order to optimize the CAM.

Finally, among the several systems for CAM calculation we want to highlight CORAM [18] and OCCAM [19]. CORAM is employed by ESA's Space Debris Office and provides the relevant informations about conjunctions, manoeuvres, and trajectories. Moreover it is capable to cope with multi-encounter and multi-manoeuvre cases. OCCAM, on the other hand, allows fast CAM computations based on an analytical formulation of the collision problem. This system is able to cope with conjunction with just one debris and supports three optimization goals: fuel consumption optimization, collision probability minimization and Miss Distance maximization.

1.2.2. Relevant literature about analytical and semi-analytical models

Let us to analyse some relevant works on the analytical and semi-analytical models for the CAM problem. The model for the impulsive CAM is fully analytical while that for low thrust CAMs is semi-analytical. This means that the main procedure is analytical but some numerical procedures (e.g. small amount of numerical integrations) are required. Regardless to which procedure and/or technology has been chosen, the main objective is to compute the Miss Distance and the PoC of two approaching objects. To do so, a maximization/minimization problem (sometimes collapsing into a root finding problem) is set up; i.e. in other words the goal is maximizing Miss Distance and/or minimizing the PoC. A very detailed explanation of what has been briefly introduced in this paragraph can be found in Gonzalo et al. [20]. Now, let us see the basically different methodologies about CAMs: the impulsive approach versus the low thrust one.

1.2.2.1. Impulsive CAMs

In Bombardelli [21] the investigation of an optimal solution for the impulsive CAM problem is performed. The mathematical formulation relies on the Dromo orbital elements. The main assumptions are: short term encounter, impulsive burn and elliptical Keplerian orbits. The main objective in this work is the maximization of the Miss Distance for a fixed manoeuvre location, optimizing the impulse direction. Closed form analytical expressions to predict the dynamics of the two bodies in the encounter B-plane are provided. A relevant aspect of this work is: it opens the doors to further developments. Those generalizations have been indeed achieved by Bombardelli et al. in [22] and [23]. Starting from the analytical formulation for the computation of the Miss Distance described in [21], the authors proceed to generalize the process taking into account the PoC (using Chan method), the initially non zero Miss Distance vector at close approach and the presence of environmental perturbations. The formulation hinged on a relation between the applied impulse and the objects' relative motion in the B-plane, which allowed the treatment of the manoeuvre optimization problem as an eigenvalue problem coupled to a simple non-linear algebraic equation. This important technique of reducing the maximum deviation optimal control problem to an eigenvalue problem was previously obtained by Conway [24].

In Gonzalo et al. [25], following the procedure proposed by Vasile et al. [26] for the optimal deflection of asteroids, the computation[7] of the instantaneous change in orbital elements

[7] through Gauss Planetary Equations.

due to an impulsive manoeuvre is presented. Since the change in orbital elements is typically small, the deviation at the CA can then be computed through linearized relative motion equations, leading to a linear model with a matrix depending on the nominal orbital elements of the deflected body and the lead time of the manoeuvre. This again reduces to an eigenvalue problem by means of Conway [24]. The main novelty is that the formulation is extended to the optimization of minimum PoC following the method proposed by Bombardelli et al. [23].

Dharmarajan et al. [27] investigate collision avoidance applications for formation flying in LEO combining the two approaches presented in Bombardelli et al. [23] and Slater et al. [28]. Neglecting the uncertainties in the knowledge of the kinematic state of the two colliding objects, the proposed optimization technique solves an eigenvalue problem for a case of non direct approach. The effect of the manoeuvre anticipation time with respect to the foreseen possible collision is highlighted, and specific detail is given to the in-plane and out of plane components of the impulsive manoeuvre indicated in order to avoid such an event.

In Reiter et al. [29] the investigation is focused on rapid collision avoidance manoeuvres: their optimization relies on the so called finite burn analysis and aims to find the optimal burn locations and directions. The linear regression technique is applied to determine an useful expression for the thrusting duration for any of the sample scenarios. It was found that, if the notification time is less than around 20 minutes, it is best to decrease the PoC as much as the available fuel allows. On the contrary, if it is higher than 20 minutes, the time required to perform the manoeuvre acts a more relevant role. Finally, simultaneously minimizing the manoeuvre time and PoC, overestimates the slight extra fuel required.

1.2.2.2. Low thrust CAMs

The main difference between the impulsive CAM and the low thrust one is that, while in the former the propulsion system acts instantaneously, while in the latter the external action is distributed over a certain thrust arc. As already said, nowadays many satellites operate with low thrust propulsion systems. This leads to the need of models and tools for the analysis and design of low thrust CAMs. An introductory work, but not directly related to CAM topic, is Colombo et al. [30]. The main idea of the low thrust preliminary design is to develop a simple but reliable semi-analytical mathematical framework where some explicit and computational efficient formulas can be obtained. Starting from Gauss Planetary Equations the main assumptions made in [30] are that no thrust action is present in the normal and out of plane directions while the tangential direction is affected by a tangential thrust proportional to the inverse of the square of the modulus of the

distance. This valuable assumption allows to express the small variations of the orbital elements in closed from, i.e. by means of incomplete elliptic integrals of first and second kind.

Proceeding in such a similar fashion the semi analytical expressions for the variations of the orbital parameters can be obtained for the generic low thrust problem. In Gonzalo et al. [31] those relations are obtained and their accuracy is assessed using various test cases with comparisons with the full numerical solution. This new model is part of the Manoeuvre Intelligence for Space Safety (MISS) software tool, currently being developed by the European Research Council-funded COMPASS project (see Gonzalo et al. [13] and COMPASS website [32]). In Gonzalo et al. [33] the same path of [31] is followed but the main novelty of this work is that those solutions are then decomposed into a sum of two contributions: a mean value and an oscillatory term. Such a decoupling yields both to an easier way to handle such solutions and a faster and more efficient evaluation of the time law. This is somehow a precursor of what we will do in this thesis work. Another relevant work that goes in this direction is Gonzalo et al. [34], where the mathematical model is furthermore refined and contextualized with respect to the current mission scenarios, e.g. the e.Cube mission. Furthermore, many numerical tests are carried out to assess the robustness of the method.

Finally, we want to highlight that all the works already presented about low thrust models deal with the case where only the tangential thrust action is present. On the contrary in Gao [35] the problem is analysed in terms of three types of control laws: the perigee centred tangential steering, the apogee centred inertial steering and the piecewise constant yaw steering. Those are performed over different orbital arcs within each transfer revolution to simultaneously change semimajor axis, eccentricity and inclination. The main novelty of this work is: it tries to build up a complete model for the low thrust CAM (i.e. with thrust in all directions) relying its argumentation on a sort of *superposition principle* suitably adapted for non linear equations.

1.3. Objectives

The main goal of this work is to develop a semi-analytical model for the 3D low thrust CAM problem, i.e. comprehensive of all three thrust actions: tangential, normal and out of plane. This specific requirement for the method of being semi-analytical, on one hand requires a more complicated mathematical formulation, but, on the other, leads to an easier and more effective way to obtain and analyse the results.

1.4. Novelties

The main novelty of this work is the use of the Fourier Series tool to perform the integrations, once the Gauss Planetary Equations are led to quadratures. This kind of solution is possible since, after some manipulations, it turns out that the integrations to be performed are those of 2π-periodic functions in the true anomaly. This Fourier Series approach gives great advantages both in terms of computational efficiency and capability of getting simple analytical formulas. In fact, for a given periodic function, once a few terms are computed, most of the function information are already captured with a high level of accuracy. Moreover, notice that the numerical part of the procedure could be possibly addressed to the evaluation of the Fourier Series coefficients only and not on the evaluation of the functional law.

The general procedure to lead the problem to quadratures strongly relies on the Taylor expansion in the neighborhood of the reference condition. This is another element of novelty with respect to the current literature; indeed in this way it is possible to increase the accuracy level of certain orbital parameters. Of course, the higher is the number of the terms included, the higher will be the complexity of the integrations to be performed. We will see how this procedure will lead us to first order linear ODEs with variable coefficients.

1.5. Thesis Structure

This thesis work is organised into four main parts:

- **Chapter 1: Introduction**. In this chapter we present the current state of the art about the topic of CAMs. After a general presentation of the current status of the space environment and the main organizations playing an important role at international level, we go to describe the main techniques adopted nowadays to deal with the mitigation of the problem of space debris. Among the many mitigations strategies, we underlined why collision avoidance manoeuvres play an important role in the prevention of catastrophic events. Then, a general overview of the current scientific literature about the collision avoidance problem is presented.
- **Chapter 2: Mathematical model**. In this chapter we present the main features of our new semi-analytical model in two main sections. The first regards the so called *full model* while the second is about the *small thrust model*. In both sections we provide the main steps to obtain the semi-analytical solution for the six Keplerian elements by means of the Fourier Series tool.

- **Chapter 3: Simulations**. In this chapter we first present some background notions about the probability of collision, the Miss Distance and the B-plane. After this short introduction we move to the analysis of the various test cases. All simulations are performed with Matlab®.
- **Chapter 4: Conclusions**. The results are here briefly discussed in relation to the aim of the thesis.

2 | Mathematical model

In this chapter we are going to analyse the mathematical model of the Low Thrust problem. After a brief introduction on the Gauss Planetary Equations, we will then move to the solution of them by means of a semi-analytical method which relies on the Fourier Series tool; this is used to analyse the involved functions and to perform the integrations. We carried out two models: the first, also denoted as *full model*, is the solution for arbitrary thrust actions while the second, denoted as *small thrust model*, is the solution when the assumption of small thrust parameters is applied. The hypothesis of *small thrust parameters* actually is equivalent of performing a first order MacLaurin expansion of the equations for $\{a_t, a_n, a_h\} \to 0$; the resulting equations are then easier to be manipulated. We will carry out a deep analysis of both models, showing how to perform all the integrations in closed form by exploiting the properties of the Fourier Series. Finally, for the small parameters approach, we evaluated analytically the Fourier Series coefficients of all functions involved (a brief summary is presented in Table 2.3).

2.1. Preliminary definitions

Let $f(\theta)$ be a 2π-periodic function, then its Fourier series expansion $\mathfrak{F}[f](\theta)$ is:

$$\mathfrak{F}[f](\theta) = \frac{\alpha_0[f]}{2} + \mathcal{P}_{2\pi}\left(\begin{array}{c} \alpha_n[f] \\ \beta_n[f] \end{array} \middle| \theta \right) \tag{2.1.1}$$

where $\mathcal{P}_{2\pi}$ is the Periodic P function of period 2π defined as:

$$\mathcal{P}_{2\pi}\left(\begin{array}{c} \alpha_n[f] \\ \beta_n[f] \end{array} \middle| \theta \right) = \sum_{n=1}^{+\infty} \{\alpha_n[f]\cos(n\theta) + \beta_n[f]\sin(n\theta)\} \tag{2.1.2}$$

and $\alpha_0[f]$, $\alpha_n[f]$ and $\beta_n[f]$ are the coefficients of the Fourier series expansion. This notation

underlines that such operators are applied to a certain function, i.e.:

$$\alpha_0[f] = \frac{1}{\pi}\int_{-\pi}^{\pi} f(\theta)\mathrm{d}\theta, \quad \alpha_n[f] = \frac{1}{\pi}\int_{-\pi}^{\pi} f(\theta)\cos(n\theta)\mathrm{d}\theta, \quad \beta_n[f] = \frac{1}{\pi}\int_{-\pi}^{\pi} f(\theta)\sin(n\theta)\mathrm{d}\theta$$

It is clear that the main advantage of expanding f in the form Equation 2.1.1 is that the operations of derivation and integration becomes straightforward. In particular:

Definition 2.1.1. The θ-integral of $\mathfrak{F}[f](\theta)$ is:

$$\int \mathfrak{F}[f](\theta)\mathrm{d}\theta = \frac{\alpha_0[f]}{2}\theta + \mathcal{P}_{2\pi}\left(\begin{array}{c} -\beta_n[f]/n \\ \alpha_n[f]/n \end{array}\middle|\,\theta\right) \tag{2.1.3}$$

where in particular:

$$\int \mathcal{P}_{2\pi}\left(\begin{array}{c} \alpha_n[f] \\ \beta_n[f] \end{array}\middle|\,\theta\right)\mathrm{d}\theta = \mathcal{P}_{2\pi}\left(\begin{array}{c} -\beta_n[f]/n \\ \alpha_n[f]/n \end{array}\middle|\,\theta\right) \tag{2.1.4}$$

Definition 2.1.2. The θ-derivative of $\mathfrak{F}[f](\theta)$ is:

$$\frac{\mathrm{d}}{\mathrm{d}\theta}\left\{\mathfrak{F}[f](\theta)\right\} = \mathcal{P}_{2\pi}\left(\begin{array}{c} n\beta_n[f] \\ -n\alpha_n[f] \end{array}\middle|\,\theta\right)$$

Definition 2.1.3. The θ-integral of the product $\theta\cdot\mathfrak{F}[f](\theta)$ is:

$$\int \theta\cdot\mathfrak{F}[f](\theta)\mathrm{d}\theta = \frac{\alpha_0[f]}{4}\theta^2 + \mathcal{P}_{2\pi}\left(\begin{array}{c} -\beta_n[f]/n \\ \alpha_n[f]/n \end{array}\middle|\,\theta\right)\theta + \mathcal{P}_{2\pi}\left(\begin{array}{c} \alpha_n[f]/n^2 \\ \beta_n[f]/n^2 \end{array}\middle|\,\theta\right) \tag{2.1.5}$$

Proof. The proof of Equation 2.1.5 can be obtained integrating by parts:

$$\int \theta\cdot\mathfrak{F}[f](\theta)\mathrm{d}\theta = \theta\int \mathfrak{F}[f](\theta)\mathrm{d}\theta - \int\left[\int \mathfrak{F}[f](\theta)\mathrm{d}\theta\right]\mathrm{d}\theta$$

The first integral is directly given by Equation 2.1.3 while for the second double integration the integral of the linear term in θ is straightforward while for the periodic part we rely on Equation 2.1.4 ■

Definition 2.1.4. The θ-integral of the product $\theta^2 \cdot \mathfrak{F}[f](\theta)$ is:

$$\begin{aligned}\int \theta^2 \cdot \mathfrak{F}[f](\theta)\mathrm{d}\theta = \frac{\alpha_0[f]}{6}\theta^3 + \mathcal{P}_{2\pi}\left(\begin{array}{c} 2\beta_n[f]/n^3 \\ -2\alpha_n[f]/n^3 \end{array}\middle|\,\theta\right) + \\ + \mathcal{P}_{2\pi}\left(\begin{array}{c} 2\alpha_n[f]/n^2 \\ 2\beta_n[f]/n^2 \end{array}\middle|\,\theta\right)\theta + \mathcal{P}_{2\pi}\left(\begin{array}{c} -\beta_n[f]/n \\ \alpha_n[f]/n \end{array}\middle|\,\theta\right)\theta^2\end{aligned} \tag{2.1.6}$$

Proof. The proof is analogous to the one of Equation 2.1.5, but this time the integration by parts has to be applied twice. ■

Definition 2.1.5. The θ-integral of the product $\exp[-k\theta] \cdot \mathfrak{F}[f](\theta)$ is:

$$\begin{aligned}\int \exp[-k\theta] \cdot \mathfrak{F}[f](\theta)\mathrm{d}\theta = -\frac{\alpha_0[f]}{2k}\exp[-k\theta] + \\ + \mathcal{P}_{2\pi}\left(\begin{array}{c} -(k\alpha_n[f] + n\beta_n[f])/(k^2+n^2) \\ (n\alpha_n[f] - k\beta_n[f])/(k^2+n^2) \end{array}\middle|\,\theta\right)\exp[-k\theta]\end{aligned} \tag{2.1.7}$$

Proof. Assuming $k \in \mathbb{R}$ and assuming also $k \neq 0$ we have:

$$\int \exp[-k\theta]\mathrm{d}\theta = -\exp[-k\theta]/k$$

and $\forall n \in \mathbb{N}$ we have:

$$\begin{aligned}\int \exp[-k\theta]\cos(n\theta)\mathrm{d}\theta &= \frac{n\sin(n\theta) - k\cos(n\theta)}{k^2+n^2}\exp[-k\theta] \\ \int \exp[-k\theta]\sin(n\theta)\mathrm{d}\theta &= -\frac{k\sin(n\theta) + n\cos(n\theta)}{k^2+n^2}\exp[-k\theta]\end{aligned}$$

Thus it follows Equation 2.1.7. ■

Definition 2.1.6. The θ-integral of the product $\theta \cdot \exp[-k\theta] \cdot \mathfrak{F}[f](\theta)$ is:

$$\begin{aligned}\int \theta \cdot \exp[-k\theta] \cdot \mathfrak{F}[f](\theta)\mathrm{d}\theta = -\frac{\alpha_0[f]}{2k^2}(1+k\theta)\exp[-k\theta] + \\ + \theta\mathcal{P}_{2\pi}\left(\begin{array}{c} -(k\alpha_n[f] + n\beta_n[f])/(k^2+n^2) \\ (n\alpha_n[f] - k\beta_n[f])/(k^2+n^2) \end{array}\middle|\,\theta\right)\exp[-k\theta] + \\ + \mathcal{P}_{2\pi}\left(\begin{array}{c} [\alpha_n[f](n^2-k^2) - 2kn\beta_n[f]]/(k^2+n^2)^2 \\ [2kn\alpha_n[f] + \beta_n[f](n^2-k^2)]/(k^2+n^2)^2 \end{array}\middle|\,\theta\right)\exp[-k\theta]\end{aligned} \tag{2.1.8}$$

Proof. The proof is analogous to the one of Equation 2.1.7. ■

Definition 2.1.7. The θ-integral of the product $\theta^2 \cdot \exp[-k\theta] \cdot \mathfrak{F}[f](\theta)$ is:

$$\begin{aligned}
&\int \theta^2 \cdot \exp[-k\theta] \cdot \mathfrak{F}[f](\theta)\mathrm{d}\theta = \\
&\left\{ -\frac{\alpha_0[f]}{k^3} + 2\mathcal{P}_{2\pi}\left(\begin{array}{c} \dfrac{n\left(n^2-3k^2\right)\beta_n[f] - k\left(k^2-3n^2\right)\alpha_n[f]}{\left(k^2+n^2\right)^3} \\ -\dfrac{n\left(n^2-3k^2\right)\alpha_n[f] + k\left(k^2-3n^2\right)\beta_n[f]}{\left(k^2+n^2\right)^3} \end{array} \middle| \theta \right) \right\} \exp[-k\theta] + \\
&\left\{ -\frac{\alpha_0[f]}{k^2} + 2\mathcal{P}_{2\pi}\left(\begin{array}{c} \dfrac{\left(n^2-k^2\right)\alpha_n[f] - 2kn\beta_n[f]}{\left(k^2+n^2\right)^2} \\ \dfrac{\left(n^2-k^2\right)\beta_n[f] + 2kn\alpha_n[f]}{\left(k^2+n^2\right)^2} \end{array} \middle| \theta \right) \right\} \theta \exp[-k\theta] + \\
&+ \left\{ -\frac{\alpha_0[f]}{2k} + \mathcal{P}_{2\pi}\left(\begin{array}{c} -\dfrac{k\alpha_n[f] + n\beta_n[f]}{k^2+n^2} \\ \dfrac{n\alpha_n[f] - k\beta_n[f]}{k^2+n^2} \end{array} \middle| \theta \right) \right\} \theta^2 \exp[-k\theta]
\end{aligned} \tag{2.1.9}$$

Proof. The proof is analogous to the one of Equation 2.1.7. ■

The Fourier Series approach to solve differential problems has been analysed in Bocci et. al [36] and [37]. Here the solution for periodic bounded problems is carried out and also the procedure for the time law inversion is presented. This goes far beyond the scope of this thesis, but it could be an hint for future developments. An important result (which will be used in next chapters) is the following convolution theorem:

Theorem 2.1.1 (Convolution of two periodic functions). Let $f(\theta)$ and $g(\theta)$ be 2π-periodic functions in θ, then:

$$\begin{aligned}
\alpha_0[f\cdot g] &= \frac{1}{2}\alpha_0[f]\alpha_0[g] + \sum_{m=1}^{+\infty}\left\{\alpha_m[f]\alpha_m[g] + \beta_m[f]\beta_m[g]\right\} \\
\alpha_n[f\cdot g] &= \frac{1}{2}\alpha_0[f]\alpha_n[g] + \frac{1}{2}\sum_{m=1}^{+\infty}\alpha_m[f]\left\{\alpha_{|n-m|}[g] + \alpha_{n+m}[g]\right\} + \\
&\quad - \frac{1}{2}\sum_{m=1}^{+\infty}\beta_m[f]\left\{\mathrm{sgn}(n-m)\beta_{|n-m|}[g] - \beta_{n+m}[g]\right\} \\
\beta_n[f\cdot g] &= \frac{1}{2}\alpha_0[f]\beta_n[g] + \frac{1}{2}\sum_{m=1}^{+\infty}\alpha_m[f]\left\{\mathrm{sgn}(n-m)\beta_{|n-m|}[g] + \beta_{n+m}[g]\right\} + \\
&\quad + \frac{1}{2}\sum_{m=1}^{+\infty}\beta_m[f]\left\{\alpha_{|n-m|}[g] - \alpha_{n+m}[g]\right\}
\end{aligned} \tag{2.1.10}$$

where:

$$\operatorname{sgn}(x) = \begin{cases} 1 & x > 0 \\ 0 & x = 0 \\ -1 & x < 0 \end{cases} \tag{2.1.11}$$

Proof. Since f and g are 2π-periodic functions we can evaluate their Fourier series expansion coefficients separately. Then, for instance, putting in the product only the expansion of f we get:

$$\begin{aligned} \alpha_0[f \cdot g] &= \frac{1}{2}\alpha_0[f] \cdot \frac{1}{\pi}\int_{-\pi}^{\pi} g(\theta)\mathrm{d}\theta + \\ &+ \sum_{m=1}^{+\infty}\left[\alpha_m[f] \cdot \frac{1}{\pi}\int_{-\pi}^{\pi} g(\theta)\cos(m\theta)\mathrm{d}\theta + \beta_m[f] \cdot \frac{1}{\pi}\int_{-\pi}^{\pi} g(\theta)\sin(m\theta)\mathrm{d}\theta\right] = \\ &= \frac{1}{2}\alpha_0[f]\alpha_0[g] + \sum_{m=1}^{+\infty}\{\alpha_m[f]\alpha_m[g] + \beta_m[f]\beta_m[g]\} \end{aligned}$$

and:

$$\begin{aligned} \alpha_n[f \cdot g] &= \frac{1}{2}\alpha_0[f] \cdot \frac{1}{\pi}\int_{-\pi}^{\pi} g(\theta)\cos(n\theta)\mathrm{d}\theta + \sum_{m=1}^{+\infty}\alpha_m[f] \cdot \frac{1}{\pi}\int_{-\pi}^{\pi} g(\theta)\cos(m\theta)\cos(n\theta)\mathrm{d}\theta + \\ &+ \sum_{m=1}^{+\infty}\beta_m[f] \cdot \frac{1}{\pi}\int_{-\pi}^{\pi} g(\theta)\sin(m\theta)\cos(n\theta)\mathrm{d}\theta = \\ &= \frac{1}{2}\alpha_0[f]\alpha_n[g] + \frac{1}{2}\sum_{m=1}^{+\infty}\alpha_m[f] \cdot \frac{1}{\pi}\int_{-\pi}^{\pi} g(\theta)\left\{\cos[|n-m|\theta] + \cos[(n+m)\theta]\right\}\mathrm{d}\theta + \\ &- \frac{1}{2}\sum_{m=1}^{+\infty}\beta_m[f] \cdot \frac{1}{\pi}\int_{-\pi}^{\pi} g(\theta)\left\{\operatorname{sgn}(n-m)\sin[|n-m|\theta] - \sin[(n+m)\theta]\right\}\mathrm{d}\theta = \\ &= \frac{1}{2}\alpha_0[f]\alpha_n[g] + \frac{1}{2}\sum_{m=1}^{+\infty}\alpha_m[f]\left\{\alpha_{|n-m|}[g] + \alpha_{n+m}[g]\right\} + \\ &- \frac{1}{2}\sum_{m=1}^{+\infty}\beta_m[f]\left\{\operatorname{sgn}(n-m)\beta_{|n-m|}[g] - \beta_{n+m}[g]\right\} \end{aligned}$$

and:

$$
\begin{aligned}
\beta_n[f\cdot g] &= \frac{1}{2}\alpha_0[f]\cdot\frac{1}{\pi}\int_{-\pi}^{\pi} g(\theta)\sin(n\theta)\mathrm{d}\theta + \sum_{m=1}^{+\infty}\alpha_m[f]\cdot\frac{1}{\pi}\int_{-\pi}^{\pi} g(\theta)\cos(m\theta)\sin(n\theta)\mathrm{d}\theta + \\
&+ \sum_{m=1}^{+\infty}\beta_m[f]\cdot\frac{1}{\pi}\int_{-\pi}^{\pi} g(\theta)\sin(m\theta)\sin(n\theta)\mathrm{d}\theta = \\
&= \frac{1}{2}\alpha_0[f]\beta_n[g] + \\
&+ \frac{1}{2}\sum_{m=1}^{+\infty}\alpha_m[f]\cdot\frac{1}{\pi}\int_{-\pi}^{\pi} g(\theta)\left\{\mathrm{sgn}(n-m)\sin[|n-m|\theta] + \sin[(n+m)\theta]\right\}\mathrm{d}\theta + \\
&+ \frac{1}{2}\sum_{m=1}^{+\infty}\beta_m[f]\cdot\frac{1}{\pi}\int_{-\pi}^{\pi} g(\theta)\left\{\cos[|n-m|\theta] - \cos[(n+m)\theta]\right\}\mathrm{d}\theta = \\
&= \frac{1}{2}\alpha_0[f]\beta_n[g] + \frac{1}{2}\sum_{m=1}^{+\infty}\alpha_m[f]\left\{\mathrm{sgn}(n-m)\beta_{|n-m|}[g] + \beta_{n+m}[g]\right\} + \\
&+ \frac{1}{2}\sum_{m=1}^{+\infty}\beta_m[f]\left\{\alpha_{|n-m|}[g] - \alpha_{n+m}[g]\right\}
\end{aligned}
$$

■

2.2. Gauss Planetary Equations overview

The general formulation of Gauss Planetary equations is:

$$
\begin{aligned}
\frac{\mathrm{d}a}{\mathrm{d}t} &= \frac{2a^2 v}{\mu}a_t \\
\frac{\mathrm{d}e}{\mathrm{d}t} &= \frac{1}{v}\left\{2\left[e+\cos(\theta)\right]a_t - \frac{r}{a}\sin(\theta)a_n\right\} \\
\frac{\mathrm{d}i}{\mathrm{d}t} &= \frac{r\cos(\theta+\omega)}{h}a_h \\
\frac{\mathrm{d}\Omega}{\mathrm{d}t} &= \frac{r\sin(\theta+\omega)}{h\sin(i)}a_h \\
\frac{\mathrm{d}\omega}{\mathrm{d}t} &= \frac{1}{ev}\left\{2\sin(\theta)a_t + \left[2e + \frac{r}{a}\cos(\theta)\right]a_n\right\} - \frac{r\sin(\theta+\omega)\cos(i)}{h\sin(i)}a_h \\
\frac{\mathrm{d}\theta}{\mathrm{d}t} &= \frac{h}{r^2} - \frac{1}{ev}\left\{2\sin(\theta)a_t + \left[2e + \frac{r}{a}\cos(\theta)\right]a_n\right\}
\end{aligned}
\tag{2.2.1}
$$

with:

$$
r = \frac{a(1-e^2)}{1+e\cos(\theta)}, \quad v = \sqrt{\frac{2\mu}{r} - \frac{\mu}{a}}, \quad h = \sqrt{\mu a(1-e^2)} \tag{2.2.2}
$$

In our notation: a is the semimajor axis of the orbit, e is the eccentricity, i is the inclination, Ω is the Right Ascension of the Ascending Node (also denoted as RAAN), ω is the argument of perigee and θ is the true anomaly. Moreover, in order to simplify the notation, we introduced in Equation 2.2.1 the quantities indicated in Equation 2.2.2, i.e. h is the specific angular momentum, r is the norm of the position vector, v is the norm of the velocity vector and μ is the standard gravitational parameter of a celestial body[1]. Finally we indicate with a_t the thrust in the tangential direction, with a_n the thrust in the normal direction and with a_h the thrust in the out of plane[2] direction.

In the most general sense the system Equation 2.2.1 is a time domain set of ordinary differential equations. Exploiting all the functional dependencies, the ODEs system can be reduced to the kind:

$$\begin{aligned}
\frac{\mathrm{d}a}{\mathrm{d}t} &= \alpha(a, e, \theta; a_t) \\
\frac{\mathrm{d}e}{\mathrm{d}t} &= \beta(a, e, \theta; a_t, a_n) \\
\frac{\mathrm{d}i}{\mathrm{d}t} &= \gamma(a, e, \omega, \theta; a_h) \\
\frac{\mathrm{d}\Omega}{\mathrm{d}t} &= \delta(a, e, i, \omega, \theta; a_h) \\
\frac{\mathrm{d}\omega}{\mathrm{d}t} &= \epsilon(a, e, i, \omega, \theta; a_t, a_n, a_h) \\
\frac{\mathrm{d}\theta}{\mathrm{d}t} &= \zeta(a, e, \theta; a_t, a_n)
\end{aligned} \tag{2.2.3}$$

where α, β, γ, δ, ϵ and ζ can be easily obtained from Equation 2.2.1.

Remark 2.2.1. Referring to Equation 2.2.3, the **shape problem** $\{a, e, \theta\}$ is decoupled from the **orientation problem** $\{i, \Omega, \omega\}$. The main reason is that, since the thrust accelerations components $\{a_t, a_n, a_h\}$ are constant, the functions α, β and ζ form a self consisting subsystem of ODEs.

Now, assuming as independent variable the true anomaly θ and indicating with $()'$ all the θ-derivatives, the system Equation 2.2.3 is led to:

[1] i.e. $\mu = GM$, where G is the gravitational constant and M is the mass of the body.
[2] i.e. the plane containing the spacecraft orbit.

$$
\begin{aligned}
a' &= \alpha(a,e,\theta;a_t,a_n)/\zeta(a,e,\theta;a_t,a_n) = R(a,e,\theta;a_t,a_n)\\
e' &= \beta(a,e,\theta;a_t,a_n)/\zeta(a,e,\theta;a_t,a_n) = S(a,e,\theta;a_t,a_n)\\
t' &= 1/\zeta(a,e,\theta;a_t,a_n) = \tau(a,e,\theta;a_t,a_n)\\
i' &= \gamma(a,e,\omega,\theta;a_t,a_n,a_h)/\zeta(a,e,\theta;a_t,a_n) = \mathfrak{I}(a,e,\omega,\theta;a_t,a_n,a_h)\\
\Omega' &= \delta(a,e,i,\omega,\theta;a_t,a_n,a_h)/\zeta(a,e,\theta;a_t,a_n) = \mathfrak{O}(a,e,i,\omega,\theta;a_t,a_n,a_h)\\
\omega' &= \epsilon(a,e,i,\omega,\theta;a_t,a_n,a_h)/\zeta(a,e,\theta;a_t,a_n) = \mathcal{O}(a,e,i,\omega,\theta;a_t,a_n,a_h)
\end{aligned}
\tag{2.2.4}
$$

The constant small thrust parameters are present inside these functions in terms of complicated algebraic forms. Nevertheless they are not referred to in the functional dependencies in the computations hereafter in order to have a simpler notation.

2.3. Arbitrary thrust actions solution - *full model*

The solution procedure consists in expanding in Taylor series all the previous functions near the reference condition $\boldsymbol{x}_0 = \{a_0, e_0, i_0, \omega_0\}$. All functions are expanded up to first order with the exception of S which characterizes the eccentricity. Moreover, we assume that the inclination is affected in its variation from a and e much more than from ω.

The system Equation 2.2.4 reduces to:

$$a' = R_0(\theta) + R_a(\theta)(a-a_0) + R_e(\theta)(e-e_0) \tag{2.3.1a}$$
$$e' = S_0(\theta) \tag{2.3.1b}$$
$$t' = \tau_0(\theta) + \tau_a(\theta)(a-a_0) + \tau_e(\theta)(e-e_0) \tag{2.3.1c}$$
$$i' = \mathfrak{I}_0(\theta) + \mathfrak{I}_a(\theta)(a-a_0) + \mathfrak{I}_e(\theta)(e-e_0) \tag{2.3.1d}$$
$$\Omega' = \mathfrak{O}_0(\theta) + \mathfrak{O}_a(\theta)(a-a_0) + \mathfrak{O}_e(\theta)(e-e_0) + \mathfrak{O}_i(\theta)(i-i_0) + \mathfrak{O}_\omega(\theta)(\omega-\omega_0) \tag{2.3.1e}$$
$$\omega' = \mathcal{O}_0(\theta) + \mathcal{O}_a(\theta)(a-a_0) + \mathcal{O}_e(\theta)(e-e_0) + \mathcal{O}_i(\theta)(i-i_0) + \mathcal{O}_\omega(\theta)(\omega-\omega_0) \tag{2.3.1f}$$

In the present notation (and also further in this work) if $f(\boldsymbol{x},\theta)$ is a generic function, then:

$$f_0(\theta) = f(\boldsymbol{x}_0,\theta) \quad \text{and} \quad f_{x_i}(\theta) = \left.\frac{\partial f}{\partial x_i}\right|_{(\boldsymbol{x}_0,\theta)} \tag{2.3.2}$$

Remark 2.3.1. The two hypotheses previously done are supported by numerical evidences as presented in Figure 2.1. In the simulations we compared the solutions of the Gauss Planetary Equations in the form Equation 2.2.4 with the numerical solution of the system in Equation 2.3.1 (namely Reduced First Order system - rfo) and also with the

numerical solution of the system composed by same set of equations but where Equation 2.3.1a and Equation 2.3.1d are replaced with:

$$e' = S_0(\theta) + S_a(\theta)(a - a_0) + S_e(\theta)(e - e_0)$$
$$i' = \mathfrak{I}_0(\theta) + \mathfrak{I}_a(\theta)(a - a_0) + \mathfrak{I}_e(\theta)(e - e_0) + \mathfrak{I}_\omega(\theta)(\omega - \omega_0)$$

(namely Complete First Order system - cfo). From Figure 2.1 we can see that passing from the cfo-model to the rfo-model the relative error increases but it remains low. This is even more true if we take into account the fact that these simulations are carried out imposing a continuous thrust action for two orbital revolutions.[3] In the common practice, indeed, the thrust arc should be as short as possible to not interfere too much with the satellite operations. Finally we observe that, in order to test the strength of the method, the selected thrust actions are relatively high in magnitude, but this not true in reality; in particular the thrust level in the out of plane direction a_h is typically vary low. Putting together all these considerations we conclude that the reduction in Equation 2.3.1 is an effective and reliable method to approximate the solution of Equation 2.2.4.

[3] this choice is done just to test the strength of the method and of the hypothesis.

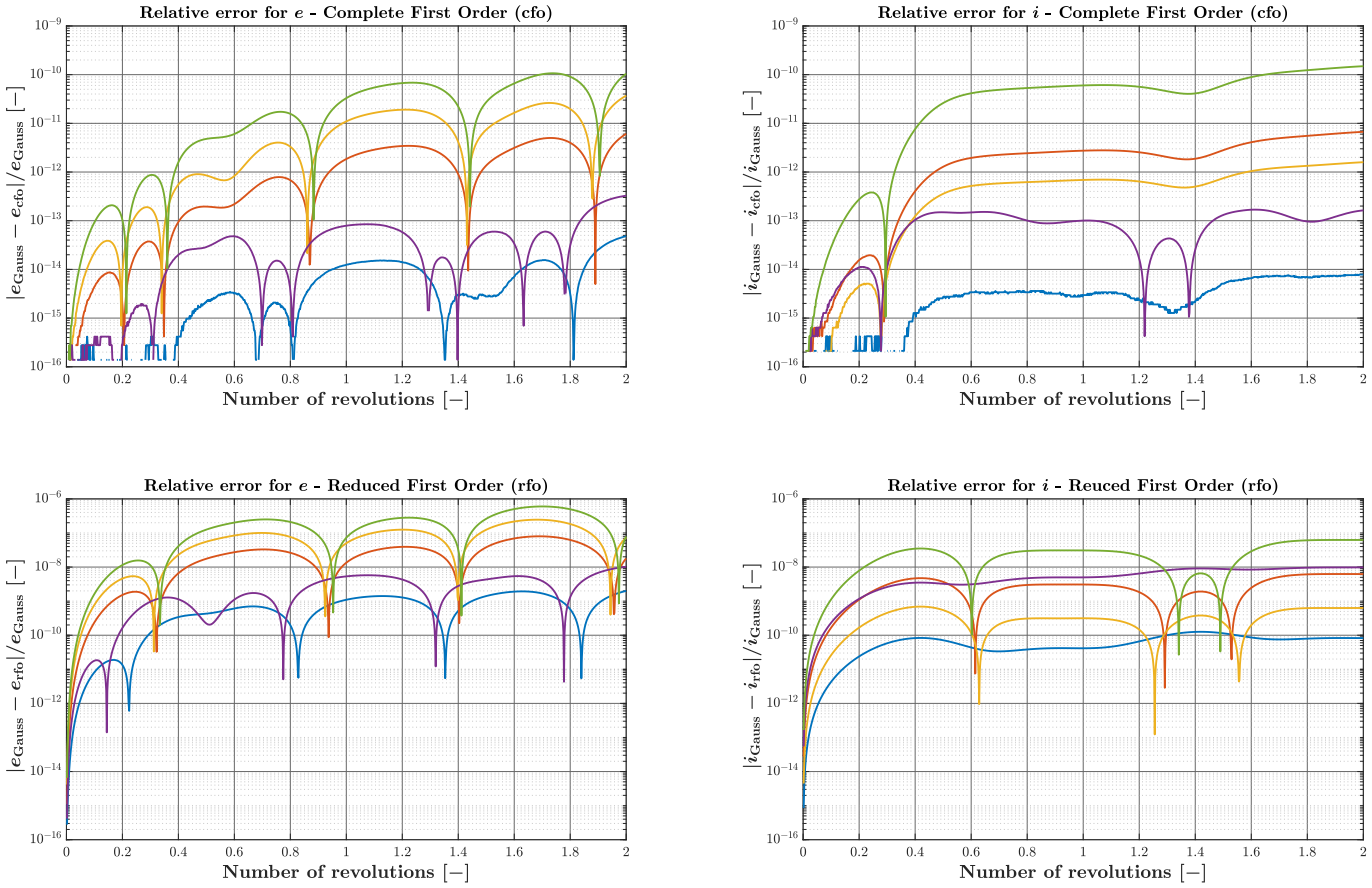

Figure 2.1: Relative errors for e and i for different thrust levels. (Reference orbit: $a_0 = 12000$ km, $e_0 = 0.1$, $i_0 = 30$ deg, $\Omega_0 = 10$ deg, $\omega_0 = 29$ deg, $\theta_0 = 5$ deg. Orbital period: $T_0 = 3.634$ h. Initial time: $t_0 = 0$ s.)

Remark 2.3.2. The variation of the eccentricity is more affected by the variation of the semimajor axis than from the variation of the eccentricity itself. Therefore, replacing Equation 2.3.1b with a first order approximation of the kind:

$$e' = S_0(\theta) + S_e(\theta)(e - e_0) \tag{2.3.3}$$

would lead to a small increase in precision. On the contrary the approximation:

$$e' = S_0(\theta) + S_a(\theta)(a - a_0) \tag{2.3.4}$$

would be more beneficial. Referring to Figure 2.2 we can see what previously explained. Here we present the solutions for different thrust levels and for different values of the reference eccentricity e_0. We can appreciate that the numerical solution of Equation 2.3.4 (denoted by e_{S_a}) is slightly more accurate than the solution of Equation 2.3.3 (denoted by e_{Se}) specially when the number of revolutions increases. Nevertheless this small gain in accuracy does not justify the corresponding increase in difficulty of the mathematical model.

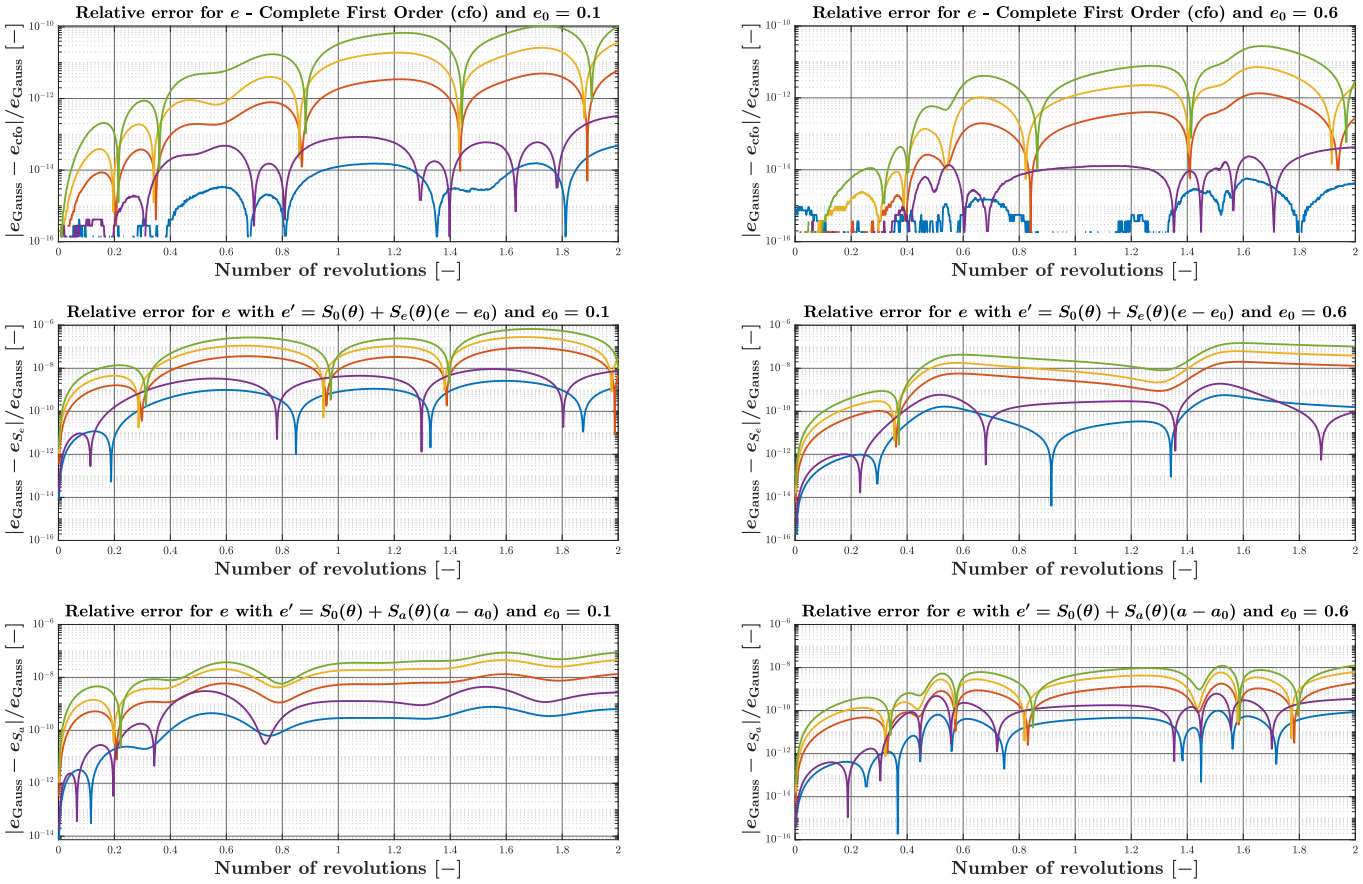

Figure 2.2: Relative errors for e for different thrust levels and reference eccentricities. (Reference orbit: $a_0 = 12000$ km, $i_0 = 30$ deg, $\Omega_0 = 10$ deg, $\omega_0 = 29$ deg, $\theta_0 = 5$ deg and $e_0 = 0.1, 0.6$. Orbital period: $T_0 = 3.634$ h. Initial time: $t_0 = 0$ s.)

Remark 2.3.3. A final remark has to be done on the behaviours of the errors. As we can appreciate in Figure 2.2 the behaviours of the relative error are not so much affected by the reference value of the eccentricity (and in general from the reference value of any other orbital parameter). This is because our model in Equation 2.3.1 is the result of a Taylor expansion in the neighbourhood of the reference condition. Therefore one of its strength point is that the accuracy will be high till the solution will not differ too much from the reference.

2.3.1. Zero order solution for the orbital shape problem

Referring to Remark 2.2.1 we now proceed to derive a very simple solution for the shape problem. The main assumption is to consider that both the variations of a and e are driven by the zero order terms. In this case Equation 2.3.1a and Equation 2.3.1b become:

$$a' = R_0(\theta) \quad \text{and} \quad e' = S_0(\theta)$$

But R_0 and S_0 are 2π-periodic in θ so the integrations come directly from Equation 2.1.4:

$$a(\theta) - a_0 = \left[\frac{\alpha_0[R_0]}{2}\xi + \mathcal{P}_{2\pi}\left(\begin{array}{c|c} -\beta_n[R_0]/n & \\ \alpha_n[R_0]/n & \xi \end{array} \right) \right]_{\theta_0}^{\theta}$$
$$e(\theta) - e_0 = \left[\frac{\alpha_0[S_0]}{2}\xi + \mathcal{P}_{2\pi}\left(\begin{array}{c|c} -\beta_n[S_0]/n & \\ \alpha_n[S_0]/n & \xi \end{array} \right) \right]_{\theta_0}^{\theta}$$

These expressions can be rewritten as:

$$\boxed{a(\theta) - a_0 = \frac{\alpha_0[R_0]}{2}\theta + \Xi_a(\theta)} \tag{2.3.5}$$

$$\boxed{e(\theta) - e_0 = \frac{\alpha_0[S_0]}{2}\theta + \Xi_e(\theta)} \tag{2.3.6}$$

with:

$$\Xi_a(\theta) = -\frac{\alpha_0[R_0]}{2}\theta_0 + \left[\mathcal{P}_{2\pi}\left(\begin{array}{c|c} -\beta_n[R_0]/n & \\ \alpha_n[R_0]/n & \xi \end{array} \right) \right]_{\theta_0}^{\theta}, \quad \Xi_a(\theta) = \Xi_a(\theta + 2\pi)$$
$$\Xi_e(\theta) = -\frac{\alpha_0[S_0]}{2}\theta_0 + \left[\mathcal{P}_{2\pi}\left(\begin{array}{c|c} -\beta_n[S_0]/n & \\ \alpha_n[S_0]/n & \xi \end{array} \right) \right]_{\theta_0}^{\theta}, \quad \Xi_e(\theta) = \Xi_e(\theta + 2\pi)$$

The main advantage of rewriting the solutions for a and e in the form of Equation 2.3.5 and Equation 2.3.6 is that we take apart the periodic contributions (i.e. Ξ_a and Ξ_e) from the linear increasing ones. This technique will allow us to achieve the further integrations in an easier way.

2.3.1.1. Time law computation

Plugging Equation 2.3.5 and Equation 2.3.6 into Equation 2.3.1c we get:

$$t - t_0 = \int_{\theta_0}^{\theta} \mathfrak{X}_0(\xi)\mathrm{d}\xi + \int_{\theta_0}^{\theta} \mathfrak{X}_1(\xi)\xi\mathrm{d}\xi \tag{2.3.7}$$

where:

$$\begin{aligned} \mathfrak{X}_0(\theta) &= \tau_0(\theta) + \tau_a(\theta)\Xi_a(\theta) + \tau_e(\theta)\Xi_e(\theta), & \mathfrak{X}_0(\theta) &= \mathfrak{X}_0(\theta + 2\pi) \\ \mathfrak{X}_1(\theta) &= \left[\alpha_0[R_0]\tau_a(\theta) + \alpha_0[S_0]\tau_e(\theta)\right]/2, & \mathfrak{X}_1(\theta) &= \mathfrak{X}_1(\theta + 2\pi) \end{aligned}$$

Now combining Equation 2.1.3 and Equation 2.1.5 we obtain:

$$\boxed{t - t_0 = A\theta^2 + B(\theta)\theta + C(\theta) - \left[A\theta_0^2 + B(\theta_0)\theta_0 + C(\theta_0)\right]} \tag{2.3.8}$$

with:

$$A = \frac{\alpha_0[\mathfrak{X}_1]}{4}, \quad B(\theta) = \frac{\alpha_0[\mathfrak{X}_0]}{2} + \mathcal{P}_{2\pi}\left(\begin{array}{c|c} -\beta_n[\mathfrak{X}_1]/n & \\ \alpha_n[\mathfrak{X}_1]/n & \theta \end{array}\right)$$
$$C(\theta) = \mathcal{P}_{2\pi}\left(\begin{array}{c|c} -\beta_n[\mathfrak{X}_0]/n + \alpha_n[\mathfrak{X}_1]/n^2 & \\ \alpha_n[\mathfrak{X}_0]/n + \beta_n[\mathfrak{X}_1]/n^2 & \theta \end{array}\right)$$

Notice that A is a constant, while $B(\theta)$ and $C(\theta)$ are both 2π-periodic functions.

A more refined model for the time law can be achieved considering a second order approximation. Expanding in Taylor series and performing the substitutions the Equation 2.3.1c becomes:

$$t' = \mathfrak{T}_0(\theta) + \mathfrak{T}_1(\theta)\theta + \mathfrak{T}_2(\theta)\theta^2$$

with:

$$\begin{aligned} \mathfrak{T}_0(\theta) &= \frac{1}{2}\Xi_a^2(\theta)\tau_{\mathrm{aa}}(\theta) + \Xi_a(\theta)\tau_{\mathrm{ae}}(\theta)\Xi_e(\theta) + \Xi_a(\theta)\tau_a(\theta) + \\ &\quad + \frac{1}{2}\Xi_e^2(\theta)\tau_{\mathrm{ee}}(\theta) + \Xi_e(\theta)\tau_e(\theta) + \tau_0(\theta) \\ \mathfrak{T}_1(\theta) &= \frac{1}{2}\alpha_0\left[R_0\right]\left[\Xi_a(\theta)\tau_{\mathrm{aa}}(\theta) + \tau_a(\theta) + \tau_{\mathrm{ae}}(\theta)\Xi_e(\theta)\right] + \\ &\quad + \frac{1}{2}\alpha_0\left[S_0\right]\left[\Xi_a(\theta)\tau_{\mathrm{ae}}(\theta) + \Xi_e(\theta)\tau_{\mathrm{ee}}(\theta) + \tau_e(\theta)\right] \\ \mathfrak{T}_2(\theta) &= \frac{1}{8}\left[\alpha_0^2\left[R_0\right]\tau_{\mathrm{aa}}(\theta) + 2\alpha_0\left[R_0\right]\alpha_0\left[S_0\right]\tau_{\mathrm{ae}}(\theta) + \alpha_0^2\left[S_0\right]\tau_{\mathrm{ee}}(\theta)\right] \end{aligned}$$

Now combining Equation 2.1.3, Equation 2.1.5 and Equation 2.1.6 we obtain:

$$\boxed{t - t_0 = \tilde{A}\theta^3 + \tilde{B}(\theta)\theta^2 + \tilde{C}(\theta)\theta + \tilde{D}(\theta) - [\tilde{A}\theta_0^3 + \tilde{B}(\theta_0)\theta_0^2 + \tilde{C}(\theta_0)\theta_0 + \tilde{D}(\theta_0)]} \quad (2.3.9)$$

with:

$$\tilde{A} = \frac{\alpha_0[\mathfrak{T}_2]}{6}, \quad \tilde{B}(\theta) = \left[\frac{\alpha_0[\mathfrak{T}_1]}{4} + \mathcal{P}_{2\pi}\left(\begin{array}{c|c} -\beta_n[\mathfrak{T}_2]/n & \\ \alpha_n[\mathfrak{T}_2]/n & \theta \end{array}\right)\right]$$

$$\tilde{C}(\theta) = \frac{\alpha_0[\mathfrak{T}_0]}{2} + \mathcal{P}_{2\pi}\left(\begin{array}{c|c} -\beta_n[\mathfrak{T}_1]/n + 2\alpha_n[\mathfrak{T}_2]/n^2 & \\ \alpha_n[\mathfrak{T}_1]/n + 2\beta_n[\mathfrak{T}_2]/n^2 & \theta \end{array}\right)$$

$$\tilde{D}(\theta) = \mathcal{P}_{2\pi}\left(\begin{array}{c|c} -\beta_n[\mathfrak{T}_0]/n + \alpha_n[\mathfrak{T}_1]/n^2 + 2\beta_n[\mathfrak{T}_2]/n^3 & \\ \alpha_n[\mathfrak{T}_0]/n + \beta_n[\mathfrak{T}_1]/n^2 - 2\alpha_n[\mathfrak{T}_2]/n^3 & \theta \end{array}\right)$$

Remark 2.3.4. The expressions obtained in Equation 2.3.8 and Equation 2.3.9 provide time t as a function of the true anomaly θ. This means that an inversion has to be performed in order to obtain the functional relationship $\theta = \theta(t)$. This is done by solving for each value of t a non linear root finding problem by means of Newton-Raphson method.

2.3.2. First order approximation for the semi-major axis

The general statement is expressed[4] by Equation 2.3.1a and Equation 2.3.1b:

$$a' = R_0(\theta) + R_a(\theta)(a - a_0) + R_e(\theta)(e - e_0)$$
$$e' = S_0(\theta)$$

Taking the θ-integral of Equation 2.3.1b and plugging that solution into Equation 2.3.1a we obtain:

$$a' = \mathfrak{R}_0(\theta) + R_a(\theta)(a - a_0), \quad \mathfrak{R}_0(\theta) = R_0(\theta) + R_e(\theta)\int_{\theta_0}^{\theta} S_0(\xi)\mathrm{d}\xi$$

Setting $\bar{a} = a - a_0$ and defining:

$$\bar{a} = \exp[\mathfrak{R}_a(\theta)]v(\theta), \quad \mathfrak{R}_a(\theta) = \int R_a(\theta)\mathrm{d}\theta$$

the ODE reduces to:

$$v' = \exp[-\mathfrak{R}_a(\theta)]\mathfrak{R}_0(\theta), \quad v(\theta_0) = 0$$

[4] we recall it here in order to be more clear.

Hence the overall solution is given by:

$$a - a_0 = \exp[\mathfrak{R}_a(\theta)] \int_{\theta_0}^{\theta} \exp[-\mathfrak{R}_a(\xi)]\mathfrak{R}_0(\xi)\mathrm{d}\xi \tag{2.3.10}$$

The relevant integral to be performed in Equation 2.3.10 is:

$$\mathfrak{I}_t(\theta) = \int \exp[-\mathfrak{R}_a(\theta)]\mathfrak{R}_0(\theta)\mathrm{d}\theta \tag{2.3.11}$$

Since $\mathfrak{R}_a$ assumes the form Equation 2.1.3:

$$\mathfrak{R}_a(\theta) = \frac{\alpha_0[R_a]}{2}\theta + \mathcal{P}_{2\pi}\left(\begin{array}{c} -\beta_n[R_a]/n \\ \alpha_n[R_a]/n \end{array} \middle| \theta \right)$$

then its exponential can be conveniently decomposed as:

$$\exp[\mathfrak{R}_a(\theta)] = \exp\left[k\theta\right] \Xi_{+\mathfrak{R}_a}(\theta) \quad \text{and} \quad \exp[-\mathfrak{R}_a(\theta)] = \exp\left[-k\theta\right] \Xi_{-\mathfrak{R}_a}(\theta)$$

where the parameter $k \neq 0$ and the periodic functions $\Xi_{+\mathfrak{R}_a}$ and $\Xi_{-\mathfrak{R}_a}$ are defined as:

$$k = \frac{\alpha_0[R_a]}{2}, \quad \Xi_{\pm\mathfrak{R}_a}(\theta) = \exp\left[\pm\mathcal{P}_{2\pi}\left(\begin{array}{c} -\beta_n[R_a]/n \\ \alpha_n[R_a]/n \end{array} \middle| \theta \right)\right]$$

Moreover, recalling Equation 2.3.6 the expression of $\mathfrak{R}_0$ becomes:

$$\mathfrak{R}_0(\theta) = R_0(\theta) + R_e(\theta)\left[\frac{\alpha_0[S_0]}{2}\theta + \Xi_e(\theta)\right] = \mathfrak{R}_{01}(\theta) + \mathfrak{R}_{02}(\theta)\theta$$

with:

$$\mathfrak{R}_{01}(\theta) = R_0(\theta) + R_e(\theta)\Xi_e(\theta), \qquad \mathfrak{R}_{01}(\theta) = \mathfrak{R}_{01}(\theta + 2\pi)$$
$$\mathfrak{R}_{02}(\theta) = \frac{\alpha_0[S_0]}{2}R_e(\theta), \qquad \mathfrak{R}_{02}(\theta) = \mathfrak{R}_{02}(\theta + 2\pi)$$

Then the integrand in Equation 2.3.11 becomes:

$$\exp[-\mathfrak{R}_a(\theta)]\mathfrak{R}_0(\theta) = \hat{\mathfrak{R}}_{01}(\theta)\exp[-k\theta] + \hat{\mathfrak{R}}_{02}(\theta)\exp[-k\theta]\theta$$

where:

$$\hat{\mathfrak{R}}_{01}(\theta) = \Xi_{-\mathfrak{R}_a}(\theta)\mathfrak{R}_{01}(\theta) = \Xi_{-\mathfrak{R}_a}(\theta)[R_0(\theta) + R_e(\theta)\Xi_e(\theta)]$$
$$\hat{\mathfrak{R}}_{02}(\theta) = \Xi_{-\mathfrak{R}_a}(\theta)\mathfrak{R}_{02}(\theta) = \Xi_{-\mathfrak{R}_a}(\theta)\alpha_0[S_0]R_e(\theta)/2$$

It follows that the integral reduces to:

$$\mathfrak{I}_t(\theta) = \int \left\{\hat{\mathfrak{R}}_{01}(\theta) + \hat{\mathfrak{R}}_{02}(\theta)\theta\right\} \exp[-k\theta]\mathrm{d}\theta$$

which solution can be obtained combining the integration properties provided by Equation 2.1.7 and Equation 2.1.8; it follows:

$$\mathfrak{I}_t(\theta) = [\mathfrak{B}_0(\theta) + \mathfrak{B}_1(\theta)\theta]\exp[-k\theta] \tag{2.3.12}$$

with:

$$\mathfrak{B}_0(\theta) = -\left[\frac{\alpha_0[\hat{\mathfrak{R}}_{01}]}{2k} + \frac{\alpha_0[\hat{\mathfrak{R}}_{02}]}{2k^2}\right] + \\ + \mathcal{P}_{2\pi}\left(\begin{array}{c} \dfrac{\alpha_n[\hat{\mathfrak{R}}_{02}](n^2-k^2) - 2kn\beta_n[\hat{\mathfrak{R}}_{02}]}{(k^2+n^2)^2} - \dfrac{k\alpha_n[\hat{\mathfrak{R}}_{01}] + n\beta_n[\hat{\mathfrak{R}}_{01}]}{k^2+n^2} \\ \dfrac{2kn\alpha_n[\hat{\mathfrak{R}}_{02}] + \beta_n[\hat{\mathfrak{R}}_{02}](n^2-k^2)}{(k^2+n^2)^2} + \dfrac{n\alpha_n[\hat{\mathfrak{R}}_{01}] - k\beta_n[\hat{\mathfrak{R}}_{01}]}{k^2+n^2} \end{array}\middle|\, \theta\right)$$
$$\mathfrak{B}_1(\theta) = -\frac{\alpha_0[\hat{\mathfrak{R}}_{02}]}{2k} + \mathcal{P}_{2\pi}\left(\begin{array}{c} -\dfrac{k\alpha_n[\hat{\mathfrak{R}}_{02}] + n\beta_n[\hat{\mathfrak{R}}_{02}]}{k^2+n^2} \\ \dfrac{n\alpha_n[\hat{\mathfrak{R}}_{02}] - k\beta_n[\hat{\mathfrak{R}}_{02}]}{k^2+n^2} \end{array}\middle|\, \theta\right)$$

So finally, plugging Equation 2.3.12 into Equation 2.3.10 we get:

$$\boxed{a - a_0 = \tilde{\mathfrak{B}}_0(\theta) + \tilde{\mathfrak{B}}_1(\theta)\theta + \tilde{\mathfrak{B}}_2(\theta)\exp[k\theta]} \tag{2.3.13}$$

with:

$$\tilde{\mathfrak{B}}_0(\theta) = \Xi_{+\mathfrak{R}_a}(\theta)\mathfrak{B}_0(\theta), \quad \tilde{\mathfrak{B}}_1(\theta) = \Xi_{+\mathfrak{R}_a}(\theta)\mathfrak{B}_1(\theta), \quad \tilde{\mathfrak{B}}_2(\theta) = -\Xi_{+\mathfrak{R}_a}(\theta)\mathfrak{I}_t(\theta_0)$$

2.3.2.1. Time law computation

Plugging Equation 2.3.13 and Equation 2.3.6 into Equation 2.3.1c we get:

$$t - t_0 = \int_{\theta_0}^{\theta} \left\{ \hat{\mathfrak{T}}_0(\xi) + \hat{\mathfrak{T}}_1(\xi)\xi + \hat{\mathfrak{T}}_2(\xi) \exp[k\xi] \right\} \mathrm{d}\xi \tag{2.3.14}$$

with:

$$\begin{aligned}
\hat{\mathfrak{T}}_0(\theta) &= \tilde{\mathfrak{B}}_0(\theta)\tau_a(\theta) + \Xi_e(\theta)\tau_e(\theta) + \tau_0(\theta) \\
\hat{\mathfrak{T}}_1(\theta) &= \tilde{\mathfrak{B}}_1(\theta)\tau_a(\theta) + \frac{1}{2}\alpha_0\left[S_0\right]\tau_e(\theta) \\
\hat{\mathfrak{T}}_2(\theta) &= \tilde{\mathfrak{B}}_2(\theta)\tau_a(\theta)
\end{aligned}$$

Then, by means of the integration properties provided by Equation 2.1.3, Equation 2.1.5 and Equation 2.1.7 we get:

$$\boxed{\begin{aligned} t - t_0 = {} & \hat{A}\theta^2 + \hat{B}(\theta)\theta + \hat{C}(\theta) + \hat{D}(\theta)\exp[k\theta] + \\ & - \left\{ \hat{A}\theta_0^2 + \hat{B}(\theta_0)\theta_0 + \hat{C}(\theta_0) + \hat{D}(\theta_0)\exp[k\theta_0] \right\} \end{aligned}} \tag{2.3.15}$$

with:

$$\hat{A} = \frac{\alpha_0[\hat{\mathfrak{T}}_1]}{4}, \quad \hat{B}(\theta) = \frac{\alpha_0[\hat{\mathfrak{T}}_0]}{2} + \mathcal{P}_{2\pi}\left(\begin{array}{c} -\beta_n[\hat{\mathfrak{T}}_1]/n \\ \alpha_n[\hat{\mathfrak{T}}_1]/n \end{array} \middle| \theta \right)$$

$$\hat{C}(\theta) = \mathcal{P}_{2\pi}\left(\begin{array}{c} -\beta_n[\hat{\mathfrak{T}}_0]/n + \alpha_n[\hat{\mathfrak{T}}_1]/n^2 \\ \alpha_n[\hat{\mathfrak{T}}_0]/n + \beta_n[\hat{\mathfrak{T}}_1]/n^2 \end{array} \middle| \theta \right)$$

$$\hat{D}(\theta) = \frac{\alpha_0[\hat{\mathfrak{T}}_2]}{2k} + \mathcal{P}_{2\pi}\left(\begin{array}{c} (k\alpha_n[\hat{\mathfrak{T}}_2] - n\beta_n[\hat{\mathfrak{T}}_2])/(k^2+n^2) \\ (n\alpha_n[\hat{\mathfrak{T}}_2] + k\beta_n[\hat{\mathfrak{T}}_2])/(k^2+n^2) \end{array} \middle| \theta \right)$$

2.3.3. Orientation problem

Once the shape problem is solved and so $\{a, e, \theta\}$ are computed, we can proceed to evaluate the remaining three Keplerian elements Ω, ω and i. The procedure is similar to what we have already seen in previous sections; nevertheless we will recall the main steps for the solutions.

Starting from Equation 2.3.1d, the ODE for the inclination can be rewritten as:

$$i' = A_{i'}(\theta) + \frac{1}{2}B_{i'}(\theta)\theta \tag{2.3.16}$$

with:

$$A_{i'}(\theta) = \mathfrak{I}_0(\theta) + \mathfrak{I}_a(\theta)\Xi_a(\theta) + \mathfrak{I}_e(\theta)\Xi_e(\theta)$$
$$B_{i'}(\theta) = \alpha_0[R_0]\mathfrak{I}_a(\theta) + \alpha_0[S_0]\mathfrak{I}_e(\theta)$$

Integrating Equation 2.3.16 in the same way of Equation 2.3.7 we get:

$$\boxed{i(\theta) - i_0 = A_i\theta^2 + B_i(\theta)\theta + C_i(\theta) - k_i, \quad k_i = A_i\theta_0^2 + B_i(\theta_0)\theta_0 + C_i(\theta_0)} \tag{2.3.17}$$

Plugging Equation 2.3.17 into Equation 2.3.1f we obtain the form:

$$\omega' = A_{\omega'}(\theta)\theta^2 + B_{\omega'}(\theta)\theta + C_{\omega'}(\theta) + \mathcal{O}_\omega(\theta)(\omega - \omega_0) \tag{2.3.18}$$

with:

$$A_{\omega'}(\theta) = A_i\mathcal{O}_i(\theta)$$
$$B_{\omega'}(\theta) = \frac{1}{2}\alpha_0\left[R_0\right]\mathcal{O}_a(\theta) + B_i(\theta)\mathcal{O}_i(\theta) + \frac{1}{2}\alpha_0\left[S_0\right]\mathcal{O}_e(\theta)$$
$$C_{\omega'}(\theta) = \Xi_a(\theta)\mathcal{O}_a(\theta) + [C_i(\theta) - k_i]\mathcal{O}_i(\theta) + \Xi_e(\theta)\mathcal{O}_e(\theta) + \mathcal{O}_0(\theta)$$

Proceeding similarly to what done in Section 2.3.2 we set $\bar{\omega} = \omega - \omega_0$ and we perform the following change of variable:

$$\bar{\omega} = \exp[Y(\theta)]v(\theta)$$

where:

$$Y(\theta) = \int \mathcal{O}_\omega(\theta)\mathrm{d}\theta = k\theta + \mathcal{P}_{2\pi}\left(\begin{array}{c|c} -\beta_n[\mathcal{O}_\omega]/n & \\ \alpha_n[\mathcal{O}_\omega]/n & \theta \end{array}\right) \quad \text{with} \quad k = \frac{\alpha_0[\mathcal{O}_\omega]}{2}$$

after performing the substitutions, leading Equation 2.3.18 to the quadratures, we obtain:

$$\omega - \omega_0 = \exp[Y(\theta)]\int_{\theta_0}^{\theta}\left\{A_{\omega'}(\xi)\xi^2 + B_{\omega'}(\xi)\xi + C_{\omega'}(\xi)\right\}\exp[-Y(\xi)]\mathrm{d}\xi \tag{2.3.19}$$

The exponentials appearing into Equation 2.3.19 can be conveniently rewritten as:

$$\exp[Y(\theta)] = \exp[k\theta]\exp[\Xi_{+Y}(\theta)] \quad \text{and} \quad \exp[-Y(\theta)] = \exp[-k\theta]\exp[\Xi_{-Y}(\theta)]$$

where:

$$\Xi_{\pm Y}(\theta) = \exp\left[\pm\mathcal{P}_{2\pi}\left(\begin{array}{c|c} -\beta_n[\mathcal{O}_\omega]/n & \\ \alpha_n[\mathcal{O}_\omega]/n & \theta \end{array}\right)\right]$$

Then the relevant integral inside Equation 2.3.19 becomes:

$$J(\theta) = \int \left\{ \bar{Y}_2(\theta)\theta^2 + \bar{Y}_1(\theta)\theta + \bar{Y}_0(\theta) \right\} \exp[-k\theta] \mathrm{d}\theta \tag{2.3.20}$$

with:

$$\bar{Y}_2(\theta) = \Xi_{-Y}(\theta) A_{\omega'}(\theta), \quad \bar{Y}_1(\theta) = \Xi_{-Y}(\theta) B_{\omega'}(\theta), \quad \bar{Y}_0 = \Xi_{-Y}(\theta) C_{\omega'}(\theta)$$

The integral in Equation 2.3.20 can be solved by means of the integration properties provided by Equation 2.1.7, Equation 2.1.8 and Equation 2.1.9; we get:

$$J(\theta) = \left\{ \hat{Y}_0(\theta) + \hat{Y}_1(\theta)\theta + \hat{Y}_2(\theta)\theta^2 \right\} \exp[-k\theta] \tag{2.3.21}$$

where:

$$\begin{aligned}
\hat{Y}_0(\theta) = &- \left[\frac{\alpha_0[\bar{Y}_0]}{2k} + \frac{\alpha_0[\bar{Y}_1]}{2k^2} + \frac{\alpha_0[\bar{Y}_2]}{k^3} \right] + \\
&+ \mathcal{P}_{2\pi} \left(\begin{array}{c} \dfrac{\alpha_n[\bar{Y}_1](n^2-k^2) - 2kn\beta_n[\bar{Y}_1]}{(k^2+n^2)^2} - \dfrac{k\alpha_n[\bar{Y}_0] + n\beta_n[\bar{Y}_0]}{k^2+n^2} \\ \dfrac{2kn\alpha_n[\bar{Y}_1] + \beta_n[\bar{\Re}_1](n^2-k^2)}{(k^2+n^2)^2} + \dfrac{n\alpha_n[\bar{Y}_0] - k\beta_n[\bar{Y}_0]}{k^2+n^2} \end{array} \middle| \theta \right) + \\
&+ \mathcal{P}_{2\pi} \left(\begin{array}{c} 2\dfrac{n\left(n^2-3k^2\right)\beta_n[\bar{Y}_2] - \left(k^3-3kn^2\right)\alpha_n[\bar{Y}_2]}{\left(k^2+n^2\right)^3} \\ -2\dfrac{\left(n^3-3k^2n\right)\alpha_n[\bar{Y}_2] + k\left(k^2-3n^2\right)\beta_n[\bar{Y}_2]}{\left(k^2+n^2\right)^3} \end{array} \middle| \theta \right) \\
\hat{Y}_1(\theta) = &- \left[\frac{\alpha_0[\bar{Y}_1]}{2k} + \frac{\alpha_0[\bar{Y}_2]}{k^2} \right] + \\
&+ \mathcal{P}_{2\pi} \left(\begin{array}{c} -\dfrac{k\alpha_n[\bar{Y}_1] + n\beta_n[\bar{Y}_1]}{k^2+n^2} + 2\dfrac{\left(n^2-k^2\right)\alpha_n[\bar{Y}_2] - 2kn\beta_n[\bar{Y}_2]}{\left(k^2+n^2\right)^2} \\ \dfrac{n\alpha_n[\bar{Y}_1] - k\beta_n[\bar{Y}_1]}{k^2+n^2} + 2\dfrac{\left(n^2-k^2\right)\beta_n[\bar{Y}_2] + 2kn\alpha_n[\bar{Y}_2]}{\left(k^2+n^2\right)^2} \end{array} \middle| \theta \right) \\
\hat{Y}_2(\theta) = &- \frac{\alpha_0[\bar{Y}_2]}{2k} + \mathcal{P}_{2\pi} \left(\begin{array}{c} -\dfrac{k\alpha_n[\bar{Y}_2] + n\beta_n[\bar{Y}_2]}{k^2+n^2} \\ \dfrac{n\alpha_n[\bar{Y}_2] - k\beta_n[\bar{Y}_2]}{k^2+n^2} \end{array} \middle| \theta \right)
\end{aligned}$$

So finally plugging Equation 2.3.21 into Equation 2.3.19 we get:

$$\boxed{\omega(\theta) - \omega_0 = A_\omega(\theta)\theta^2 + B_\omega(\theta)\theta + C_\omega(\theta) + D_\omega(\theta)\exp[k\theta]} \tag{2.3.22}$$

where:

$$A_\omega(\theta) = \Xi_{+Y}(\theta)\hat{Y}_2(\theta), \quad B_\omega(\theta) = \Xi_{+Y}(\theta)\hat{Y}_1(\theta),$$
$$C_\omega(\theta) = \Xi_{+Y}(\theta)\hat{Y}_0(\theta), \quad D_\omega(\theta) = -J(\theta_0)\Xi_{+Y}(\theta)$$

Finally plugging Equation 2.3.22 into Equation 2.3.1e we get:

$$\Omega' = A_{\Omega'}(\theta)\theta^2 + B_{\Omega'}(\theta)\theta + C_{\Omega'}(\theta) + D_{\Omega'}(\theta)\exp[k\theta] \tag{2.3.23}$$

with:

$$A_{\Omega'}(\theta) = A_i\mathfrak{O}_i(\theta) + A_\omega(\theta)\mathfrak{O}_\omega(\theta)$$
$$B_{\Omega'}(\theta) = \frac{1}{2}\alpha_0\left[R_0\right]\mathfrak{O}_a(\theta) + B_i(\theta)\mathfrak{O}_i(\theta) + B_\omega(\theta)\mathfrak{O}_\omega(\theta) + \frac{1}{2}\alpha_0\left[S_0\right]\mathfrak{O}_e(\theta)$$
$$C_{\Omega'}(\theta) = \Xi_a(\theta)\mathfrak{O}_a(\theta) + \mathfrak{O}_i(\theta)\left(C_i(\theta) - k_i\right) + C_\omega(\theta)\mathfrak{O}_\omega(\theta) + \Xi_e(\theta)\mathfrak{O}_e(\theta) + \mathfrak{O}_0(\theta)$$
$$D_{\Omega'}(\theta) = D_\omega(\theta)\mathfrak{O}_\omega(\theta)$$

Integrating Equation 2.3.23 by means of the integrations properties provided by Equation 2.1.3, Equation 2.1.5, Equation 2.1.6 and Equation 2.1.7 we have:

$$\boxed{\Omega(\theta) - \Omega_0 = A_\Omega\theta^3 + B_\Omega(\theta)\theta^2 + C_\Omega(\theta)\theta + D_\Omega(\theta) + E_\Omega(\theta)\exp[k\theta] - k_\Omega} \tag{2.3.24}$$

with:

$$A_\Omega = \frac{1}{6}\alpha_0\left[A_{\Omega'}\right]$$
$$B_\Omega(\theta) = \frac{1}{4}\alpha_0\left[B_{\Omega'}\right] + \mathcal{P}_{2\pi}\left(\begin{array}{c|c} -\dfrac{\beta_n\left[A_{\Omega'}\right]}{n} & \\ \dfrac{\alpha_n\left[A_{\Omega'}\right]}{n} & \theta \end{array}\right)$$
$$C_\Omega(\theta) = \frac{1}{2}\alpha_0\left[C_{\Omega'}\right] + \mathcal{P}_{2\pi}\left(\begin{array}{c|c} \dfrac{2\alpha_n\left[A_{\Omega'}\right] - n\beta_n\left[B_{\Omega'}\right]}{n^2} & \\ \dfrac{2\beta_n\left[A_{\Omega'}\right] + n\alpha_n\left[B_{\Omega'}\right]}{n^2} & \theta \end{array}\right)$$
$$D_\Omega(\theta) = \mathcal{P}_{2\pi}\left(\begin{array}{c|c} \dfrac{2\beta_n\left[A_{\Omega'}\right] + n\left(\alpha_n\left[B_{\Omega'}\right] - n\beta_n\left[C_{\Omega'}\right]\right)}{n^3} & \\ \dfrac{n\left(\beta_n\left[B_{\Omega'}\right] + n\alpha_n\left[C_{\Omega'}\right]\right) - 2\alpha_n\left[A_{\Omega'}\right]}{n^3} & \theta \end{array}\right)$$
$$E_\Omega(\theta) = \frac{\alpha_0\left[D_{\Omega'}\right]}{2k} + \mathcal{P}_{2\pi}\left(\begin{array}{c|c} \dfrac{k\alpha_n\left[D_{\Omega'}\right] - n\beta_n\left[D_{\Omega'}\right]}{k^2+n^2} & \\ \dfrac{k\beta_n\left[D_{\Omega'}\right] + n\alpha_n\left[D_{\Omega'}\right]}{k^2+n^2} & \theta \end{array}\right)$$
$$k_\Omega = A_\Omega\theta_0^3 + B_\Omega(\theta_0)\theta_0^2 + C_\Omega(\theta_0)\theta_0 + D_\Omega(\theta_0) + E_\Omega(\theta_0)\exp[k\theta_0]$$

In Table 2.1 a summary of all the results obtained for the full model approximation is

presented.

Table 2.1: Summary of the main results obtained for the *full model*

Quantity	**Equation number**
a, Semimajor axis (zero order approx.)	Equation 2.3.5
a, Semimajor axis (first order approx.)	Equation 2.3.13
e, Eccentricity (zero order approx.)	Equation 2.3.6
$t(\theta)$, Time law (1st order approx.) with zero order approx. for a	Equation 2.3.8
$t(\theta)$, Time law (2nd order approx.) with zero order approx. for a	Equation 2.3.9
$t(\theta)$, Time law (1st order approx.) with 1st order approx. for a	Equation 2.3.15
i, Inclination (1st order approx.) with zero order approx. for a	Equation 2.3.17
ω, arg. perigee (1st order approx.) with zero order approx. for a	Equation 2.3.22
Ω, RAAN (1st order approx.) with zero order approx. for a	Equation 2.3.24

2.4. Small thrust parameters approximation - *small thrust model*

Up to now we did consider general thrust parameters so that all the functions shown are complicated expressions of them and they operate in non linear way inside the functions. However, notice that we are talking about a low thrust problem and, in addition, a first order linearization has been performed: some information therefore has been lost. As a consequence, we can reasonably simplify the aforementioned functions by a Maclaurin expansion with respect to the thrust parameter.

For $a_t \to 0$, $a_n \to 0$ and $a_h \to 0$, performing a MacLaurin expansion truncated at first order we pass from the form Equation 2.2.4 to:

$$\begin{aligned}
a' &= R_{a_t}(a,e,\theta)a_t \\
e' &= S_{a_t}(a,e,\theta)a_t + S_{a_n}(a,e,\theta)a_n \\
t' &= \tau_0(a,e,\theta) + \tau_{a_t}(a,e,\theta)a_t + \tau_{a_n}(a,e,\theta)a_n \\
i' &= \mathfrak{I}_{a_h}(a,e,\omega,\theta)a_h \\
\omega' &= \mathcal{O}_{a_t}(a,e,i,\omega,\theta)a_t + \mathcal{O}_{a_n}(a,e,i,\omega,\theta)a_n + \mathcal{O}_{a_h}(a,e,i,\omega,\theta)a_h \\
\Omega' &= \mathfrak{O}_{a_h}(a,e,i,\omega,\theta)a_h
\end{aligned} \tag{2.4.1}$$

performing the derivatives as in Equation 2.4.1 we obtain:

$$
\begin{aligned}
a' &= -\frac{2a^3\left(e^2-1\right)\mathcal{R}(e,\theta)}{\mu\mathcal{S}(e,\theta)}a_t \\
e' &= \frac{2a^2\left(e^2-1\right)^2\left(e+\cos(\theta)\right)}{\mu\mathcal{S}(e,\theta)\mathcal{R}(e,\theta)}a_t + \frac{a^2\left(e^2-1\right)^3\sin(\theta)}{\mu\mathcal{S}^{3/2}(e,\theta)\mathcal{R}(e,\theta)}a_n \\
t' &= \frac{a^{3/2}\left(1-e^2\right)^{3/2}}{\sqrt{\mu}\mathcal{S}(e,\theta)} + \frac{2a^{7/2}\left(1-e^2\right)^{7/2}\sin(\theta)}{e\mu^{3/2}\mathcal{S}^2(e,\theta)\mathcal{R}(e,\theta)}a_t + \frac{a^{7/2}\left(1-e^2\right)^{7/2}\mathcal{Q}(e,\theta)}{e\mu^{3/2}\mathcal{S}^{5/2}(e,\theta)\mathcal{R}(e,\theta)}a_n \\
i' &= \frac{a^2\left(e^2-1\right)^2\cos(\theta+\omega)}{\mu\mathcal{S}^{3/2}(e,\theta)}a_h \\
\omega' &= \frac{2a^2\left(e^2-1\right)^2\sin(\theta)}{e\mu\mathcal{S}(e,\theta)\mathcal{R}(e,\theta)}a_t + \frac{a^2\left(e^2-1\right)^2\mathcal{Q}(e,\theta)}{e\mu\mathcal{S}^{3/2}(e,\theta)\mathcal{R}(e,\theta)}a_n - \frac{a^2\left(e^2-1\right)^2\cot(i)\sin(\theta+\omega)}{\mu\mathcal{S}^{3/2}(e,\theta)}a_h \\
\Omega' &= \frac{a^2\left(e^2-1\right)^2\csc(i)\sin(\theta+\omega)}{\mu\mathcal{S}^{3/2}(e,\theta)}a_h
\end{aligned}
$$

with:

$$
\mathcal{Q}(e,\theta) = \left(e^2+1\right)\cos(\theta)+2e, \quad \mathcal{R}(e,\theta) = \sqrt{1+e^2+2e\cos(\theta)}, \quad \mathcal{S}(e,\theta) = (e\cos(\theta)+1)^2 \tag{2.4.2}
$$

Then, following the notation Equation 2.3.2 and linearizing the equations near to the reference condition $\boldsymbol{x}_0 = \{a_0, e_0, i_0, \omega_0\}$, we get:

$$
a' = \{\bar{R}_{a_t,0}(\theta) + \bar{R}_{a_t,a}(\theta)(a-a_0) + \bar{R}_{a_t,e}(e-e_0)\}\tilde{a}_t \tag{2.4.3}
$$

$$
e' = \bar{S}_{a_t,0}(\theta)\tilde{a}_t + \bar{S}_{a_n,0}(\theta)\tilde{a}_n \tag{2.4.4}
$$

$$
i' = \{\bar{\mathfrak{I}}_{a_h,0}(\theta) + \bar{\mathfrak{I}}_{a_h,a}(\theta)(a-a_0) + \bar{\mathfrak{I}}_{a_h,e}(\theta)(e-e_0)\}\tilde{a}_h \tag{2.4.5}
$$

$$
\begin{aligned}
t' = {} & \{\bar{\tau}_{a_t,0}(\theta) + \bar{\tau}_{a_t,a}(\theta)(a-a_0) + \bar{\tau}_{a_t,e}(\theta)(e-e_0)\}\tilde{a}_t + \\
& + \{\bar{\tau}_{a_n,0}(\theta) + \bar{\tau}_{a_n,a}(\theta)(a-a_0) + \bar{\tau}_{a_n,e}(\theta)(e-e_0)\}\tilde{a}_n + \\
& + \tau_{0,0}(\theta) + \tau_{0,a}(\theta)(a-a_0) + \tau_{0,e}(\theta)(e-e_0)
\end{aligned} \tag{2.4.6}
$$

$$
\begin{aligned}
\omega' = {} & \{\bar{\mathcal{O}}_{a_t,0}(\theta) + \bar{\mathcal{O}}_{a_t,a}(\theta)(a-a_0) + \bar{\mathcal{O}}_{a_t,e}(\theta)(e-e_0)\}\tilde{a}_t + \\
& + \{\bar{\mathcal{O}}_{a_n,0}(\theta) + \bar{\mathcal{O}}_{a_n,a}(\theta)(a-a_0) + \bar{\mathcal{O}}_{a_n,e}(\theta)(e-e_0)\}\tilde{a}_n + \\
& + \{\bar{\mathcal{O}}_{a_h,0}(\theta) + \bar{\mathcal{O}}_{a_h,a}(\theta)(a-a_0) + \bar{\mathcal{O}}_{a_h,e}(\theta)(e-e_0) + \\
& + \bar{\mathcal{O}}_{a_h,i}(\theta)(i-i_0) + \bar{\mathcal{O}}_{a_h,\omega}(\theta)(\omega-\omega_0)\}\tilde{a}_h
\end{aligned} \tag{2.4.7}
$$

$$
\begin{aligned}
\Omega' = {} & \{\bar{\mathfrak{O}}_{a_h,0}(\theta) + \bar{\mathfrak{O}}_{a_h,a}(\theta)(a-a_0) + \bar{\mathfrak{O}}_{a_h,e}(\theta)(e-e_0) + \\
& + \bar{\mathfrak{O}}_{a_h,i}(\theta)(i-i_0) + \bar{\mathfrak{O}}_{a_h,\omega}(\theta)(\omega-\omega_0)\}\tilde{a}_h
\end{aligned} \tag{2.4.8}
$$

where we defined the adimentional thrust parameters:

$$\tilde{a}_t = \frac{a_0^2}{\mu} a_t, \quad \tilde{a}_n = \frac{a_0^2}{\mu} a_n, \quad \tilde{a}_h = \frac{a_0^2}{\mu} a_h \tag{2.4.9}$$

and if $x(\theta)$ is the generic function then:

$$\bar{x}(\theta) = \frac{\mu}{a_0^2} x(\theta)$$

2.4.1. Semimajor axis solution

The ODE for the semimajor axis is given by Equation 2.4.3. Now, for analogous reasons of those seen in Remark 2.3.1 and Remark 2.3.2 not reported here to avoid redundancies, assuming that the variation of the semi-major axis is not so much affected by the variation of the eccentricity we get:

$$a' = 2(1-e_0^2) g(\theta) [a_0 + 3(a-a_0)] \tilde{a}_t, \quad g(\theta) = \frac{\mathcal{R}(e_0, \theta)}{\mathcal{S}(e_0, \theta)} \tag{2.4.10}$$

Let now be:

$$\mathfrak{R}_a^*(\theta) = \tilde{a}_t \cdot 6(1-e_0^2) \int g(\theta) \mathrm{d}\theta$$

$$\mathfrak{R}_0^*(\theta) = \tilde{a}_t \cdot 2(1-e_0^2) a_0 g(\theta) = \frac{a_0}{3} \cdot \frac{\mathrm{d}[\mathfrak{R}_a^*(\theta)]}{\mathrm{d}\theta}$$

Then:

$$a - a_0 = \exp[\mathfrak{R}_a^*(\theta)] \int_{\theta_0}^{\theta} \exp[-\mathfrak{R}_a^*(\xi)] \mathfrak{R}_0^*(\xi) \mathrm{d}\xi = -\frac{a_0}{3} \left(1 - \exp[\mathfrak{R}_a^*(\theta) - \mathfrak{R}_a^*(\theta_0)]\right)$$

with:

$$\mathfrak{R}_a^*(\theta) = \tilde{a}_t \cdot 6(1-e_0^2) \left[\frac{\alpha_0[g]}{2} \theta + \mathcal{P}_{2\pi} \left(\begin{array}{c} 0 \\ \alpha_n[g]/n \end{array} \middle| \theta \right) \right]$$

Then we have:

$$\exp[\mathfrak{R}_a^*(\theta)] = \exp[k_a \theta] \Xi_{+\mathfrak{R}_a^*}(\theta)$$

with:

$$k_a = \tilde{a}_t \cdot 3(1-e_0^2)\alpha_0[g], \quad \Xi_{+\mathfrak{R}_a^*}(\theta) = \exp\left[\tilde{a}_t \cdot 6(1-e_0^2) \mathcal{P}_{2\pi} \left(\begin{array}{c} 0 \\ \alpha_n[g]/n \end{array} \middle| \theta \right) \right] \tag{2.4.11}$$

Finally we can observe that, since the argument of the exponential inside $\Xi_{+\mathfrak{R}_a^*}$ is bounded we can approximate it for small $\tilde{a}_t$:

$$\Xi_{+\mathfrak{R}_a^*}(\theta) \approx 1 + \tilde{a}_t \cdot 6(1-e_0^2)\mathcal{P}_{2\pi}\left(\begin{array}{c} 0 \\ \alpha_n[g]/n \end{array} \middle| \theta \right) = 1 + \tilde{a}_t Q_a(\theta)$$

Then we can rewrite the variation of the semi-major axis with respect to the reference condition in matrix form as:

$$\begin{aligned} a - a_0 &= k_0[1 - \exp(k_a\theta + k_1) - \tilde{a}_t Q_a(\theta)\exp(k_a\theta + k_1)] = \\ &= k_0[1 - \exp(k_a\theta + k_1), -Q_a(\theta)\exp(k_a\theta + k_1)] \begin{bmatrix} 1 \\ \tilde{a}_t \end{bmatrix} \end{aligned} \tag{2.4.12}$$

with:

$$k_0 = -\frac{a_0}{3}, \quad k_1 = -\mathfrak{R}_a(\theta_0), \quad Q_a(\theta) = 6(1-e_0^2)\mathcal{P}_{2\pi}\left(\begin{array}{c} 0 \\ \alpha_n[g]/n \end{array} \middle| \theta \right)$$

2.4.1.1. Fourier series coefficients

With reference to Appendix B, Equation B.0.17, it can be proved that :

$$g(\theta) = \frac{1}{2}\pi^{1/2}(1+e_0^2)^{1/2}\sum_{m=0}^{+\infty} q_m(e_0)\cos^m(\theta)$$

where the coefficients q_m are given by:

$$q_m(e_0) = \frac{(2e_0)^m\,(e_0^2+1)^{\,-m}}{\Gamma\,(3/2-m)\,\Gamma(m+1)}\,{}_2F_1\left(\begin{array}{cc} 2 & -m \\ 3/2-m & \end{array} \middle| \frac{1+e_0^2}{2} \right)$$

where Γ is the complete Gamma Function and ${}_2F_1$ is the Gauss Hypergeometric function (see Appendix A for a short general presentation or Slater [38] for mare details).

It follows that the relevant integral to be performed is:

$$\frac{1}{\pi}\int_{-\pi}^{\pi} \cos^m(\theta)\cos(n\theta)\mathrm{d}\theta = p_m(n)$$

with:

$$p_m(n) = -\frac{\pi(-2)^m(n+m-1)\Gamma(m+1)}{\Gamma\left((-n-m+3)/2\right)\Gamma\left((n-m+1)/2\right)\Gamma(-n+m+1)\Gamma(n+m+1)} \tag{2.4.13}$$

So finally the expression of the coefficients is:

$$\boxed{\begin{aligned}\alpha_0[g] &= \frac{2}{\pi}\left[\frac{1}{1+e_0}\mathbf{E}(\kappa) + \frac{1}{1-e_0}\mathbf{K}(\kappa)\right] \\ \alpha_n[g] &= \frac{1}{2}\pi^{1/2}(1+e_0^2)^{1/2}\sum_{m=0}^{+\infty} q_m(e_0)p_m(n) \\ \beta_n[g] &= 0\end{aligned}} \tag{2.4.14}$$

Where $\mathbf{K}(\kappa)$ and $\mathbf{E}(\kappa)$ are the complete elliptic integrals of first and second kind respectively with elliptic modulus:

$$\kappa = -\frac{4e_0}{(e_0-1)^2} \tag{2.4.15}$$

2.4.2. Eccentricity solution

Starting from Equation 2.4.4 the θ-derivative of the eccentricity becomes:

$$e' = \bar{S}_{a_t,0}(\theta)\tilde{a}_t + \bar{S}_{a_n,0}(\theta)\tilde{a}_n = 2(1-e_0^2)^2\bar{\bar{S}}_{a_t,0}(\theta)\tilde{a}_t + (e_0^2-1)^3\bar{\bar{S}}_{a_n,0}(\theta)\tilde{a}_n$$

where:

$$\begin{aligned}\bar{\bar{S}}_{a_t,0}(\theta) &= \frac{S_{a_t,0}(\theta)}{2(1-e_0^2)^2} = \frac{e_0+\cos(\theta)}{\mathcal{S}(e_0,\theta)\mathcal{R}(e_0,\theta)} \\ \bar{\bar{S}}_{a_n,0}(\theta) &= \frac{S_{a_n,0}(\theta)}{(e_0^2-1)^3} = \frac{\sin(\theta)}{\mathcal{S}^{3/2}(e_0,\theta)\mathcal{R}(e_0,\theta)}\end{aligned}$$

So that the solution can be expressed as:

$$\begin{aligned}e - e_0 = 2\tilde{a}_t(1-e_0^2)^2\left[\frac{\alpha_0[\bar{\bar{S}}_{a_t,0}]}{2}\theta + \mathcal{P}_{2\pi}\left(\begin{array}{c}0\\ \alpha_n[\bar{\bar{S}}_{a_t,0}]/n\end{array}\middle|\,\xi\right)\right]_{\theta_0}^{\theta} + \\ + \tilde{a}_n(e_0^2-1)^3\left[\mathcal{P}_{2\pi}\left(\begin{array}{c}-\beta_n[\bar{\bar{S}}_{a_n,0}]/n\\ 0\end{array}\middle|\,\xi\right)\right]_{\theta_0}^{\theta}\end{aligned}$$

which can be rewritten in matrix form as:

$$e - e_0 = \tilde{a}_t[k_e\theta + Q_{1e}(\theta)] + \tilde{a}_n Q_{2e}(\theta) = [k_e\theta + Q_{1e}(\theta), Q_{2e}(\theta)] \begin{bmatrix} \tilde{a}_t \\ \tilde{a}_n \end{bmatrix} \tag{2.4.16}$$

with:

$$\begin{aligned} k_e &= \alpha_0[\bar{\bar{S}}_{a_t,0}](1-e_0^2)^2 \\ Q_{1e}(\theta) &= -k_e\theta_0 + 2(1-e_0^2)^2 \left[\mathcal{P}_{2\pi}\left(\begin{array}{c|c} 0 & \\ \alpha_n[\bar{\bar{S}}_{a_t,0}]/n & \xi \end{array}\right)\right]_{\theta_0}^{\theta} \\ Q_{2e}(\theta) &= (e_0^2-1)^3 \left[\mathcal{P}_{2\pi}\left(\begin{array}{c|c} -\beta_n[\bar{\bar{S}}_{a_n,0}]/n & \\ 0 & \xi \end{array}\right)\right]_{\theta_0}^{\theta} \end{aligned}$$

2.4.2.1. Fourier series coefficients

It can be proved that:

$$\begin{aligned} \bar{\bar{S}}_{a_t,0}(\theta) &= \frac{1}{e_0}\sqrt{\frac{\pi}{1+e_0^2}} \sum_{m=0}^{+\infty} u_m(e_0)\cos^m(\theta) \\ \bar{\bar{S}}_{a_n,0}(\theta) &= \frac{1}{2(e_0^2-1)}\sqrt{\frac{\pi}{1+e_0^2}} \cdot \sin(\theta) \sum_{m=0}^{+\infty} v_m(e_0)\cos^m(\theta) \end{aligned}$$

with:

$$\begin{aligned} u_m(e_0) &= \frac{(2e)^m}{\Gamma(m+1)(1+e_0^2)^m} \cdot \left[\mathfrak{u}_m(e_0) - (1-e_0^2)\mathfrak{v}_m(e_0)\right] \\ v_m(e_0) &= \frac{(2e)^m}{\Gamma(m+1)(1+e_0^2)^m} \cdot \left[(3+2m)\mathfrak{u}_m(e_0) + (e_0^2(m+2) - m - 5)\mathfrak{v}_m(e_0)\right] \end{aligned}$$

and:

$$\begin{aligned} \mathfrak{u}_m(e_0) &= \frac{1}{\Gamma(1/2-m)}\, {}_2F_1\left(\begin{array}{cc|c} 1 & -m & \\ 1/2-m & & \frac{1+e_0^2}{2} \end{array}\right) \\ \mathfrak{v}_m(e_0) &= \frac{1}{\Gamma(1/2-m)}\, {}_2F_1\left(\begin{array}{cc|c} 2 & -m & \\ 1/2-m & & \frac{1+e_0^2}{2} \end{array}\right) \end{aligned}$$

Then:

$$\begin{aligned}
\alpha_0[\bar{\bar{S}}_{a_t,0}] &= \frac{2}{\pi e_0}\left[\frac{\mathbf{E}(\kappa)}{1+e_0}+\frac{\mathbf{K}(\kappa)}{1-e_0}-\frac{2}{(1-e_0)^2}\mathbf{\Pi}\left(\zeta|\kappa\right)\right]\\
\alpha_n[\bar{\bar{S}}_{a_t,0}] &= \frac{1}{e_0}\sqrt{\frac{\pi}{1+e_0^2}}\sum_{m=0}^{+\infty}u_m(e_0)p_m(n)\\
\beta_n[\bar{\bar{S}}_{a_t,0}] &= \alpha_0[\bar{\bar{S}}_{a_n,0}] = \alpha_n[\bar{\bar{S}}_{a_n,0}] = 0\\
\beta_n[\bar{\bar{S}}_{a_n,0}] &= \frac{n}{2(e_0^2-1)}\sqrt{\frac{\pi}{1+e_0^2}}\sum_{m=0}^{+\infty}\frac{v_m(e_0)p_{m+1}(n)}{m+1}
\end{aligned} \tag{2.4.17}$$

where p_m is defined in Equation 2.4.13, κ comes from Equation 2.4.15, $\mathbf{\Pi}(\zeta|\kappa)$ is the complete elliptic integral of third kind with elliptic modulus:

$$\zeta = \frac{2e_0}{e_0-1} \tag{2.4.18}$$

2.4.3. Time law solution

Rewriting Equation 2.4.6 in matrix form notation and substituting into that the expressions of $a-a_0$ and $e-e_0$ given by Equation 2.4.12 and Equation 2.4.16 respectively we get:

$$\begin{aligned}
t' = {} & [1,\tilde{a}_t,\tilde{a}_n]\begin{bmatrix}\tau_{00}(\theta)\\ \bar{\tau}_{0,a_t}(\theta)\\ \bar{\tau}_{0,a_n}(\theta)\end{bmatrix}+\\
& + k_0[1,\tilde{a}_t,\tilde{a}_n]\begin{bmatrix}\left(-\exp[k_a\theta+k_1]+1\right)\tau_{a,0}(\theta) & -Q_a(\theta)\tau_{a,0}(\theta)\exp[k_a\theta+k_1]\\ \left(-\exp[k_a\theta+k_1]+1\right)\bar{\tau}_{a,a_t}(\theta) & -Q_a(\theta)\bar{\tau}_{a,a_t}(\theta)\exp[k_a\theta+k_1]\\ \left(-\exp[k_a\theta+k_1]+1\right)\bar{\tau}_{a,a_n}(\theta) & -Q_a(\theta)\bar{\tau}_{a,a_n}(\theta)\exp[k_a\theta+k_1]\end{bmatrix}\begin{bmatrix}1\\ \tilde{a}_t\end{bmatrix}+\\
& + [1,\tilde{a}_t,\tilde{a}_n]\begin{bmatrix}\left(\theta k_e+Q_{1e}(\theta)\right)\tau_{e,0}(\theta) & Q_{2e}(\theta)\tau_{e,0}(\theta)\\ \left(\theta k_e+Q_{1e}(\theta)\right)\bar{\tau}_{e,a_t}(\theta) & Q_{2e}(\theta)\bar{\tau}_{e,a_t}(\theta)\\ \left(\theta k_e+Q_{1e}(\theta)\right)\bar{\tau}_{e,a_n}(\theta) & Q_{2e}(\theta)\bar{\tau}_{e,a_n}(\theta)\end{bmatrix}\begin{bmatrix}\tilde{a}_t\\ \tilde{a}_n\end{bmatrix}
\end{aligned}$$

Now neglecting all terms higher than first order we get:

$$t' = [1,\tilde{a}_t,\tilde{a}_n]\begin{bmatrix}\mathfrak{T}_1(\theta)+\mathfrak{T}_2(\theta)\exp[k_a\theta+k_1]\\ \mathfrak{T}_3(\theta)+\mathfrak{T}_4(\theta)\theta+\mathfrak{T}_5(\theta)\exp[k_a\theta+k_1]\\ \mathfrak{T}_6(\theta)+\mathfrak{T}_7(\theta)\exp[k_a\theta+k_1]\end{bmatrix}$$

with:

$$
\begin{aligned}
\mathfrak{T}_1(\theta) &= \tau_{00}(\theta) + k_0\tau_{a,0}(\theta) = \tau_{00}(\theta)/2 \\
\mathfrak{T}_2(\theta) &= -k_0\tau_{a,0}(\theta) = \tau_{00}(\theta)/2 \\
\mathfrak{T}_3(\theta) &= \bar{\tau}_{0,a_t}(\theta) + k_0\bar{\tau}_{a,a_t}(\theta) + Q_{1e}(\theta)\tau_{e,0}(\theta) = -\bar{\tau}_{0,a_t}(\theta)/6 + Q_{1e}(\theta)\tau_{e,0}(\theta) \\
\mathfrak{T}_4(\theta) &= k_e\tau_{e,0}(\theta) \\
\mathfrak{T}_5(\theta) &= -k_0\bar{\tau}_{a,a_t}(\theta) - k_0Q_a(\theta)\tau_{a,0}(\theta) = 7/6\cdot\bar{\tau}_{0,a_t}(\theta) + 1/2\cdot\tau_{00}(\theta)Q_a(\theta) \\
\mathfrak{T}_6(\theta) &= \bar{\tau}_{0,a_n}(\theta) + k_0\bar{\tau}_{a,a_n}(\theta) + Q_{2e}(\theta)\tau_{e,0}(\theta) = -\bar{\tau}_{0,a_n}(\theta)/6 + Q_{2e}(\theta)\tau_{e,0}(\theta) \\
\mathfrak{T}_7(\theta) &= -k_0\bar{\tau}_{a,a_n}(\theta) = 7/6\cdot\bar{\tau}_{0,a_n}(\theta)
\end{aligned}
$$

We have already seen how to deal with integrals of these kinds in Section 2.3.2.1, Equation 2.3.14 and Equation 2.3.15.

2.4.3.1. Fourier series coefficients

The first function to be expanded is τ_{00}, which is an even function defined as:

$$\tau_{00}(\theta) = \frac{a_0^{3/2}(1-e_0^2)^{3/2}}{\mu^{1/2}}\cdot\frac{1}{\mathcal{S}(e_0,\theta)}$$

Now we recall a result from Gradshteyn et al. [39], rearranging formula 1.[6] page 391 we have:

$$Y(\mathfrak{p},\mathfrak{q},n) = \frac{1}{\pi}\int_{-\pi}^{\pi}\frac{\cos(n\theta)}{\mathfrak{p}-\mathfrak{q}\cos(\theta)}\mathrm{d}\theta = \frac{2}{\sqrt{\mathfrak{p}^2-\mathfrak{q}^2}}\left(\frac{\mathfrak{p}-\sqrt{\mathfrak{p}^2-\mathfrak{q}^2}}{\mathfrak{q}}\right)^n \tag{2.4.19}$$

for $|\mathfrak{q}| < \mathfrak{p}$. In our case $\mathfrak{p} = 1$ and $\mathfrak{q} = -e_0$. Then:

$$\frac{1}{\pi}\int_{-\pi}^{\pi}\frac{\cos(n\theta)}{(e_0\cos(\theta)+1)^2}\mathrm{d}\theta = -\left[\frac{\partial Y(\mathfrak{p},\mathfrak{q},n)}{\partial\mathfrak{p}}\right]_{\substack{\mathfrak{p}=1\\ \mathfrak{q}=-e_0}} = \frac{2\left[-1+\lambda^{1/2}\right]^n\left[1+n\lambda^{1/2}\right]}{e_0^n\lambda^{3/2}} \tag{2.4.20}$$

Then the coefficients are:

$$\boxed{\begin{aligned}
\alpha_0[\tau_{00}] &= 2a_0^{3/2}\mu^{-1/2} \\
\alpha_n[\tau_{00}] &= 2a_0^{3/2}\mu^{-1/2}\cdot e_0^{-n}\left[-1+\lambda^{1/2}\right]^n\left[1+n\lambda^{1/2}\right] \\
\beta_n[\tau_{00}] &= 0
\end{aligned}} \tag{2.4.21}$$

with:

$$\lambda = 1 - e_0^2 \tag{2.4.22}$$

The function $\bar{\tau}_{0,a_t}$ is an odd function defined as:

$$\bar{\tau}_{0,a_t}(\theta) = \frac{2a_0^{3/2}(1-e_0^2)^{7/2}}{e_0\mu^{1/2}} \cdot \frac{\sin(\theta)}{\mathcal{S}^2(e_0,\theta)\mathcal{R}(e_0,\theta)}$$

Then we observe that:

$$\bar{\tau}_{0,a_t}(\theta) = \frac{\pi^{1/2}a_0^{3/2}\left(1-e_0^2\right)^{3/2}}{3e_0(e_0^2+1)^{1/2}\mu^{1/2}} \cdot \sin(\theta) \sum_{m=0}^{+\infty} w_m(e_0)\cos^m(\theta)$$

with:

$$w_m(e_0) = \frac{1}{m!}\left(\frac{2e_0}{1+e_0^2}\right)^m \cdot \Big\{[2(e_0^2-1)m^2 + (9e_0^2-19)m + 9e_0^2 - 24]\mathfrak{u}_m(e_0) + \\ + [(1-e_0^2)^2m^2 + (9-14e_0^2+5e_0^4)m + 30 - 21e_0^2 + 6e_0^4]\mathfrak{v}_m(e_0)\Big\}$$

Then the coefficients are:

$$\boxed{\begin{aligned} &\alpha_0[\bar{\tau}_{0,a_t}] = 0 \\ &\alpha_n[\bar{\tau}_{0,a_t}] = 0 \\ &\beta_n[\bar{\tau}_{0,a_t}] = \frac{\pi^{1/2}a_0^{3/2}\left(1-e_0^2\right)^{3/2}}{3e_0(e_0^2+1)^{1/2}\mu^{1/2}} \cdot n\sum_{m=0}^{+\infty}\frac{w_m(e_0)p_{m+1}(n)}{m+1} \end{aligned}} \tag{2.4.23}$$

where p_m is defined in Equation 2.4.13. The function $\tau_{e,0}$ is an even function defined as:

$$\tau_{e,0}(\theta) = -\frac{a_0^{3/2}(1-e_0^2)^{1/2}}{\mu^{1/2}} \cdot \frac{(e_0^2+2)\cos(\theta)+3e_0}{\mathcal{S}(e_0,\theta)^{3/2}}$$

Then the coefficients are:

$$\boxed{\begin{aligned} &\alpha_0[\tau_{e,0}] = 0 \\ &\alpha_n[\tau_{e,0}] = 2\frac{a_0^{3/2}}{\mu^{1/2}e_0\eta} \cdot n\zeta^n(1+\eta)^{-2n}(1+e_0+\eta n) \\ &\beta_n[\tau_{e,0}] = 0 \end{aligned}} \tag{2.4.24}$$

where ζ is defined in Equation 2.4.18 and:

$$\eta = \sqrt{\frac{1+e_0}{1-e_0}} \tag{2.4.25}$$

Regarding the coefficients of the product $Q_{1e} \cdot \tau_{e,0}$, we first observe that:

$$Q_{1e}(\theta) = \hat{Q}_0 + \hat{Q}_{1e}(\theta)$$

with:

$$\hat{Q}_0 = -k_e\theta_0 - 2\lambda^2 \mathcal{P}_{2\pi}\left(\begin{array}{c} 0 \\ \alpha_n[\bar{\bar{S}}_{a_t,0}]/n \end{array} \middle| \theta_0 \right), \quad \hat{Q}_{1e}(\theta) = 2\lambda^2 \mathcal{P}_{2\pi}\left(\begin{array}{c} 0 \\ \alpha_n[\bar{\bar{S}}_{a_t,0}]/n \end{array} \middle| \theta \right)$$

Then recalling that $\tau_{e,0}$ is an even function with zero mean value and $\hat{Q}_{1e}$ is an odd function we have:

$$\begin{aligned}
\alpha_0[Q_{1e} \cdot \tau_{e,0}] &= \hat{Q}_0 \alpha_0[\tau_{e,0}] + \alpha_0[\hat{Q}_{1e} \cdot \tau_{e0}] = 0 \\
\alpha_n[Q_{1e} \cdot \tau_{e,0}] &= \hat{Q}_0 \alpha_n[\tau_{e,0}] + \alpha_n[\hat{Q}_{1e} \cdot \tau_{e0}] = \hat{Q}_0 \alpha_n[\tau_{e,0}] \\
\beta_n[Q_{1e} \cdot \tau_{e,0}] &= \hat{Q}_0 \beta_n[\tau_{e,0}] + \beta_n[\hat{Q}_{1e} \cdot \tau_{e,0}] = \beta_n[\hat{Q}_{1e} \cdot \tau_{e,0}]
\end{aligned}$$

It is now clear that the only thing we have to evaluate are the coefficients β_n of the convolution $\hat{Q}_{1e} \cdot \tau_{e,0}$; this is straightforward applying Theorem 2.1.1, Equation 2.1.10. So in conclusion:

$$\boxed{\begin{aligned}
&\alpha_0[Q_{1e} \cdot \tau_{e,0}] = 0 \\
&\alpha_n[Q_{1e} \cdot \tau_{e,0}] = \hat{Q}_0 \alpha_n[\tau_{e,0}] \\
&\beta_n[Q_{1e} \cdot \tau_{e,0}] = \lambda^2 \sum_{m=1}^{+\infty} \alpha_m[\bar{\bar{S}}_{a_t,0}]\{\alpha_{|m-n|}[\tau_{e,0}] - \alpha_{m+n}[\tau_{e,0}]\} m^{-1}
\end{aligned}} \tag{2.4.26}$$

The process to obtain the coefficients of the functions $Q_{2e} \cdot \tau_{e,0}$ and $Q_a \cdot \tau_{00}$ is analogous and the coefficients are:

$$\boxed{\begin{aligned}
&\alpha_0[Q_{2e} \cdot \tau_{e,0}] = \lambda^3 \sum_{m=1}^{+\infty} \beta_m[\bar{\bar{S}}_{a_n,0}]\alpha_m[\tau_{e,0}] m^{-1} \\
&\alpha_n[Q_{2e} \cdot \tau_{e,0}] = \tilde{Q}_0 \alpha_n[\tau_{e,0}] + \frac{\lambda^3}{2} \sum_{m=1}^{+\infty} \beta_m[\bar{\bar{S}}_{a_n,0}]\{\alpha_{|m-n|}[\tau_{e,0}] + \alpha_{m+n}[\tau_{e,0}]\} m^{-1} \\
&\beta_n[Q_{2e} \cdot \tau_{e,0}] = 0
\end{aligned}} \tag{2.4.27}$$

with:

$$\tilde{Q}_0 = -(e_0^2 - 1)^3 \mathcal{P}_{2\pi}\left(\begin{array}{c} -\beta_n[\bar{\bar{S}}_{a_n,0}]/n \\ 0 \end{array} \middle| \theta_0 \right)$$

and:

$$\boxed{\begin{aligned}&\alpha_0[Q_a \cdot \tau_{00}] = 0\\&\alpha_n[Q_a \cdot \tau_{00}] = 0\\&\beta_n[Q_a \cdot \tau_{00}] = 3\lambda \sum_{m=1}^{+\infty} \alpha_m[g]\{\alpha_{|m-n|}[\tau_{00}] - \alpha_{m+n}[\tau_{00}]\}m^{-1}\end{aligned}} \tag{2.4.28}$$

Finally:

$$\bar{\tau}_{0,a_n}(\theta) = \frac{a_0^{3/2}(1-e_0^2)^{7/2}}{e_0\mu^{1/2}} \cdot \frac{(1+e_0^2)\cos(\theta) + 2e_0}{\mathcal{S}^{5/2}(e_0,\theta)\mathcal{R}(e_0,\theta)}$$

which can be rewritten as:

$$\bar{\tau}_{0,a_n} = \frac{a_0^{3/2}(1-e_0^2)^{3/2}\pi^{1/2}}{24e_0^2(1+e_0^2)^{1/2}\mu^{1/2}} \sum_{m=0}^{+\infty} y_m(e_0)\cos^m(\theta)$$

with:

$$\begin{aligned}y_m(e_0) = \frac{1}{m!}\left(\frac{2e_0}{1+e_0^2}\right)^m \cdot \Big\{&[2\lambda^2 m^3 + \left(25e_0^4 - 46e_0^2 + 21\right)m^2 +\\&+ \left(81e_0^4 - 188e_0^2 + 97\right)m + 3\left(24e_0^4 - 64e_0^2 + 35\right)]\mathfrak{u}_m(e_0) +\\&+ [-\lambda^3 m^3 + \left(13e_0^2 - 10\right)\lambda^2 m^2 +\\&- \lambda\left(46e_0^4 - 95e_0^2 + 42\right)m + 3\left(16e_0^6 - 56e_0^4 + 80e_0^2 - 35\right)]\mathfrak{v}_m(e_0)\Big\}\end{aligned}$$

Then:

$$\boxed{\begin{aligned}\alpha_0[\bar{\tau}_{0,a_n}] &= \frac{a_0^{3/2}}{6\pi e_0^2\lambda^{1/2}\mu^{1/2}} \cdot \Big\{8\left(e_0-1\right)\left(e_0^4 + 6e_0^2 - 10\right)\mathbf{E}(\kappa) +\\&\quad + \lambda\left(e_0+1\right)\left(8e_0^2+25\right)\mathbf{K}(\kappa) - 3(1+e_0)^2(35+13e_0^2)\mathbf{\Pi}(\zeta|\kappa)\Big\}\\\alpha_n[\bar{\tau}_{0,a_n}] &= \frac{a_0^{3/2}(1-e_0^2)^{3/2}\pi^{1/2}}{24e_0^2(1+e_0^2)^{1/2}\mu^{1/2}} \sum_{m=0}^{+\infty} y_m(e_0)p_m(n)\\\beta_n[\bar{\tau}_{0,a_n}] &= 0\end{aligned}} \tag{2.4.29}$$

where p_m is defined in Equation 2.4.13 and κ comes from Equation 2.4.15. The results are summarized in Table 2.2.

Table 2.2: Fourier series coefficients for the functions $\mathfrak{T}_i(\theta)$ characterizing the time law.

Function	α_0	α_n	β_n	Eq. Number
$\mathfrak{T}_1(\theta)$	$\alpha_0[\tau_{00}]/2$	$\alpha_n[\tau_{00}]/2$	0	Equation 2.4.21
$\mathfrak{T}_2(\theta)$	$\alpha_0[\tau_{00}]/2$	$\alpha_n[\tau_{00}]/2$	0	Equation 2.4.21
$\mathfrak{T}_3(\theta)$	0	$\alpha_n[Q_{1e}\cdot\tau_{e,0}]$	$-\beta_n[\bar{\tau}_{0,a_t}]/6+$ $+\beta_n[Q_{1e}\cdot\tau_{e,0}]$	Equation 2.4.23 Equation 2.4.26
$\mathfrak{T}_4(\theta)$	0	$k_e\alpha_n[\tau_{e,0}]$	0	Equation 2.4.24
$\mathfrak{T}_5(\theta)$	0	0	$7\beta_n[\bar{\tau}_{0,a_t}]/6+$ $+\beta_n[Q_a\cdot\tau_{00}]/2$	Equation 2.4.23 Equation 2.4.28
$\mathfrak{T}_6(\theta)$	$-\alpha_0[\bar{\tau}_{0,a_n}]/6+$ $+\alpha_0[Q_{2e}\cdot\tau_{e,0}]$	$-\alpha_n[\bar{\tau}_{0,a_n}]/6+$ $+\alpha_n[Q_{2e}\cdot\tau_{e,0}]$	0	Equation 2.4.27 Equation 2.4.29
$\mathfrak{T}_7(\theta)$	$7\alpha_0[\bar{\tau}_{0,a_n}]/6$	$7\alpha_n[\bar{\tau}_{0,a_n}]/6$	0	Equation 2.4.29

2.4.4. Inclination solution

Starting from Equation 2.4.5 the θ-derivative of the inclination becomes:

$$\begin{aligned} i' &= \{\bar{\mathfrak{I}}_{a_h,0}(\theta) + \bar{\mathfrak{I}}_{a_h,a}(\theta)(a-a_0) + \bar{\mathfrak{I}}_{a_h,e}(\theta)(e-e_0)\}\tilde{a}_h = \\ &= \{\bar{\mathfrak{I}}_{a_h,0}(\theta) + 2a_0^{-1}\bar{\mathfrak{I}}_{a_h,0}(\theta)(a-a_0) + \bar{\mathfrak{I}}_{a_h,e}(\theta)(e-e_0)\}\tilde{a}_h \end{aligned}$$

where $\tilde{a}_h$ is defined in Equation 2.4.9 and with:

$$\begin{aligned} \bar{\mathfrak{I}}_{a_h,0}(\theta) &= \lambda^2\cdot\frac{\cos(\theta+\omega_0)}{\mathcal{S}^{3/2}(e_0,\theta)} \\ \bar{\mathfrak{I}}_{a_h,e}(\theta) &= -\lambda\cdot\frac{[(e_0^2+3)\cos(\theta)+4e_0]\cos(\theta+\omega_0)}{\mathcal{S}^2(e_0,\theta)} \end{aligned} \tag{2.4.30}$$

Thus recalling Equation 2.4.12 and Equation 2.4.16 we get:

$$\begin{aligned} i' = &\frac{1}{3}\bar{\mathfrak{I}}_{a_h,0}(\theta)\left\{1+2\exp[k_a\theta+k_1]\right\}\tilde{a}_h+ \\ &+\left\{\frac{2}{3}\bar{\mathfrak{I}}_{a_h,0}(\theta)Q_a(\theta)\exp[k_a\theta+k_1]+k_e\bar{\mathfrak{I}}_{a_h,e}(\theta)\theta+\bar{\mathfrak{I}}_{a_h,e}(\theta)Q_{1e}(\theta)\right\}\tilde{a}_t\tilde{a}_h+ \\ &+\bar{\mathfrak{I}}_{a_h,e}(\theta)Q_{2e}(\theta)\tilde{a}_n\tilde{a}_h \end{aligned}$$

Thus at first order:

$$i' = \frac{1}{3}\bar{\mathfrak{I}}_{a_h,0}(\theta)\left\{1 + 2\exp[k_a\theta + k_1]\right\}\tilde{a}_h \tag{2.4.31}$$

2.4.4.1. Fourier series coefficients

The first function to be analysed is $\bar{\mathfrak{I}}_{a_h,0}$ given by Equation 2.4.30. Notice that:

$$\cos(\theta + \omega_0) = \cos(\theta)\cos(\omega_0) - \sin(\theta)\sin(\omega_0)$$

Then recalling Equation 2.4.19 and Equation 2.4.20 we observe that:

$$\frac{1}{\pi}\int_{-\pi}^{\pi}\frac{\cos(\theta)\cos(n\theta)}{\mathcal{S}^{3/2}(e_0,\theta)}\mathrm{d}\theta = -\frac{1}{2}\left[\frac{\partial^2 Y(\mathfrak{p},\mathfrak{q},n)}{\partial\mathfrak{p}\partial\mathfrak{q}}\right]_{\substack{\mathfrak{p}=1\\ \mathfrak{q}=-e_0}}$$
$$\frac{1}{\pi}\int_{-\pi}^{\pi}\frac{\sin(\theta)\sin(n\theta)}{\mathcal{S}^{3/2}(e_0,\theta)}\mathrm{d}\theta = -\frac{n}{2e_0}\cdot\frac{1}{\pi}\int_{-\pi}^{\pi}\frac{\cos(n\theta)}{\mathcal{S}(e_0,\theta)}\mathrm{d}\theta = -\frac{\mu^{1/2}}{2e_0a_0^{3/2}\lambda^{3/2}}\cdot n\alpha_n[\tau_{00}]$$

So finally the analytical expressions of the Fourier series coefficients are:

$$\boxed{\begin{aligned}
\alpha_0[\bar{\mathfrak{I}}_{a_h,0}] &= -3e_0\cos(\omega_0)\lambda^{-1/2}\\
\alpha_n[\bar{\mathfrak{I}}_{a_h,0}] &= -\frac{\cos(\omega_0)}{e_0\lambda}\cdot\left(\frac{\lambda^{1/2}-1}{e_0}\right)^n\left[\lambda^{3/2}n^2 + \left(-2e_0^4 + e_0^2 + 1\right)n + 3e_0^2\lambda^{1/2}\right]\\
\beta_n[\bar{\mathfrak{I}}_{a_h,0}] &= \frac{\sin(\omega_0)\lambda^{1/2}\mu^{1/2}}{2e_0a_0^{3/2}}\cdot n\alpha_n[\tau_{00}]
\end{aligned}} \tag{2.4.32}$$

where λ is given by Equation 2.4.22. In a similar fashion we can compute analytically the Fourier series coefficients of $\mathfrak{I}_{a_h,e}$ function. Indeed:

$$\bar{\mathfrak{I}}_{a_h,e}(\theta) = -\lambda(3 + e_0^2)\cdot\frac{\cos(\theta)\cos(\theta+\omega_0)}{\mathcal{S}^2(e_0,\theta)} - 4e_0\lambda\cdot\frac{\cos(\theta+\omega_0)}{\mathcal{S}^2(e_0,\theta)}$$

But from Equation 2.4.19 we get:

$$\frac{1}{\pi}\int_{-\pi}^{\pi}\frac{\cos^2(\theta)\cos(n\theta)}{\mathcal{S}^2(e_0,\theta)}\mathrm{d}\theta = -\frac{1}{6}\left[\frac{\partial^3 Y(\mathfrak{p},\mathfrak{q},n)}{\partial\mathfrak{p}\partial^2\mathfrak{q}}\right]_{\substack{\mathfrak{p}=1\\ \mathfrak{q}=-e_0}}$$
$$\frac{1}{\pi}\int_{-\pi}^{\pi}\frac{\cos(\theta)\cos(n\theta)}{\mathcal{S}^2(e_0,\theta)}\mathrm{d}\theta = \frac{1}{6}\left[\frac{\partial^3 Y(\mathfrak{p},\mathfrak{q},n)}{\partial^2\mathfrak{p}\partial\mathfrak{q}}\right]_{\substack{\mathfrak{p}=1\\ \mathfrak{q}=-e_0}}$$

Then the coefficients are:

$$\begin{aligned}
\alpha_0[\bar{\mathfrak{I}}_{a_h,e}] &= -3\cos(\omega_0)\lambda^{-3/2} \\
\alpha_n[\bar{\mathfrak{I}}_{a_h,e}] &= -\frac{\lambda^2 n^3 + 2e_0^2\lambda^{3/2}n^2 + \left(2e_0^6 - 8e_0^4 + 7e_0^2 - 1\right)n + 3e_0^2\lambda^{1/2}}{e_0^{2+n}\lambda^2\left[\lambda^{1/2}-1\right]^{-n}}\cos(\omega_0) \\
\beta_n[\bar{\mathfrak{I}}_{a_h,e}] &= -\frac{n\zeta^n\left[e_0^2(e_0+1)n + \eta\left(1-\lambda n^2\right)\right]}{e_0^2(e_0+1)\left(\eta+1\right)^{2n}}\sin(\omega_0)
\end{aligned} \tag{2.4.33}$$

where λ comes from Equation 2.4.22, η from Equation 2.4.25 and ζ from Equation 2.4.18. Following a procedure similar to that explained in Section 2.4.3.1 we also have:

$$\begin{aligned}
\alpha_0[\bar{\mathfrak{I}}_{a_h,0}\cdot Q_a] &= 3\frac{\lambda^{3/2}\mu^{1/2}}{e_0 a_0^{3/2}}\sin(\omega_0)\sum_{m=1}^{+\infty}\alpha_m[g]\alpha_m[\tau_{00}] \\
\alpha_n[\bar{\mathfrak{I}}_{a_h,0}\cdot Q_a] &= -\frac{3}{2}\frac{\lambda^{3/2}\mu^{1/2}}{e_0 a_0^{3/2}}\sin(\omega_0)\cdot \\
&\qquad \cdot\sum_{m=1}^{+\infty}\frac{\alpha_m[g]}{m}\left\{(n-m)\alpha_{|n-m|}[\tau_{00}] - (n+m)\alpha_{n+m}[\tau_{00}]\right\} \\
\beta_n[\bar{\mathfrak{I}}_{a_h,0}\cdot Q_a] &= 3\lambda\sum_{m=1}^{+\infty}\frac{\alpha_m[g]}{m}\left\{\alpha_{|n-m|}[\bar{\mathfrak{I}}_{a_h,0}] - \alpha_{n+m}[\bar{\mathfrak{I}}_{a_h,0}]\right\}
\end{aligned} \tag{2.4.34}$$

$$\begin{aligned}
\alpha_0[\bar{\mathfrak{I}}_{a_h,e}\cdot Q_{1e}] &= \hat{Q}_0\alpha_0[\bar{\mathfrak{I}}_{a_h,e}] + 2\lambda^2\sum_{m=1}^{+\infty}\frac{\alpha_m[\bar{\bar{S}}_{a_t,0}]}{m}\beta_m[\bar{\mathfrak{I}}_{a_h,e}] \\
\alpha_n[\bar{\mathfrak{I}}_{a_h,e}\cdot Q_{1e}] &= \hat{Q}_0\alpha_n[\bar{\mathfrak{I}}_{a_h,e}] + \\
&\quad -\lambda^2\sum_{m=1}^{+\infty}\frac{\alpha_m[\bar{\bar{S}}_{a_t,0}]}{m}\left\{\mathrm{sgn}(n-m)\beta_{|n-m|}[\bar{\mathfrak{I}}_{a_h,e}] - \beta_{n+m}[\bar{\mathfrak{I}}_{a_h,e}]\right\} \\
\beta_n[\bar{\mathfrak{I}}_{a_h,e}\cdot Q_{1e}] &= \hat{Q}_0\beta_n[\bar{\mathfrak{I}}_{a_h,e}] + \lambda^2\sum_{m=1}^{+\infty}\frac{\alpha_m[\bar{\bar{S}}_{a_t,0}]}{m}\left\{\alpha_{|n-m|}[\bar{\mathfrak{I}}_{a_h,e}] - \alpha_{n+m}[\bar{\mathfrak{I}}_{a_h,e}]\right\}
\end{aligned} \tag{2.4.35}$$

and:

$$\begin{aligned}
\alpha_0[\bar{\mathfrak{I}}_{a_h,e}\cdot Q_{2e}] &= \tilde{Q}_0\alpha_0[\bar{\mathfrak{I}}_{a_h,e}] + \lambda^3\sum_{m=1}^{+\infty}\frac{\beta_m[\bar{\bar{S}}_{a_n,0}]}{m}\alpha_m[\bar{\mathfrak{I}}_{a_h,e}]\\
\alpha_n[\bar{\mathfrak{I}}_{a_h,e}\cdot Q_{2e}] &= \tilde{Q}_0\alpha_n[\bar{\mathfrak{I}}_{a_h,e}] + \frac{\lambda^3}{2}\sum_{m=1}^{+\infty}\frac{\beta_m[\bar{\bar{S}}_{a_n,0}]}{m}\left\{\alpha_{|n-m|}[\bar{\mathfrak{I}}_{a_h,e}] + \alpha_{n+m}[\bar{\mathfrak{I}}_{a_h,e}]\right\}\\
\beta_n[\bar{\mathfrak{I}}_{a_h,e}\cdot Q_{2e}] &= \tilde{Q}_0\beta_n[\bar{\mathfrak{I}}_{a_h,e}]+\\
&\quad+\frac{\lambda^3}{2}\sum_{m=1}^{+\infty}\frac{\beta_m[\bar{\bar{S}}_{a_n,0}]}{m}\left\{\mathrm{sgn}(n-m)\beta_{|n-m|}[\bar{\mathfrak{I}}_{a_h,e}] + \beta_{n+m}[\bar{\mathfrak{I}}_{a_h,e}]\right\}
\end{aligned} \tag{2.4.36}$$

Where the sgn convention is the same as in Equation 2.1.11.

2.4.5. Argument of perigee solution

The expression of the θ-derivative of the argument of perigee provided by Equation 2.4.7 can be conveniently rewritten in matrix form as:

$$\omega' = [\tilde{a}_t, \tilde{a}_n, \tilde{a}_h]\begin{bmatrix} \bar{\mathcal{O}}_{a_t,0}(\theta) & \bar{\mathcal{O}}_{a_t,a}(\theta) & \bar{\mathcal{O}}_{a_t,e}(\theta) & 0 & 0\\ \bar{\mathcal{O}}_{a_n,0}(\theta) & \bar{\mathcal{O}}_{a_n,a}(\theta) & \bar{\mathcal{O}}_{a_n,e}(\theta) & 0 & 0\\ \bar{\mathcal{O}}_{a_h,0}(\theta) & \bar{\mathcal{O}}_{a_h,a}(\theta) & \bar{\mathcal{O}}_{a_h,e}(\theta) & \bar{\mathcal{O}}_{a_h,i}(\theta) & \bar{\mathcal{O}}_{a_h,\omega}(\theta)\end{bmatrix}\begin{bmatrix} a-a_0\\ e-e_0\\ i-i_0\\ \omega-\omega_0\end{bmatrix}$$

Thus substituting the expressions of $a-a_0$, $e-e_0$ and $i-i_0$ (given by Equation 2.4.12, Equation 2.4.16 and by solving Equation 2.4.31) and considering only the first order contributions, we get:

$$\omega' = [\tilde{a}_t, \tilde{a}_n, \tilde{a}_h]\left\{\begin{bmatrix} \bar{\mathcal{O}}_{a_t,0}(\theta) + k_0\bar{\mathcal{O}}_{a_t,a}(\theta)\left\{1-\exp[k_a\theta+k_1]\right\}\\ \bar{\mathcal{O}}_{a_n,0}(\theta) + k_0\bar{\mathcal{O}}_{a_n,a}(\theta)\left\{1-\exp[k_a\theta+k_1]\right\}\\ \bar{\mathcal{O}}_{a_h,0}(\theta) + k_0\bar{\mathcal{O}}_{a_h,a}(\theta)\left\{1-\exp[k_a\theta+k_1]\right\}\end{bmatrix}\right\} + \tilde{a}_h\bar{\mathcal{O}}_{a_h,\omega}(\theta)(\omega-\omega_0)$$

which has the same form analysed in Section 2.4.1, Equation 2.4.10. Thus, leading the problem to the quadratures we obtain:

$$\begin{aligned}
\omega-\omega_0 &= \exp[k_\omega\theta]\cdot[\tilde{a}_t,\tilde{a}_n,\tilde{a}_h]\cdot\\
&\quad\cdot\frac{1}{3}\int_{\theta_0}^{\theta}\begin{bmatrix}\left\{\exp[-k_\omega\xi]+2\exp[(k_a-k_\omega)\xi+k_1]\right\}\bar{\mathcal{O}}_{a_t,0}(\xi)\\ \left\{\exp[-k_\omega\xi]+2\exp[(k_a-k_\omega)\xi+k_1]\right\}\bar{\mathcal{O}}_{a_n,0}(\xi)\\ \left\{\exp[-k_\omega\xi]+2\exp[(k_a-k_\omega)\xi+k_1]\right\}\bar{\mathcal{O}}_{a_h,0}(\xi)\end{bmatrix}\mathrm{d}\xi
\end{aligned} \tag{2.4.37}$$

with:

$$k_\omega = \frac{\alpha_0[\bar{\mathcal{O}}_{a_h,\omega}]}{2}\tilde{a}_h = \frac{3e_0\cot(i_0)\cos(\omega_0)}{2\sqrt{1-e_0^2}}\tilde{a}_h$$

2.4.5.1. Fourier series coefficients

The three relevant functions to be expanded are:

$$\begin{aligned}
\bar{\mathcal{O}}_{a_t,0}(\theta) &= \frac{2\lambda^2\sin(\theta)}{e_0\mathcal{S}(e_0,\theta)\mathcal{R}(e_0,\theta)} \\
\bar{\mathcal{O}}_{a_n,0}(\theta) &= \frac{\lambda^2\mathcal{Q}(e_0,\theta)}{e_0\mathcal{S}^{3/2}(e_0,\theta)\mathcal{R}(e_0,\theta)} \\
\bar{\mathcal{O}}_{a_h,0}(\theta) &= -\frac{\lambda^2\cot(i_0)\sin(\theta+\omega_0)}{\mathcal{S}^{3/2}(e_0,\theta)}
\end{aligned}$$

In a fashion similar to what was done previously:

$$\begin{aligned}
\bar{\mathcal{O}}_{a_t,0}(\theta) &= \frac{2\lambda^2\pi^{1/2}}{e_0(1+e_0^2)^{1/2}}\cdot\sin(\theta)\sum_{m=0}^{+\infty} z_m(e_0)\cos^m(\theta) \\
\bar{\mathcal{O}}_{a_n,0}(\theta) &= \frac{\lambda^2\pi^{1/2}}{2e_0^2(1+e_0^2)^{1/2}}\sum_{m=0}^{+\infty} l_m(e_0)\cos^m(\theta)
\end{aligned}$$

with:

$$\begin{aligned}
z_m(e_0) &= \frac{1}{m!}\left(\frac{2e_0}{1+e_0^2}\right)^m \mathfrak{v}_m(e_0) \\
l_m(e_0) &= \frac{1}{m!}\left(\frac{2e_0}{1+e_0^2}\right)^m \left[(3+2m)\mathfrak{u}_m(e_0) + (-3+4e_0^2-\lambda m)\mathfrak{v}_m(e_0)\right]
\end{aligned}$$

thus:

$$\boxed{\begin{aligned}
&\alpha_0[\bar{\mathcal{O}}_{a_t,0}] = 0 \\
&\alpha_n[\bar{\mathcal{O}}_{a_t,0}] = 0 \\
&\beta_n[\bar{\mathcal{O}}_{a_t,0}] = \frac{2\lambda^2\pi^{1/2}}{e_0(1+e_0^2)^{1/2}}\cdot n\sum_{m=0}^{+\infty}\frac{z_m(e_0)p_{m+1}(n)}{m+1}
\end{aligned}} \tag{2.4.38}$$

and:

$$\boxed{\begin{aligned}\alpha_0[\bar{\mathcal{O}}_{a_n,0}] &= \frac{2(1+e_0)(1+\lambda)}{\pi e_0^2}\mathbf{E}(\nu) + \frac{2\lambda(1-e_0)}{\pi e_0^2}\mathbf{K}(\nu) - \frac{6(1-e_0)^2}{\pi e_0^2}\mathbf{\Pi}(\sigma|\nu)\\ \alpha_n[\bar{\mathcal{O}}_{a_n,0}] &= \frac{\lambda^2\pi^{1/2}}{2e_0^2(1+e_0^2)^{1/2}}\sum_{m=0}^{+\infty} l_m(e_0)p_m(n)\\ \beta_n[\bar{\mathcal{O}}_{a_n,0}] &= 0\end{aligned}} \tag{2.4.39}$$

with:

$$\nu = \frac{4e_0}{(1+e_0)^2}, \quad \sigma = \frac{2e_0}{1+e_0}$$

Regarding $\bar{\mathcal{O}}_{a_h,0}$ we notice that:

$$\sin(\theta+\omega_0) = \sin(\omega_0)\cos(\theta) + \cos(\omega_0)\sin(\theta)$$

thus comparing with the function $\bar{\mathfrak{I}}_{a_h,0}$ we get:

$$\boxed{\begin{aligned}\alpha_0[\bar{\mathcal{O}}_{a_h,0}] &= -\tan(\omega_0)\cot(i_0)\alpha_0[\bar{\mathfrak{I}}_{a_h,0}]\\ \alpha_n[\bar{\mathcal{O}}_{a_h,0}] &= -\tan(\omega_0)\cot(i_0)\alpha_n[\bar{\mathfrak{I}}_{a_h,0}]\\ \beta_n[\bar{\mathcal{O}}_{a_h,0}] &= \cot(\omega_0)\cot(i_0)\beta_n[\bar{\mathfrak{I}}_{a_h,0}]\end{aligned}} \tag{2.4.40}$$

2.4.6. Right ascension of the ascending node solution

Starting from Equation 2.4.8 the θ-derivative of the Right Ascension of the Ascending Node becomes:

$$\begin{aligned}\Omega' = &\{\bar{\mathfrak{O}}_{a_h,0}(\theta) + \bar{\mathfrak{O}}_{a_h,a}(\theta)(a-a_0) + \bar{\mathfrak{O}}_{a_h,e}(\theta)(e-e_0) +\\ &+ \bar{\mathfrak{O}}_{a_h,i}(\theta)(i-i_0) + \bar{\mathfrak{O}}_{a_h,\omega}(\theta)(\omega-\omega_0)\}\tilde{a}_h =\\ &= \{\bar{\mathfrak{O}}_{a_h,0}(\theta) + 2a_0^{-1}\bar{\mathfrak{O}}_{a_h,0}(\theta)(a-a_0) + \bar{\mathfrak{O}}_{a_h,e}(\theta)(e-e_0) +\\ &+ \bar{\mathfrak{O}}_{a_h,i}(\theta)(i-i_0) + \bar{\mathfrak{O}}_{a_h,\omega}(\theta)(\omega-\omega_0)\}\tilde{a}_h\end{aligned}$$

For the RAAN we make the assumption of neglecting the small variations of the inclination (i.e. the solution of Equation 2.4.31) and of the argument of perigee (i.e. the solution of Equation 2.4.37). This is done for two reasons mainly: first, they are both second order terms; furthermore, both variations are really small over one thrust arc. Then recalling Equation 2.4.12 and Equation 2.4.16 for $a-a_0$ and $e-e_0$ respectively, a similar expression

as the one for the inclination is achieved:

$$\begin{aligned}\Omega' = &\frac{1}{3}\bar{\mathfrak{O}}_{a_h,0}(\theta)\left\{1+2\exp[k_a\theta+k_1]\right\}\tilde{a}_h+\\ &+\left\{\frac{2}{3}\bar{\mathfrak{O}}_{a_h,0}(\theta)Q_a(\theta)\exp[k_a\theta+k_1]+k_e\bar{\mathfrak{O}}_{a_h,e}(\theta)\theta+\bar{\mathfrak{O}}_{a_h,e}(\theta)Q_{1e}(\theta)\right\}\tilde{a}_t\tilde{a}_h+\\ &+\bar{\mathfrak{O}}_{a_h,e}(\theta)Q_{2e}(\theta)\tilde{a}_n\tilde{a}_h\end{aligned}$$

And at first order:

$$\Omega' = \frac{1}{3}\bar{\mathfrak{O}}_{a_h,0}(\theta)\left\{1+2\exp[k_a\theta+k_1]\right\}\tilde{a}_h$$

where $\tilde{a}_h$ is defined in Equation 2.4.9 and with:

$$\bar{\mathfrak{O}}_{a_h,0}(\theta) = \frac{\lambda^2\csc(i_0)\sin(\theta+\omega_0)}{\mathcal{S}^{3/2}(e_0,\theta)} \tag{2.4.41}$$

2.4.6.1. Fourier series coefficients

Comparing Equation 2.4.41 with Equation 2.4.30, it is easy to notice that:

$$\bar{\mathfrak{O}}_{a_h,0}(\theta) = -\frac{\partial\bar{\mathfrak{I}}_{a_h,0}(\theta)}{\partial\omega_0}\csc(i_0)$$

This relation can be extended to the coefficients; considering for instance the Fourier coefficient α_0 we have:

$$\alpha_0[\bar{\mathfrak{O}}_{a_h,0}] = -\frac{\partial\alpha_0[\bar{\mathfrak{I}}_{a_h,0}]}{\partial\omega_0}\csc(i_0)$$

and this relation holds for all the other coefficients. It follows:

$$\boxed{\begin{aligned}\alpha_0[\bar{\mathfrak{O}}_{a_h,0}] &= \tan(\omega_0)\csc(i_0)\alpha_0[\bar{\mathfrak{I}}_{a_h,0}]\\ \alpha_n[\bar{\mathfrak{O}}_{a_h,0}] &= \tan(\omega_0)\csc(i_0)\alpha_n[\bar{\mathfrak{I}}_{a_h,0}]\\ \beta_n[\bar{\mathfrak{O}}_{a_h,0}] &= -\cot(\omega_0)\csc(i_0)\beta_n[\bar{\mathfrak{I}}_{a_h,0}]\end{aligned}} \tag{2.4.42}$$

$$\boxed{\begin{aligned}\alpha_0[\bar{\mathfrak{O}}_{a_h,e}] &= \tan(\omega_0)\csc(i_0)\alpha_0[\bar{\mathfrak{I}}_{a_h,e}]\\ \alpha_n[\bar{\mathfrak{O}}_{a_h,e}] &= \tan(\omega_0)\csc(i_0)\alpha_n[\bar{\mathfrak{I}}_{a_h,e}]\\ \beta_n[\bar{\mathfrak{O}}_{a_h,e}] &= -\cot(\omega_0)\csc(i_0)\beta_n[\bar{\mathfrak{I}}_{a_h,e}]\end{aligned}} \tag{2.4.43}$$

$$\begin{aligned}
\alpha_0[\bar{\mathfrak{O}}_{a_h,0}\cdot Q_a] &= -\cot(\omega_0)\csc(i_0)\alpha_0[\bar{\mathfrak{I}}_{a_h,0}\cdot Q_a]\\
\alpha_n[\bar{\mathfrak{O}}_{a_h,0}\cdot Q_a] &= -\cot(\omega_0)\csc(i_0)\alpha_n[\bar{\mathfrak{I}}_{a_h,0}\cdot Q_a]\\
\beta_n[\bar{\mathfrak{O}}_{a_h,0}\cdot Q_a] &= \tan(\omega_0)\csc(i_0)\beta_n[\bar{\mathfrak{I}}_{a_h,0}\cdot Q_a]
\end{aligned} \tag{2.4.44}$$

$$\begin{aligned}
\alpha_0[\bar{\mathfrak{O}}_{a_h,e}\cdot Q_{1e}] &= \tan(\omega_0)\csc(i_0)\hat{Q}_0\alpha_0[\bar{\mathfrak{I}}_{a_h,e}]+\\
&\quad -2\lambda^2\cot(\omega_0)\csc(i_0)\sum_{m=1}^{+\infty}\frac{\alpha_m[\bar{\bar{S}}_{a_t,0}]}{m}\beta_m[\bar{\mathfrak{I}}_{a_h,e}]\\
\alpha_n[\bar{\mathfrak{O}}_{a_h,e}\cdot Q_{1e}] &= \tan(\omega_0)\csc(i_0)\hat{Q}_0\alpha_n[\bar{\mathfrak{I}}_{a_h,e}]+\lambda^2\cot(\omega_0)\csc(i_0)\cdot\\
&\quad \cdot\sum_{m=1}^{+\infty}\frac{\alpha_m[\bar{\bar{S}}_{a_t,0}]}{m}\left\{\mathrm{sgn}(n-m)\beta_{|n-m|}[\bar{\mathfrak{I}}_{a_h,e}]-\beta_{n+m}[\bar{\mathfrak{I}}_{a_h,e}]\right\}\\
\beta_n[\bar{\mathfrak{O}}_{a_h,e}\cdot Q_{1e}] &= -\cot(\omega_0)\csc(i_0)\hat{Q}_0\beta_n[\bar{\mathfrak{I}}_{a_h,e}]+\\
&\quad +\lambda^2\tan(\omega_0)\csc(i_0)\sum_{m=1}^{+\infty}\frac{\alpha_m[\bar{\bar{S}}_{a_t,0}]}{m}\left\{\alpha_{|n-m|}[\bar{\mathfrak{I}}_{a_h,e}]-\alpha_{n+m}[\bar{\mathfrak{I}}_{a_h,e}]\right\}
\end{aligned} \tag{2.4.45}$$

and:

$$\begin{aligned}
\alpha_0[\bar{\mathfrak{O}}_{a_h,e}\cdot Q_{2e}] &= \tan(\omega_0)\csc(i_0)\alpha_0[\bar{\mathfrak{I}}_{a_h,e}\cdot Q_{2e}]\\
\alpha_n[\bar{\mathfrak{O}}_{a_h,e}\cdot Q_{2e}] &= \tan(\omega_0)\csc(i_0)\alpha_n[\bar{\mathfrak{I}}_{a_h,e}\cdot Q_{2e}]\\
\beta_n[\bar{\mathfrak{O}}_{a_h,e}\cdot Q_{2e}] &= -\cot(\omega_0)\csc(i_0)\beta_n[\bar{\mathfrak{I}}_{a_h,e}\cdot Q_{2e}]
\end{aligned} \tag{2.4.46}$$

In Table 2.3 we summarize all the results concerning the Fourier series coefficients.

Table 2.3: Summary of Fourier series coefficients of the functions

Function	Equation Number
g	Equation 2.4.14
$\bar{\bar{S}}_{a_t,0}$, $\bar{\bar{S}}_{a_n,0}$	Equation 2.4.17
τ_{00}	Equation 2.4.21
$\bar{\tau}_{0,a_t}$	Equation 2.4.23
$\tau_{e,0}$	Equation 2.4.24
$Q_{1e} \cdot \tau_{e,0}$	Equation 2.4.26
$Q_{2e} \cdot \tau_{e,0}$	Equation 2.4.27
$Q_a \cdot \tau_{00}$	Equation 2.4.28
$\bar{\tau}_{0,a_n}$	Equation 2.4.29
$\bar{\mathfrak{I}}_{a_h,0}$	Equation 2.4.32
$\bar{\mathfrak{I}}_{a_h,e}$	Equation 2.4.33
$\bar{\mathfrak{I}}_{a_h,0} \cdot Q_a$	Equation 2.4.34
$\bar{\mathfrak{I}}_{a_h,e} \cdot Q_{1e}$	Equation 2.4.35
$\bar{\mathfrak{I}}_{a_h,e} \cdot Q_{2e}$	Equation 2.4.36
$\bar{\mathfrak{O}}_{a_t,0}$	Equation 2.4.38
$\bar{\mathfrak{O}}_{a_n,0}$	Equation 2.4.39
$\bar{\mathfrak{O}}_{a_h,0}$	Equation 2.4.40
$\bar{\mathfrak{O}}_{a_h,0}$	Equation 2.4.42
$\bar{\mathfrak{O}}_{a_h,e}$	Equation 2.4.43
$\bar{\mathfrak{O}}_{a_h,0} \cdot Q_a$	Equation 2.4.44
$\bar{\mathfrak{O}}_{a_h,e} \cdot Q_{1e}$	Equation 2.4.45
$\bar{\mathfrak{O}}_{a_h,e} \cdot Q_{2e}$	Equation 2.4.46

3 | Simulations

In this chapter the previously defined analytical models are tested by means of several test cases. The first set has been carried out to compare the *full model* to the *small thrust model* as it concerns accuracy and computational time. Both beneficial and limiting aspects have been highlighted. The result is that the *small thrust model* has the best trade off between the above mentioned performances. Afterwards, several CAMs strategies have been computed. In the first one we considered only the tangential thrust (which is the quasi optimal manoeuvre in practical scenarios), while in the second both tangential and normal thrust act simultaneously. All the simulations have been carried out at several thrust levels and for different reference conditions. Special care has been due to e_0 because these kind of solutions are very sensitive towards reference eccentricity values. Several plots provide a comparative view between our semi-analytical solution and that of Gauss Planetary equations numerically obtained by means of the Adams–Bashforth-Moulton method, assessing the effectiveness of the method.

3.1. Mathematical background

The simulation methodology used in the following sections is based on the assumption of short-term conjunction. This means that it is possible to consider the relative velocity at CA sufficiently large to ensure a brief encounter time and static covariance. The calculation of the PoC relies on the assumption that the relative motion is linear without velocity uncertainty. In this case the position error ellipsoid during the encounter is constant and equal to the value at the estimated conjunction. The PoC is defined as the probability that the Miss Distance between two objects is less than the sum of the radii of their spherical envelopes. Each object's positional uncertainties are combined[1] and the resultant is projected onto a plane perpendicular to the relative velocity (the B-plane). Then the calculation of the PoC passes from an integral of the 3D Gaussian distribution to an integral of a 2D Gaussian probability density function (PDF) over the circular collision cross-sectional area. Referring to Bombardelli et al. [23] the B-plane centred on the debris

[1] combining both covariances also relies on the hypothesis that they are statistically independent.

nominal position is defined as:

$$\boldsymbol{\eta} = \frac{\boldsymbol{v}_s - \boldsymbol{v}_d}{||\boldsymbol{v}_s - \boldsymbol{v}_d||}, \quad \boldsymbol{\xi} = \frac{\boldsymbol{v}_d \wedge \boldsymbol{v}_s}{||\boldsymbol{v}_d \wedge \boldsymbol{v}_s||}, \quad \boldsymbol{\zeta} = \boldsymbol{\xi} \wedge \boldsymbol{\eta}$$

where $\boldsymbol{v}_d$ is the debris velocity and $\boldsymbol{v}_s$ is the spacecraft velocity. The Miss Distance is defined as:

$$\rho_{miss} = ||\boldsymbol{r}_s - \boldsymbol{r}_d||$$

Where $\boldsymbol{r}_s$ and $\boldsymbol{r}_d$ are the spacecraft position vector and the debris position vector, respectively. The idea is that at the time of close approach t_{CA} we have:

$$\rho_{miss}(t_{CA}) > s_A, \quad \text{with} \quad s_A = \rho_s + \rho_d$$

where ρ_s and ρ_d are the radii of the spacecraft and of the debris, respectively, assuming a spherical envelope for both objects. The relevant advantage of projecting on the B-plane is that the CA relative position in $\{\boldsymbol{\xi}, \boldsymbol{\eta}, \boldsymbol{\zeta}\}$ axes (denoted by e subscript) becomes:

$$\hat{\boldsymbol{r}}_e = [\xi_e, 0, \zeta_e]$$

For the PoC evaluation we adopt the Chan method. Chan [40] transforms the two-dimensional Gaussian PDF to a one-dimensional Rician PDF. Then the computation of the PoC reduces to a Rician integral that can be computed by the convergent series:

$$\text{PoC} = \exp\left(-\frac{v}{2}\right) \sum_{m=0}^{+\infty} \left[\frac{v^m}{2^m m!} \left(1 - \exp\left(-\frac{u}{2}\right) \sum_{k=0}^{m} \frac{u^k}{2^k k!} \right) \right]$$

with:

$$u = \frac{s_A^2}{\sigma_\xi \sigma_\zeta \sqrt{1 - \rho_{\xi\zeta}^2}}, \quad v = \left[\left(\frac{\xi_e}{\sigma_\xi}\right)^2 + \left(\frac{\zeta_e}{\sigma_\zeta}\right)^2 - 2\rho_{\xi\zeta} \frac{\xi_e \zeta_e}{\sigma_\xi \sigma_\zeta} \right] / (1 - \rho_{\xi\zeta}^2)$$

where σ_ξ, σ_ζ and $\rho_{\xi\zeta}$ can be extracted from the relative position covariance matrix in the B-plane:

$$C = \begin{bmatrix} \sigma_\xi^2 & \rho_{\xi\zeta}\sigma_\xi\sigma_\zeta \\ \rho_{\xi\zeta}\sigma_\xi\sigma_\zeta & \sigma_\zeta^2 \end{bmatrix}$$

3.2. A *full model* and *small thrust model* comparison

The first simulations have the aim of comparing the two proposed methods both in terms of accuracy and computational time. We will rely on two reference orbits outlined in

Table 3.1 and Table 3.2.

Table 3.1: First reference orbit for models comparison.

a_0 [km]	e_0 [−]	i_0 [deg]	Ω_0 [deg]	ω_0 [deg]	θ_0 [deg]	T [h]	t_0 [s]
12000	0.1	30	10	29	5	3.634	0

Table 3.2: Second reference orbit for models comparison.

a_0 [km]	e_0 [−]	i_0 [deg]	Ω_0 [deg]	ω_0 [deg]	θ_0 [deg]	T [h]	t_0 [s]
26000	0.8	63	40	270	33	11.5896	0

For our methods the number of Fourier Series coefficients is determined automatically by the code relying on the desired level of accuracy in the integrating functions approximation. For instance, referring to Equation 2.3.1b the stop criterion is defined as:

$$\max_{\theta\in[0,2\pi]}\{|\mathfrak{F}[S_0](\theta) - S_0(\theta)|\} < \text{toll}$$

where toll is the tolerance. Now, considering the decomposition of S_0 into a mean value and an oscillatory part, we have:

$$|\mathfrak{F}[S_0](\theta) - S_0(\theta)| = \left|\mathcal{P}_{2\pi}\left(\begin{array}{c|c} \alpha_n[S_0] & \\ \beta_n[S_0] & \theta \end{array}\right)\right| \leq \sqrt{\alpha_n^2[S_0] + \beta_n^2[S_0]}$$

Therefore, the stop criterion can be rewritten as:

$$\sqrt{\alpha_n^2[S_0] + \beta_n^2[S_0]} < \text{toll}$$

for our computations we set toll $= 10^{-12}$. For low eccentricities the number of terms is in the range 5-10 while for higher eccentricities it is in the range 25-30 or higher. For the truncation of the series present in the coefficients, such as Equation 2.4.14, we used a similar approach. In this case the stop criterion would be:

$$|g(\theta) - g_{\text{approx.}}(\theta)| \leq \frac{1}{2}\pi^{1/2}(1+e_0^2)^{1/2}\sum_{m=0}^{N} q_m(e_0)$$

where N is the order of approximation. For low eccentricities the number of terms is in the range 10-15, while for higher eccentricities it is in the range 90-100 or higher. All the

simulations are carried out with a MacBook Pro with a CPU 2.4 GHz Intel Core i9 8 core.

The selected reference solution is the numerical one of the Gauss Planetary Equations by means of the Adams–Bashforth-Moulton method[2]. First we start to analyse the results for the first reference orbit in Table 3.1. In Figure 3.1 the relative errors for the semimajor axis and for the eccentricity at different thrust levels are shown. As we can see, the *full model* with a first order approximation for a behaves better, specially inside the first orbital revolution. Nevertheless, it shows s a monotonically increasing behaviour, while the *small thrust model* has a lower accuracy but presents a more stationary one. For the eccentricity instead, the behaviours are more or less the same. This is due to the fact that, referring to Equation 2.3.1b and Equation 2.4.1, both rely on a zero order approximation for the θ-derivative of the eccentricity.

[2]In Matlab `ode113`. It is a variable-step, variable-order Adams-Bashforth-Moulton solver of orders 1 to 13. Relative error tolerance `RelTol` setted to 10^{-13} and absolute error tolerance `AbsTol` setted to 10^{-13}.

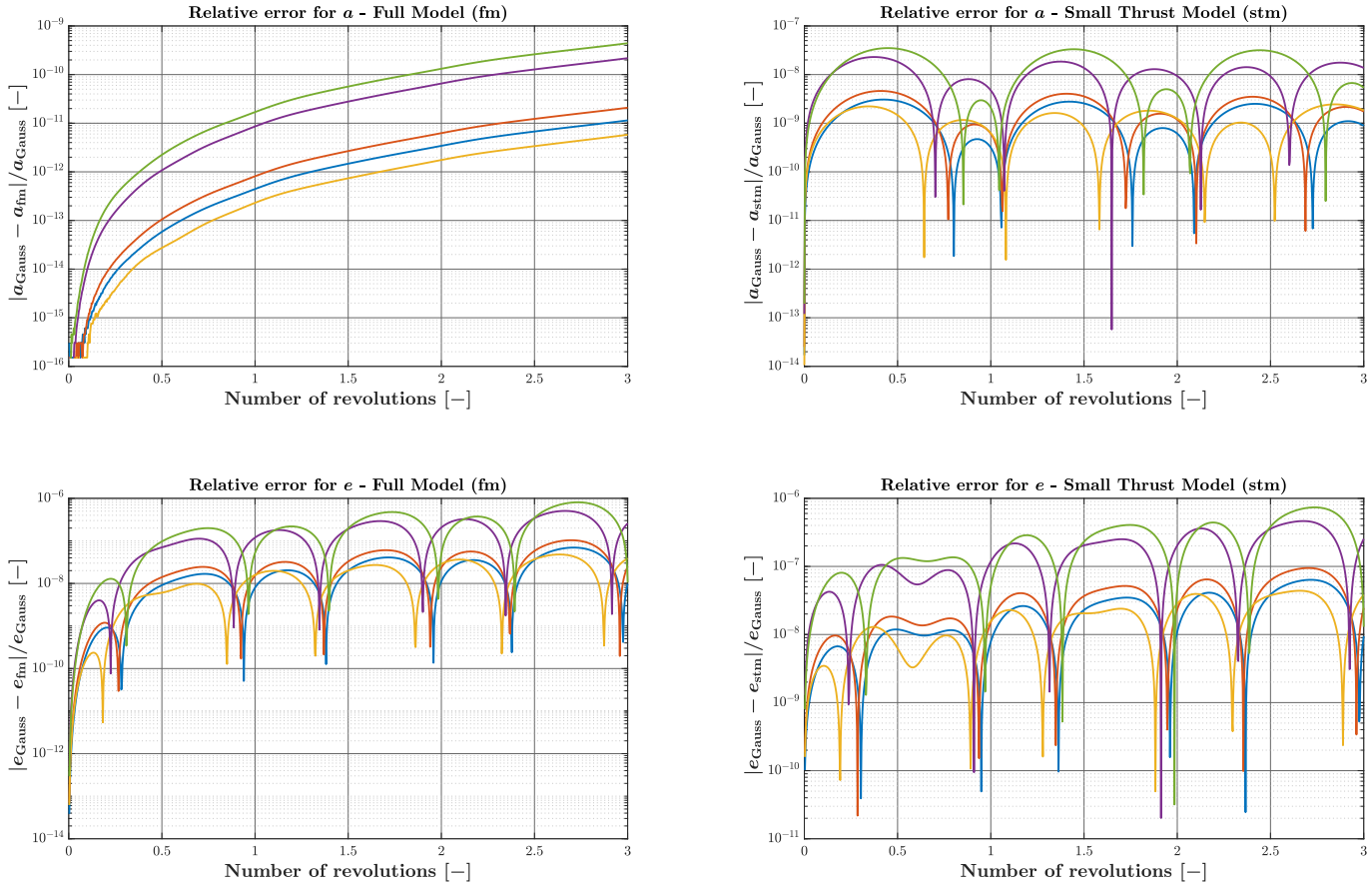

Figure 3.1: f.m. and s.t.m. comparison for a and e. Reference orbit in Table 3.1.

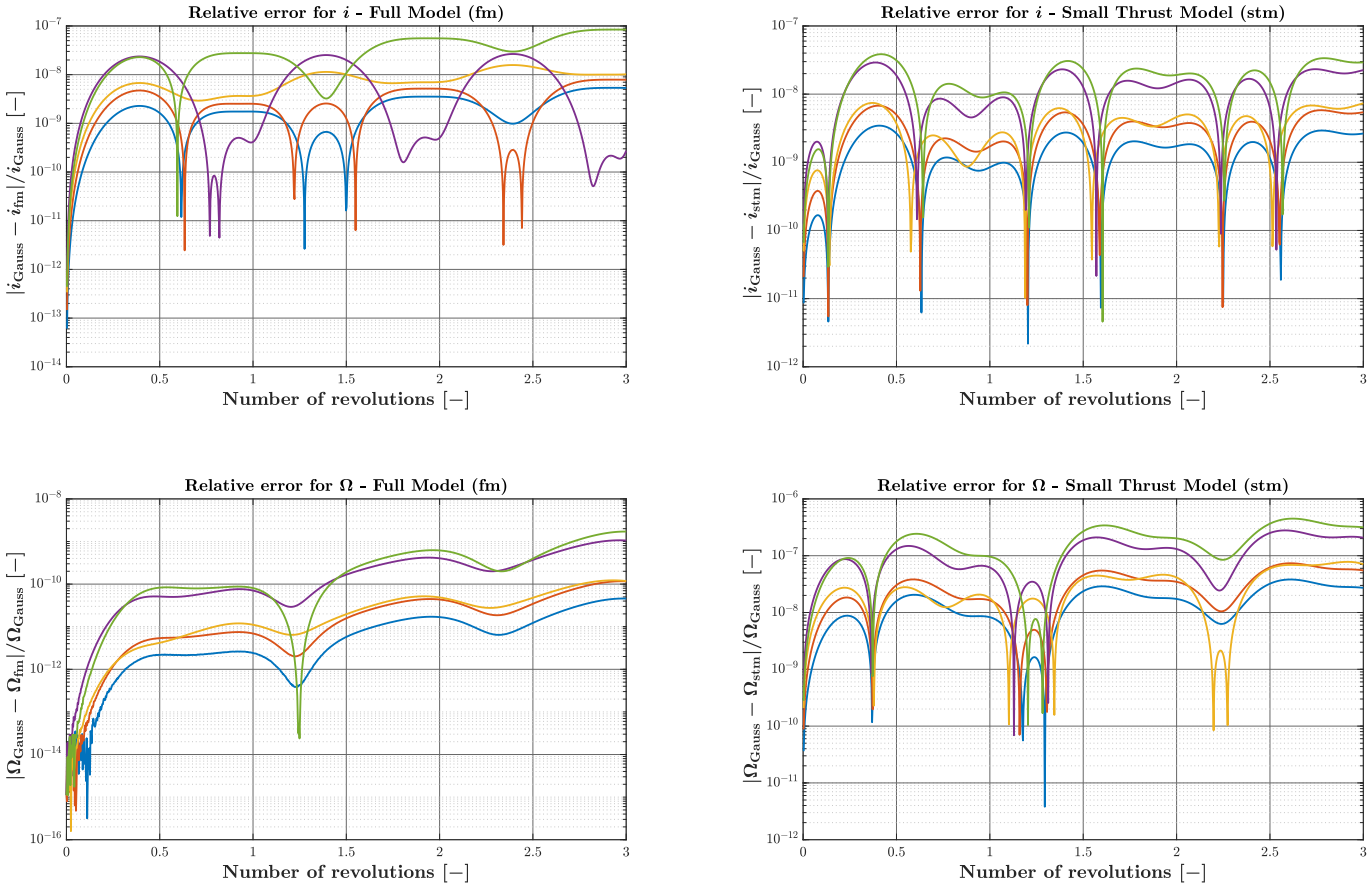

Figure 3.2: f.m. and s.t.m. comparison for i and Ω. Reference orbit in Table 3.1.

In Figure 3.2 we can appreciate analogous results for the inclination and the RAAN. The inclination relative error behaves similarly in both models while for the RAAN it is significantly lower. This is related to the approximation of the eccentricity; in other words, approximating S at order zero affects the inclination, while the RAAN is more influenced by the variation of the semimajor axis.

Finally in Figure 3.3 the results for the argument of perigee and the true anomaly are provided. These behaviours are coherent with those already discussed. In particular, notice that a better approximation of the semimajor axis leads to an increased accuracy in the time law computation and so for the true anomaly.

To better appreciate the difference between the two methods, we report in Table 3.3 the computational elapsed times for both. Notice that for the *full model* it is much higher than for the *small thrust model*. The main reasons are two. First of all, in the full model the Fourier Expansion coefficients have to be evaluated at each simulation while in the *small thrust model* they can be computed once for all at the beginning for the selected reference orbit. The second reason, which is the most heavy in terms of computational time, is that the inversion of the time law requires the solution of a non linear root finding problem.

Table 3.3: Computational times. Reference data Table 3.1.

Case	**Sym. 1**	**Sym. 2**	**Sym. 3**	**Sym. 4**	**Sym. 5**
Time f.m. [s]	1.7759	1.7736	1.7781	1.7768	1.7712
Time s.t.m. [s]	0.6043	0.6034	0.6154	0.5567	0.6657
Time `ode113` [s]	0.0345	0.0360	0.0416	0.0401	0.0415

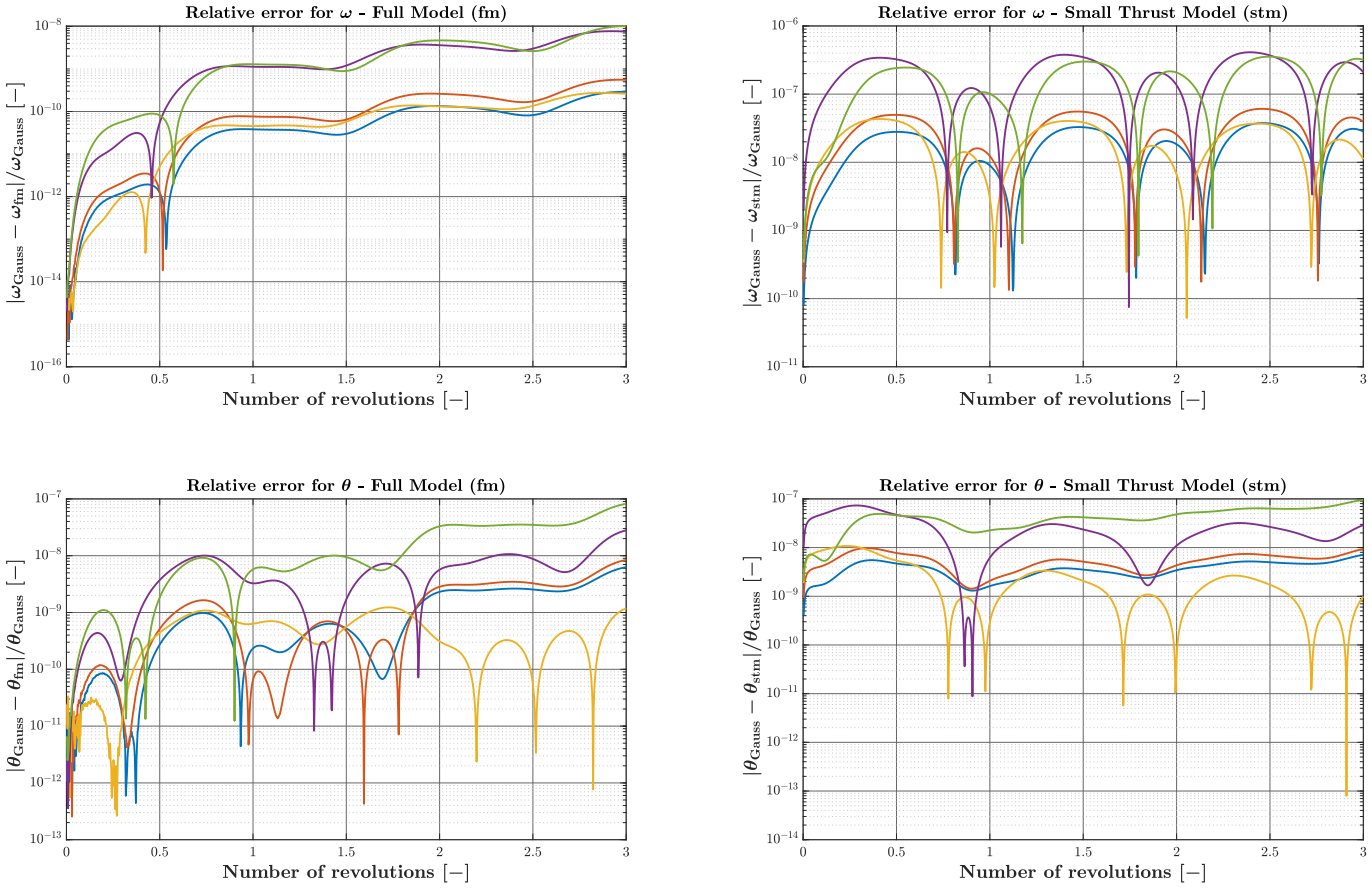

Figure 3.3: f.m. and s.t.m. comparison for ω and θ. Reference orbit in Table 3.1.

The same approach is used for the reference orbit in Table 3.2 and the results are shown in Figure 3.4, Figure 3.6 and Figure 3.7. Notice that for this kind of high elliptical orbit both methods are still capable of achieving a good approximation for the orbital parameters. For a, e, i and θ, the same considerations as previously can be applied.

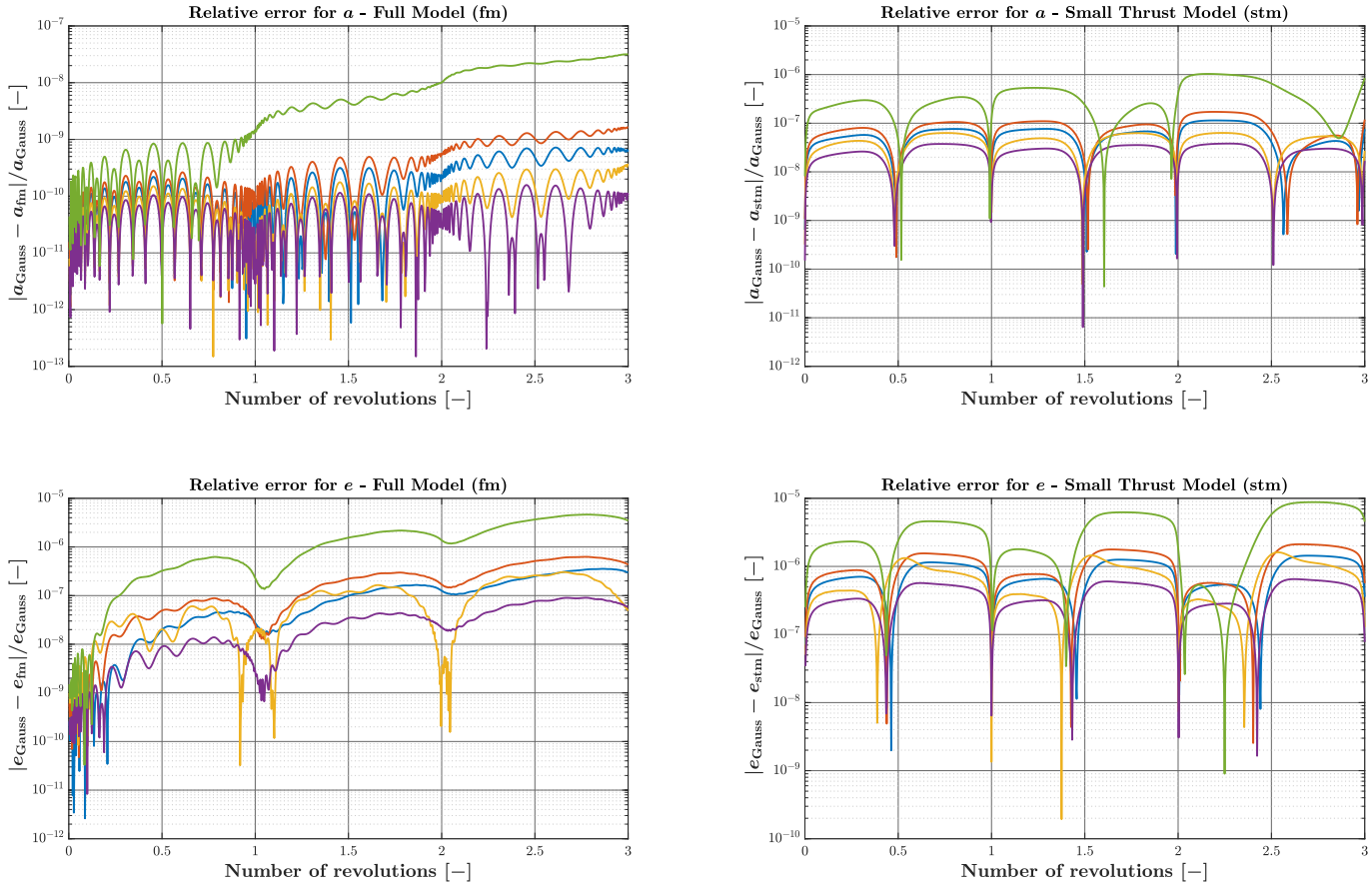

Figure 3.4: f.m. and s.t.m. comparison for i and Ω. Reference orbit in Table 3.2.

For the argument of perigee and the RANN (see Figure 3.6 and Figure 3.7) we can see a better behaviour of the *small thrust model* with respect to the *full model* for some combinations of the thrust actions. This is mainly due to two reasons. The first is that, while in the *full model* the first order approximation for the semimajor axis is used to achieve a better accuracy on itself and in the time law computation, in the *small thrust model* also the orientation problem is solved using such an approximation.

The second, which is more important, is that the functions to be expanded in Fourier Series are very sensible to the reference value of the eccentricity. In other words, the higher is the value of e_0 the higher should be the number of terms of the expansion. This

has two main consequences: the computational time increases a lot (see Table 3.4) and the precision in the numerical integrations for the coefficients decreases. Indeed, as the value of e_0 increases, the functions start to become more and more irregular, as shown in Figure 3.5, till collapsing into a singularity for $e_0 = 1$.

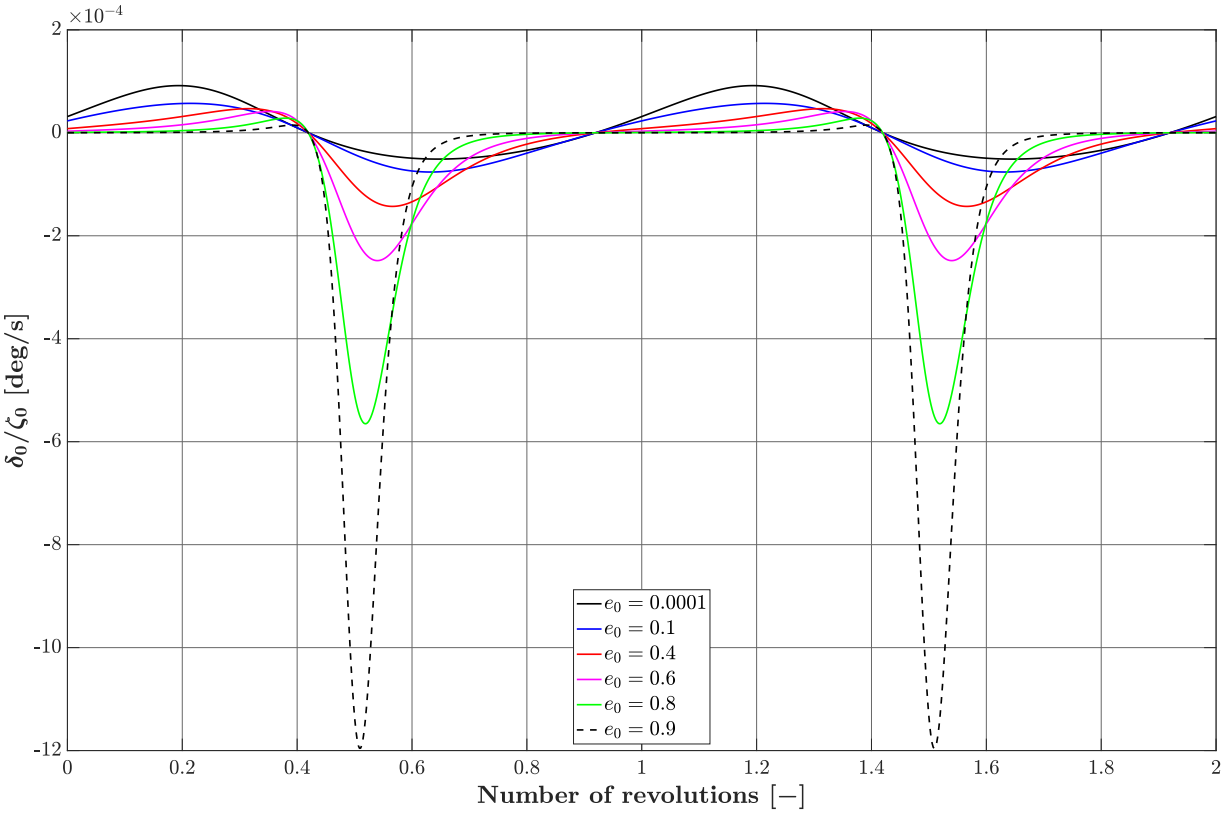

Figure 3.5: Behaviour of $\mathfrak{D}_0(\theta) = \delta_0(\theta)/\zeta_0(\theta)$ for different values of e_0.

This problem is partially overcome in the *small thrust model* because the Fourier coefficients are expressed in closed form. Nevertheless, for high value of eccentricities, the required number of terms increases and this leads to problems in terms of machine precision. For instance referring to Equation 2.4.17, if we want to truncate the series for $\alpha_n[\bar{\bar{S}}_{at,0}]$ up to the 100th term we should compute:

$$\Gamma(1/2 - 100) = 3.37046 \cdot 10^{-157}$$

For such reasons the solution for high eccentricities will be less accurate. Nevertheless, some techniques for series manipulation could be used to deal with such a problem and this could be left to a future development. Finally we report the computational times:

Table 3.4: Computational times for the *full model* and the *low thrust model*. Reference data Table 3.2.

Case	Sym. 1	Sym. 2	Sym. 3	Sym. 4	Sym. 5
Time f.m. [s]	13.4304	13.3951	13.6707	13.3480	13.6472
Time s.t.m. [s]	0.7038	0.7459	0.7177	0.7612	0.6159
Time `ode113` [s]	0.0946	0.0971	0.1060	0.1123	0.1045

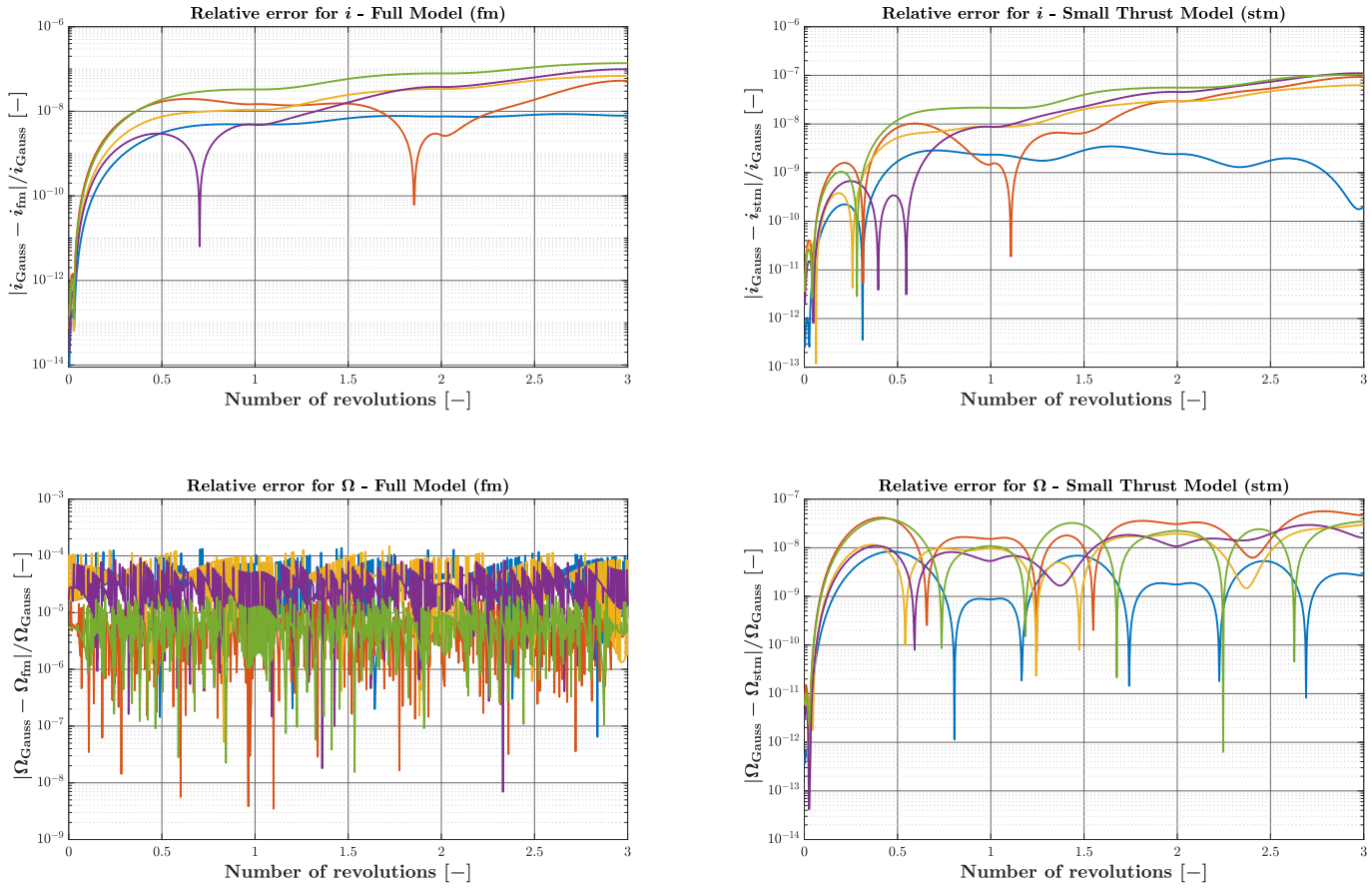

Figure 3.6: f.m. and s.t.m. comparison for i and Ω. Reference orbit in Table 3.2.

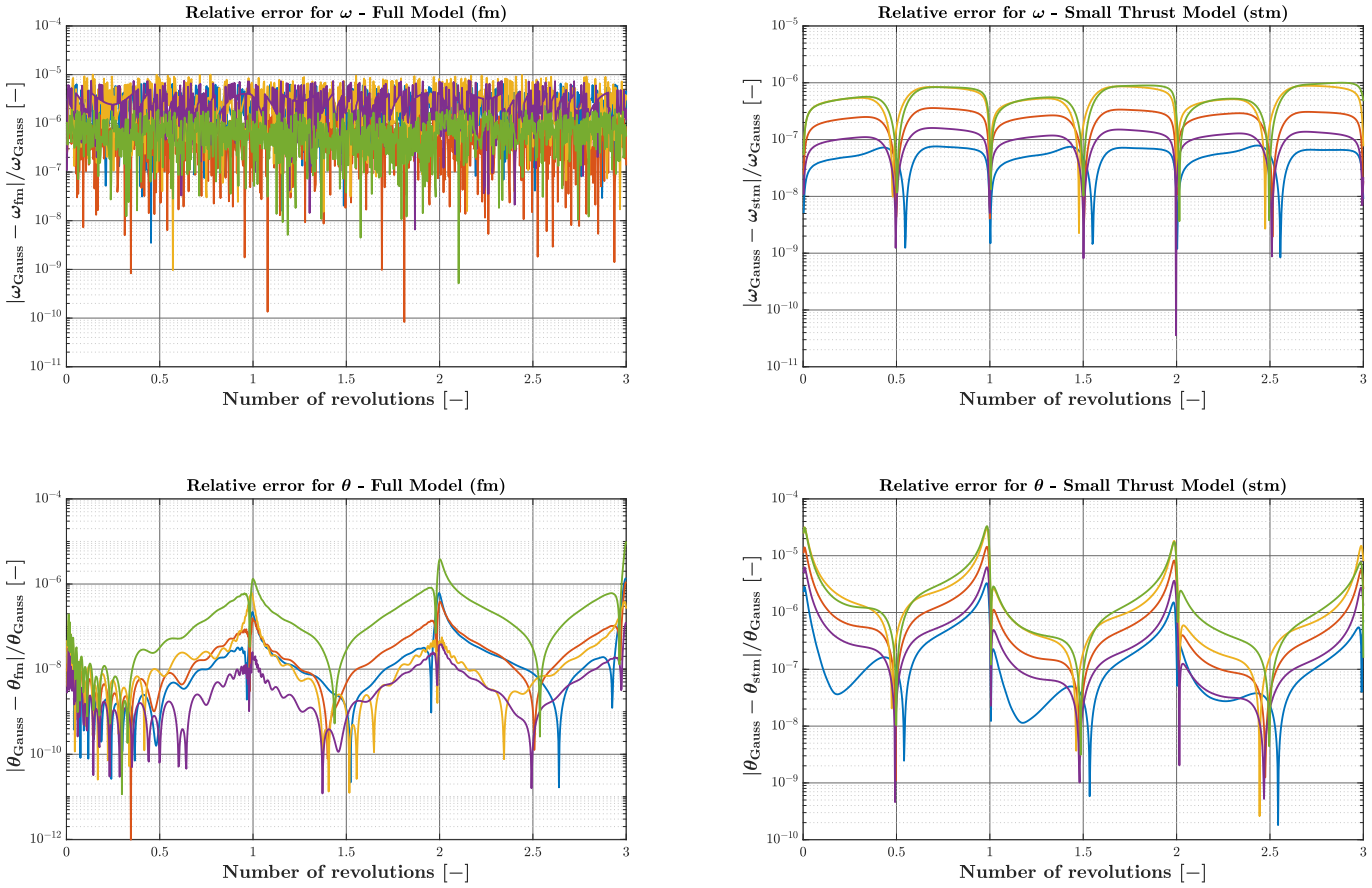

Figure 3.7: f.m. and s.t.m. comparison for i and Ω. Reference orbit in Table 3.2.

As a final remark, notice that the computational times reported in Table 3.3 and Table 3.4 are related to a full orbit propagation using the numerical ODEs solver `ode113` and compared to our semi-analytical methods. Nevertheless, the real advantage of these solutions is that, unlike the numerical method, we do not need to evaluate the entire sampling time-span to obtain the solution at a fixed instant of time. Since we have already seen that the *full model* is computationally very expensive, we now perform a different analysis using the *small thrust model*. We consider two performance parameters: the relative error related to the norm of the position vector at the end of the thrust arc and the computational time needed to compute it. We then did a comparison between `ode113` and the *small thrust*

model for different levels of the trhust vector magnitude and for different values of the reference eccentricity. Operatively, for an assigned thrust magnitude, the corresponding thrust vector components are obtained by multiplying this value for a random number between 0 and 1. The results are shown in Figure 3.8. For the error related to the norm of the position vector the results are satisfactory and show a behaviour like those already seen. The interesting aspect is about the computational time. We can see from the plot that the quantity:

$$\sigma = \frac{t_{\text{stm}} - t_{\texttt{ode113}}}{t_{\texttt{ode113}}}$$

can also assume values in the range 0.8-0.9, meaning that the computational time of our *small thrust model* could also be the $2\% - 1\%$ of the `ode113` computational time. This assesses the accuracy and the efficiency of the method.

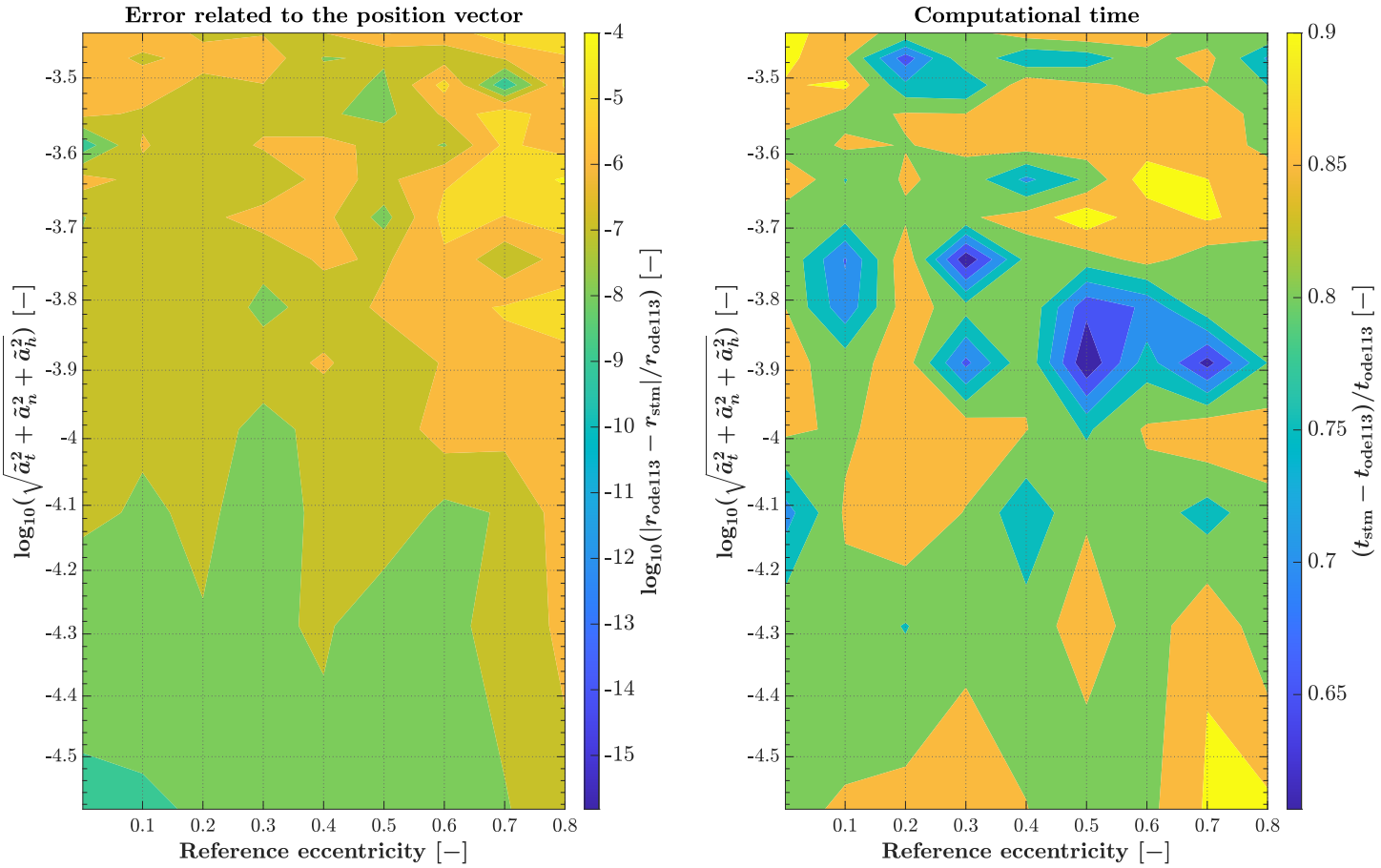

Figure 3.8: `ode113` and s.t.m. comparison: relative error related to the norm of the position vector at the end of the thrust arc and computational times. a_0, i_0, Ω_0, ω_0 as in Table 3.1.

3.3. Preliminary data for the manoeuvres simulations

To carry out the simulations, a reference spacecraft orbit has been selected; the orbital elements at $t = t_0 = 0$ s are:

Table 3.5: Spacecraft nominal orbit: Keplerian elements.

a_0 [km]	e_0 [−]	i_0 [deg]	Ω_0 [deg]	ω_0 [deg]	θ_0 [deg]	T_0 [h]
12000	0.1	30	10	29	0	3.634

The debris trajectory has been built such that at the time of close encounter t_{CA}, the position vector of the spacecraft equates to the position vector of the debris; this is done by solving a suitable Lambert problem. The procedure is the following. First the debris is assumed to be on a virtual orbit and its position vector at t_0 can be computed using the following orbital elements:

Table 3.6: Debris virtual orbit.

$a_{d,in}$ [km]	$e_{d,in}$ [−]	$i_{d,in}$ [deg]	$\Omega_{d,in}$ [deg]	$\omega_{d,in}$ [deg]	$\theta_{d,in}$ [deg]	$T_{d,in}$ [h]
3 a_0	0.03	20	0	0	0	18.8826

Then, considering the time of close approach equal to the orbital period of the reference orbit, namely $t_{CA} = T$, the boundary value problem is built up setting:

$$\boldsymbol{r}_d(t_0) = \boldsymbol{r}_{d,in} \quad \text{and} \quad \boldsymbol{r}_d(t_{CA}) = \boldsymbol{r}_s(t_{CA})$$

where $\boldsymbol{r}_d$ is the position vector of the debris which can be obtained from Table 3.6 and $\boldsymbol{r}_s$ is the position vector of the spacecraft obtained after propagating the reference orbit in Table 3.5. The resulting orbital elements characterizing the debris orbit at $t = t_0$ are:

Table 3.7: Debris orbital elements.

a_d [km]	e_d [−]	i_d [deg]	Ω_d [deg]	ω_d [deg]	θ_d [deg]	T_d [h]
18382	0.9253	23.2080	0	182.6773	177.3227	6.8899

Of course, this kind of procedure to build the debris orbit is fictitious, nevertheless it allows a simple visualization of the problem. For all our simulation cases, we consider that in

the nominal situation the uncertainties are so small that the nominal PoC obtained from calculations is in the range $95\% - 100\%$. This is, of course, not true in practical scenarios because the uncertainties on the position vectors of both objects can have higher values. Nevertheless, they would lead to a lower nominal value of the PoC; the above assumption has then to be seen as a worst case scenario where uncertainties are vary small. Moreover, we assumed the radii of the spherical envelopes for the spacecraft and the debris as reported in Table 3.8.

Table 3.8: Radius of the spacecraft and the debris (spherical envelopes assumption).

ρ_s [m]	ρ_d [m]
3	4

The general simulation procedure consists of the following steps:

1. Select a nominal orbit for the spacecraft (e.g. see Table 3.5).
2. Define the orbit of the debris: i.e. define the time of close approach t_{CA} and compute the trajectory solving the relevant Lambert Problem (e.g. see Table 3.7).
3. Apply Gaussian uncertainties with normalized distribution on both spacecraft and debris trajectories (maximum value[3] assumed to be 1 m) and evaluate also the nominal PoC.
4. Apply the thrust action and the CAM strategy.
5. Evaluate B-plane at encounter point for the nominal CA obtaining $\{\xi_e, 0, \zeta_e\}$.
6. Evaluate the covariance matrix.
7. Extract σ_ξ, σ_ζ and $\rho_{\xi\zeta}$.
8. Evaluate Miss Distance and PoC.

3.4. First case: spacecraft thrusted only tangentially

The first strategy is to perform the CAM by means of the tangential acceleration only, namely $a_n = a_h = 0$. This is a very important scenario because it is the quasi optimal solution in practical applications. The main assumptions are:

[3] coherently to what previously said, this is done to have high PoC values for the direct impact nominal case.

- The manoeuvre is performed in the last orbital revolution of the spacecraft before the close approach.
- The close approach occurs at the end of the nominal orbital period, namely $t_{CA} = T$.
- In the most general case the manoeuvre is organized as: 1 coast arc of duration $k\tau$, 1 thrust arc of duration τ and a final coast arc of duration[4] $T - (k+1)\tau$. Where $k \in [0, 1]$ is a constant parameter and τ is the length of the thrust arc. Notice that varying the k parameter means actually changing the time instant at which the thrust action begins; and so, in other words, the true anomaly θ. In such a framework, the thrust action in the tangential direction a_t is a piecewise function defined as:

$$a_t(t) = \begin{cases} 0 & \text{if} \quad t < k\tau \\ \hat{a}_t & \text{if} \quad k\tau \leq t \leq (1+k)\tau \quad \wedge \quad t \leq T \\ 0 & \text{if} \quad t > (1+k)\tau \end{cases} \tag{3.4.1}$$

  where $\hat{a}_t$ is the assigned value of the thrust action in the tangential direction. We can underline some limit cases:

  1. If $k = 0$ there is no first coast arc ant the CAM consists only in one thrust arc and one final coast arc.
  2. If $k = 0$ and $\tau = T$ there are no coast arcs and the CAM consists only in one thrust arc.
  3. If $k = 0$ and $\tau = t_0$ the CAM reduces to an impulse manoeuvre at the initial time t_0.
  4. $\forall k$ and $\forall \tau$ such that $T - (k+1)\tau < 0$ the CAM consists in one coast arc and one thrust arc.
  5. If $k = 1$ and $\tau = T$ the CAM reduces to an impulsive manoeuvre at TCA.

- The maximum value of the length of the thrust arc is fixed at $\tau_{\max} = T$. This is done to explore all the possible combinations and see if some optimal solution can be achieved.

The main goal of such a simulation is to compute both the PoC and the Miss Distance. In particular, the objective is to determine the optimal values of the tangential thrust magnitude a_t and of the length of the thrust arc τ such that the PoC is less than a certain threshold or equivalently such that the Miss Distance is greater that a certain threshold.

[4] the final coast arc is defined only if $T - (k+1)\tau > 0$.

The main architecture of the simulation is the following:

1. The PoC is built up as function of the three main variables, i.e. $\text{PoC} = \text{PoC}(a_t, \tau, k)$.
2. The parameter k is forced to assume up to 6 values: $k = 0, 0.2, 0.4, 0.6, 0.8, 1$.
3. For each value of k, say $\bar{k}$, the function of two variables $\bar{\text{PoC}} = \text{PoC}(a_t, \tau, \bar{k})$ is obtained.
4. A mesh of the domain formed by the two independent variables a_t and τ is done, i.e. a mesh-grid 80×80.
5. Finally the PoC level lines are obtained for different k values .

In Figure 3.9 the results in terms of the PoC are presented for different values of the parameter k. As we can see, as k increases in magnitude, the region of low PoC decreases in size. Moreover, the 2D contour lines, namely the curves representing the function $\tilde{a}_t = \tilde{a}_t(\tau)$, progressively pass from a monotonically decreasing behaviour to an increasing one. This is even more clear looking to Figure 3.9(6) where minima points are clearly outlined.

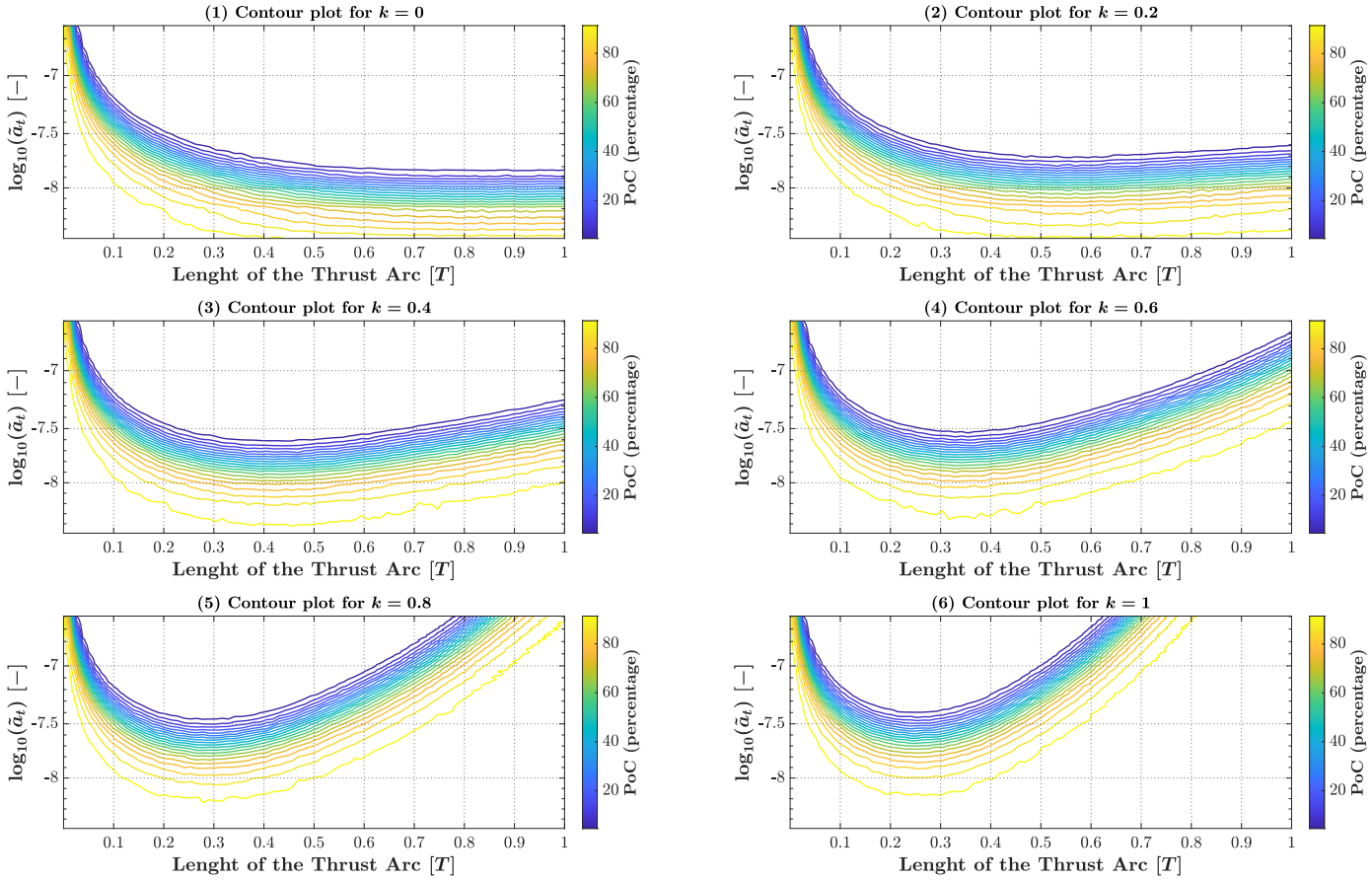

Figure 3.9: Contour plots for different values of the k parameter.

As in literature (see ESA [11] and Aida et al. [14]) the PoC shall be less than 10^{-4}; this is assumed as threshold and the results are shown in Figure 3.10. For $k = 0$ the length of the thrust arc is $\tau = 0.84T$ and the minimum thrust required is approximately $a_t = 0.61 \cdot 10^{-10}$ km/s^2, while as k increases, τ starts to decrease but the thrust level drastically increases, e.g. for $k = 0.8$, a_t is already $1.5 \cdot 10^{-10}$ km/s^2 which is more than twice the case $k = 0$. Therefore, a trade off between the cost of the manoeuvre and the maximum manoeuvring time to avoid operational problems has to be performed.

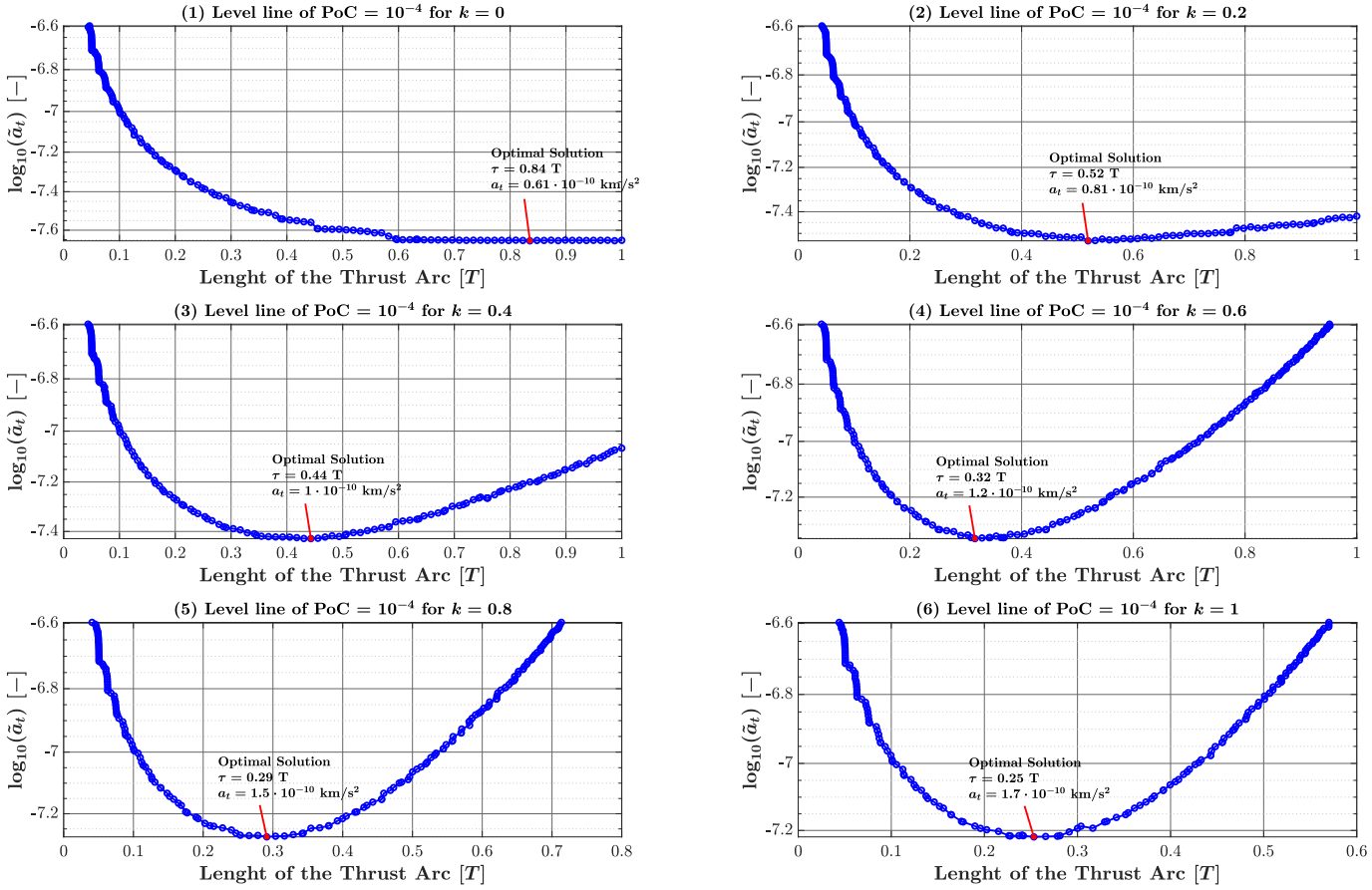

Figure 3.10: Level lines for fixed PoC for different values of the k parameter.

To assess the accuracy of the semi-analytical approximation (subscript sa), we define the following relative errors:

$$\text{err}(a) = \left| \frac{a_{\text{num}} - a_{\text{sa}}}{a_{\text{num}}} \right|, \quad \text{err}(e) = \left| \frac{e_{\text{num}} - e_{\text{sa}}}{e_{\text{num}}} \right|$$

which are the errors over the semimajor axis and eccentricity, respectively. Notice that both a and e vary with time and so, from a computational point of view, we will consider the maximum error over the overall time span, e.g. for a we have:

$$\text{err}_{\text{eval}} = \max([a(t_1), a(t_2), \dots a(t_i)])$$

where t_i is the i-th time instant of which the sampling time is subdivided. In Figure 3.11 the results of the analysis are presented. Coherently to what was seen in Section 3.2-Figure 3.1 the approximation works better for short thrust arcs and low thrust actions

(blue zone) while it decreases in accuracy for higher values (worst accuracy in the yellow-orange zone). Nevertheless, the results are still accurate and this assesses the effectiveness of our semi-analytical solution.

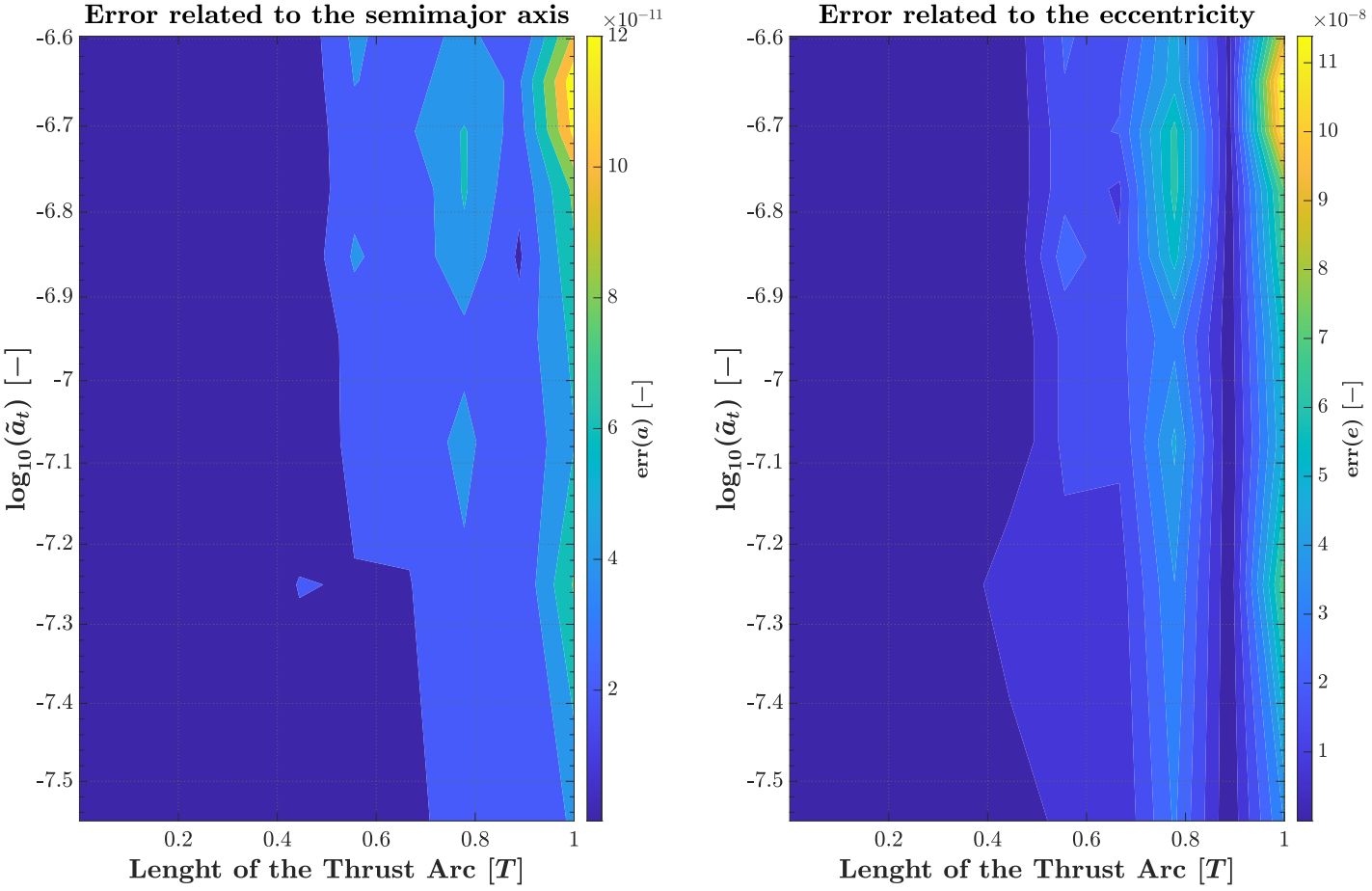

Figure 3.11: Contour plots for the relative errors related a and e.

For completeness we report the results of the analysis with the same reference data in Table 3.5 but with $e_0 = 0.8$. Comparing Figure 3.12 with Figure 3.10 we can see that the minimum thrust level required to achieve the PoC threshold is lower. Comparing Figure 3.13 with Figure 3.11 the error in the orbital parameters estimation is higher in agreement with the results already presented in Section 3.2-Figure 3.4.

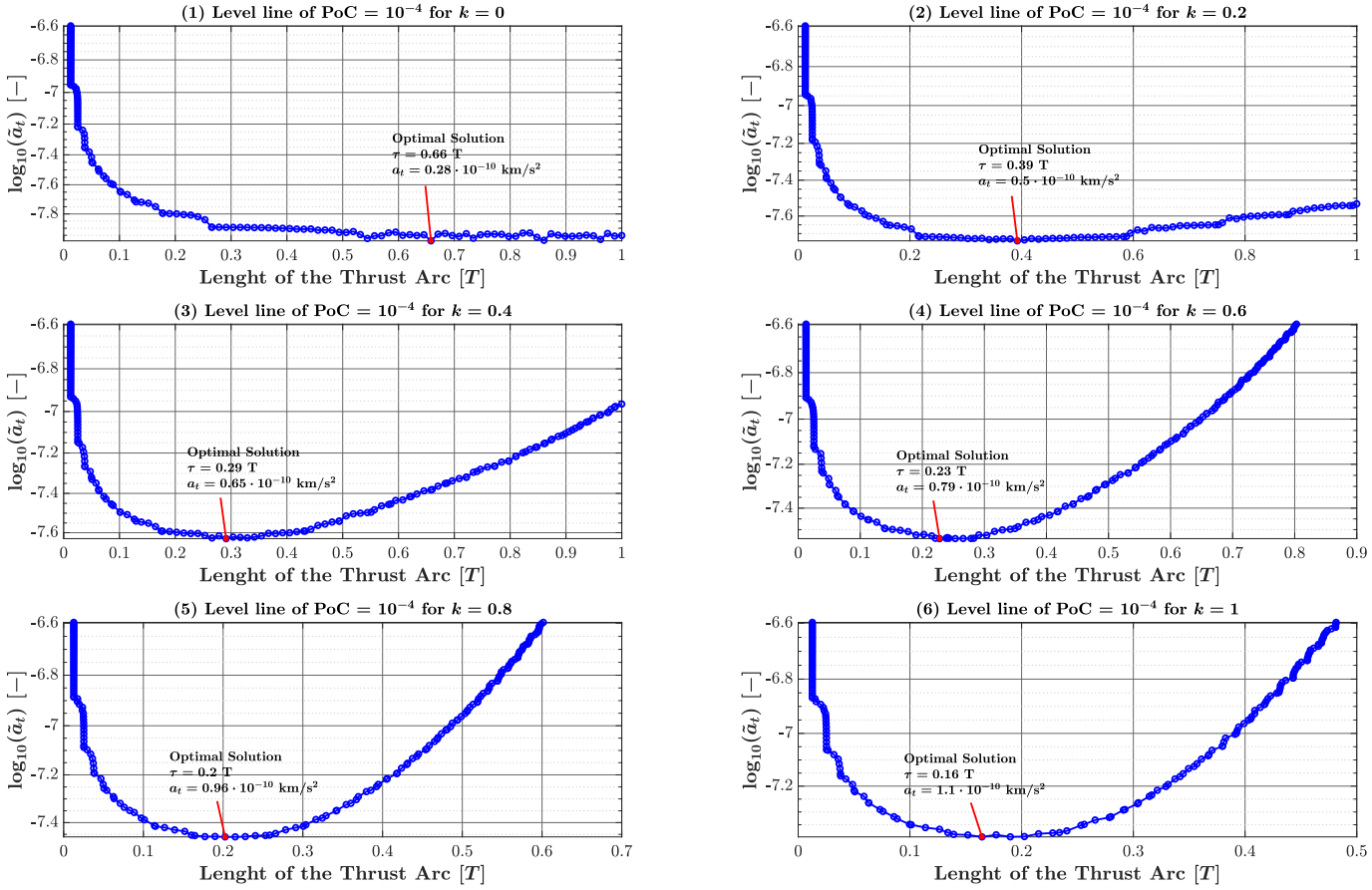

Figure 3.12: Level lines for fixed PoC for different values of the k parameter with $e_0 = 0.8$.

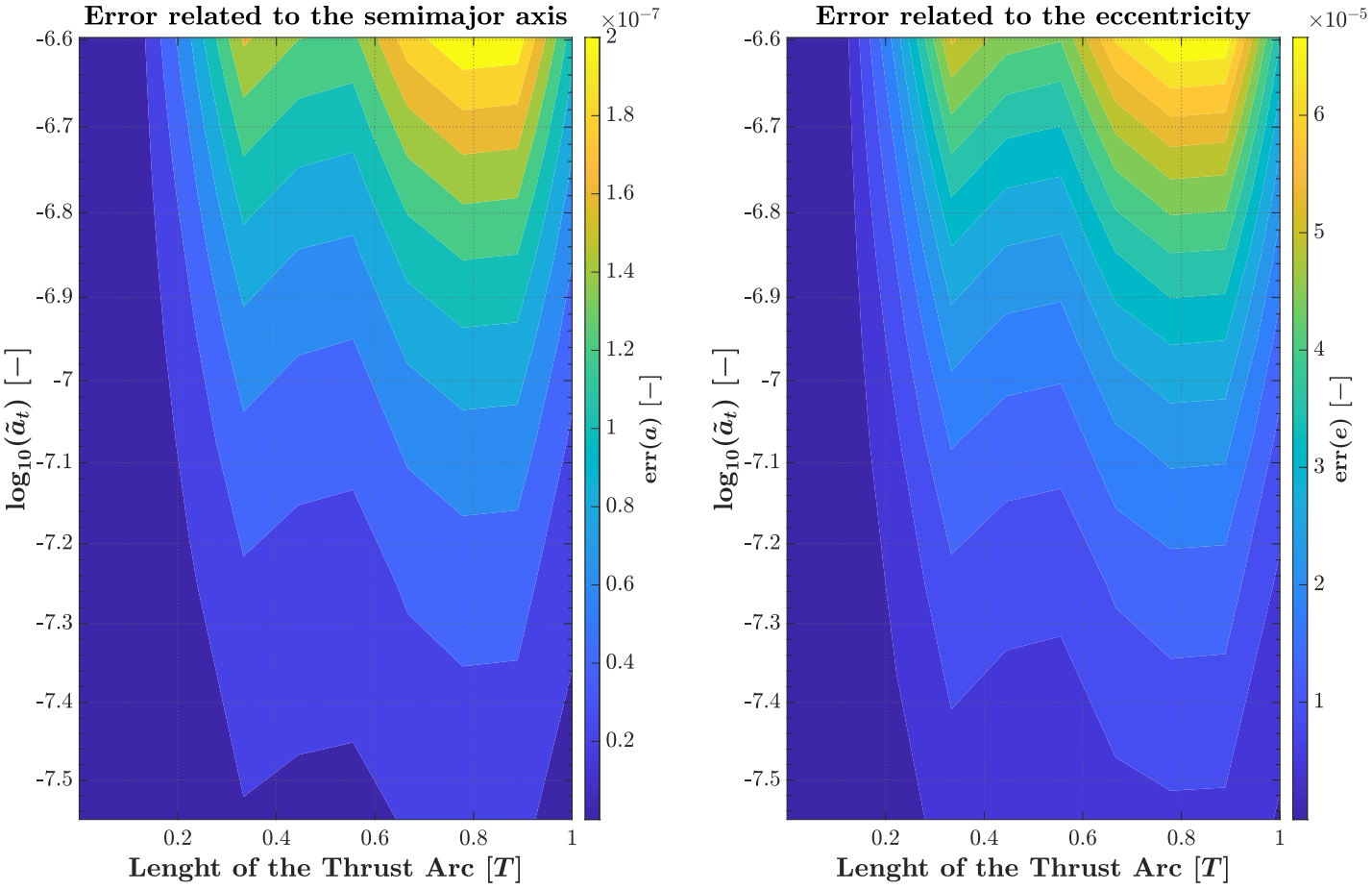

Figure 3.13: Contour plots for the relative errors related a and e with $e_0 = 0.8$.

3.5. Second case: spacecraft thrusted in tangential and normal directions

Similarly to what was done in Section 3.4, we now proceed to analyse the case where both the tangential and the normal thrust actions are applied. The reference values for the spacecraft orbit adopted for these simulations are those of Table 3.5. Moreover, we considered a large interval of values of a_n thrust action. Of course this is not for some practical interest because the optimal CAM is typically nearly tangential, but this allows to visualize better the results. In Figure 3.14 and Figure 3.15 the contour plots of the PoC as a function of both thrust levels are presented. In particular, in Figure 3.14 we considered the case with $k = 0$ and we evaluated the PoC for different values of τ. The same procedure is followed setting $k = 0.6$ and the results are shown in Figure 3.15. In both figures we can see that the PoC decreases faster as the value of τ increases. On the

other hand, for a fixed value of τ the contour lines are actually similar to ellipses: the maximum PoC is reached in correspondence of the smaller ellipses while the minimum PoC is reached in correspondence to the bigger ones.

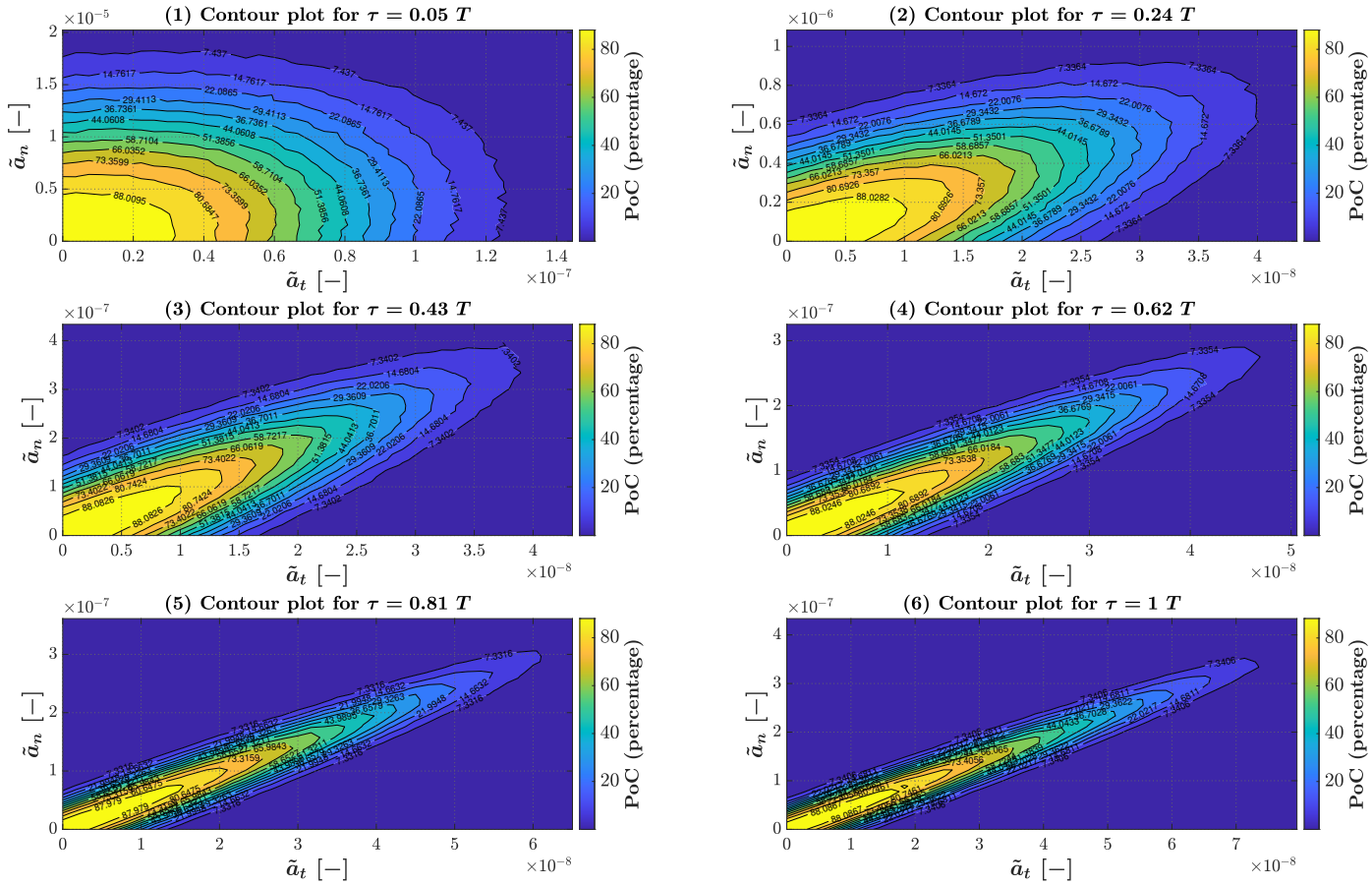

Figure 3.14: Contour Plots for different values of τ and for $k = 0$.

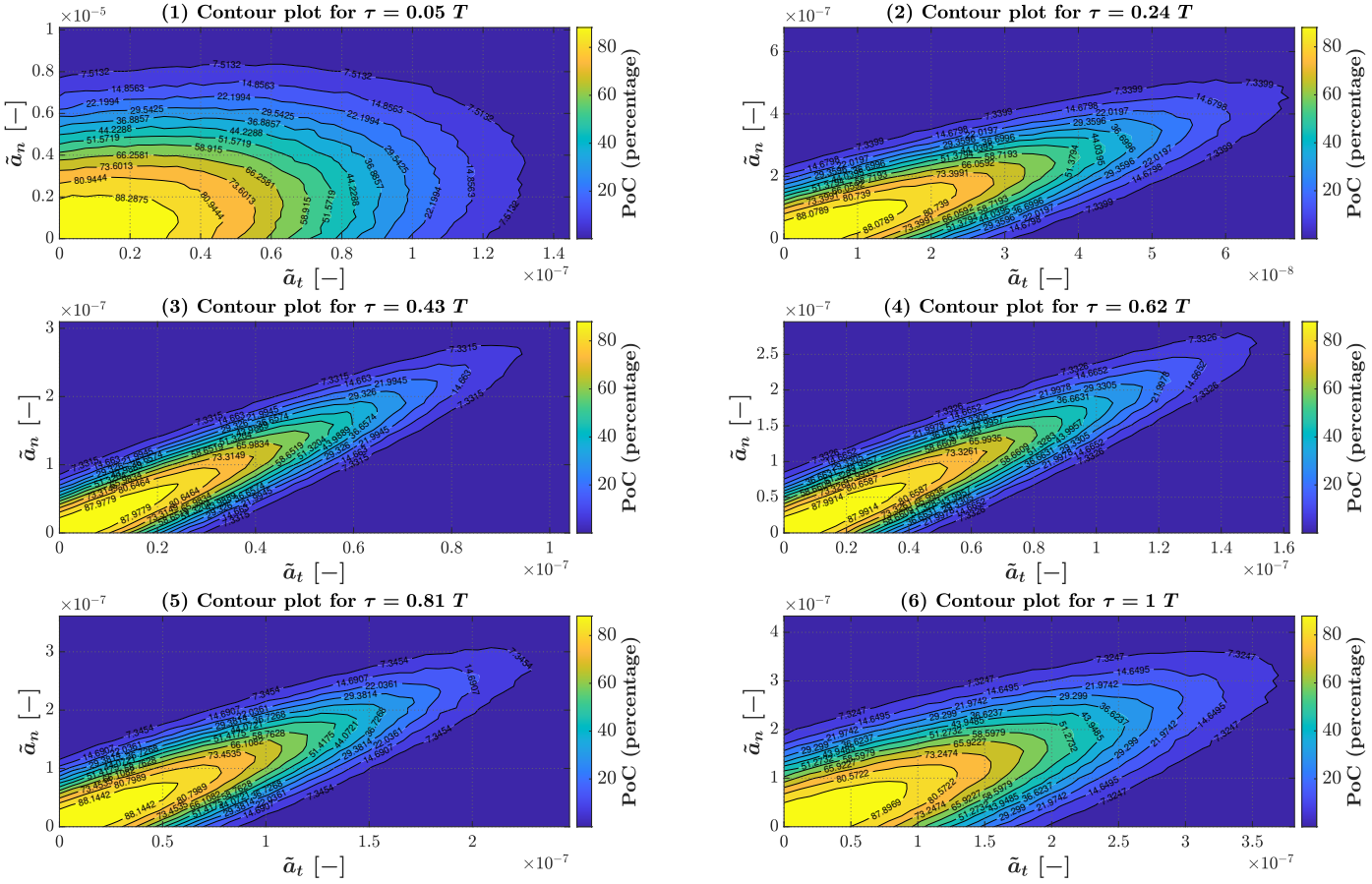

Figure 3.15: Contour Plots for different values of τ and for $k = 0.6$.

To better understand such a behaviour, we present the same results in a different fashion in Figure 3.16 and Figure 3.17. Here the level lines are displayed as a function of the norm of the thrust vector and the angle that the latter forms with respect to the tangential direction. Notice that, the norm of the thrust vector linearly increases for a big interval of angles and then starts increasing till it reaches a maximum. In other words the lowest thrust levels are reached with a pure tangential action and the higher thrust levels are reached with high normal accelerations. The region in-between could be very interesting if the propulsion system is not capable of providing the required tangential action. Indeed the increasing linear behaviour has a small rate of change before entering the critical zone dominated by the normal acceleration. Finally notice that as k and τ increase the contribution of the normal acceleration also increase till the limit case where $k = 1$ shown in Figure 3.16(6) and Figure 3.17(6). This means that, progressively, we are meeting the condition of last-minute CAM. Indeed, as already said in Section 3.4-Equation 3.4.1, if

we consider the case $k = 1$ and $\tau > 2T/3$ this means that the length of the thrust arc is $\tau = T/3$ which correspond with the remaining time before the CA.

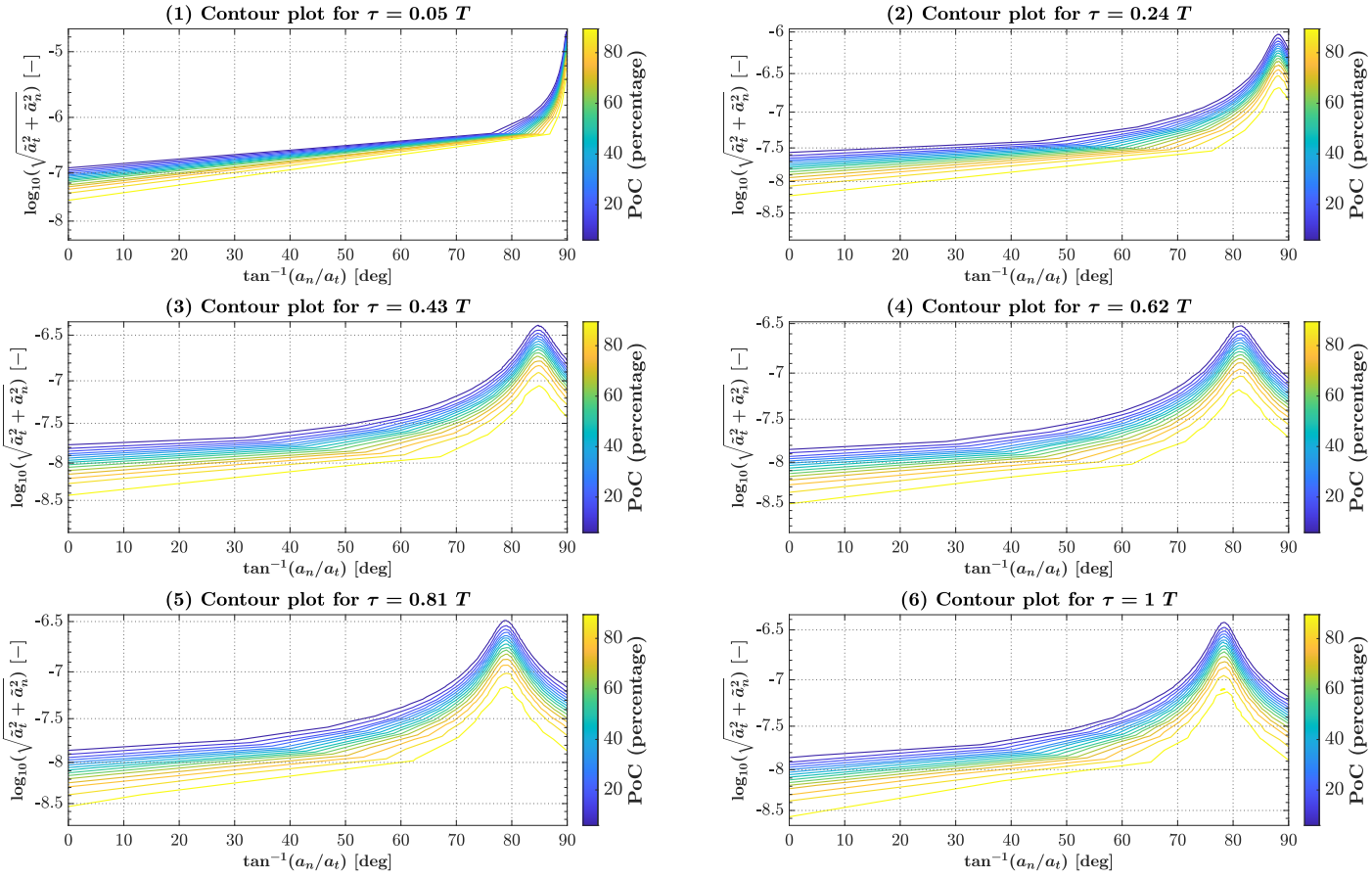

Figure 3.16: Level lines when the independent variables are switched to the norm of the thrust vector and the angle with respect to the tangential direction (for $k = 0$).

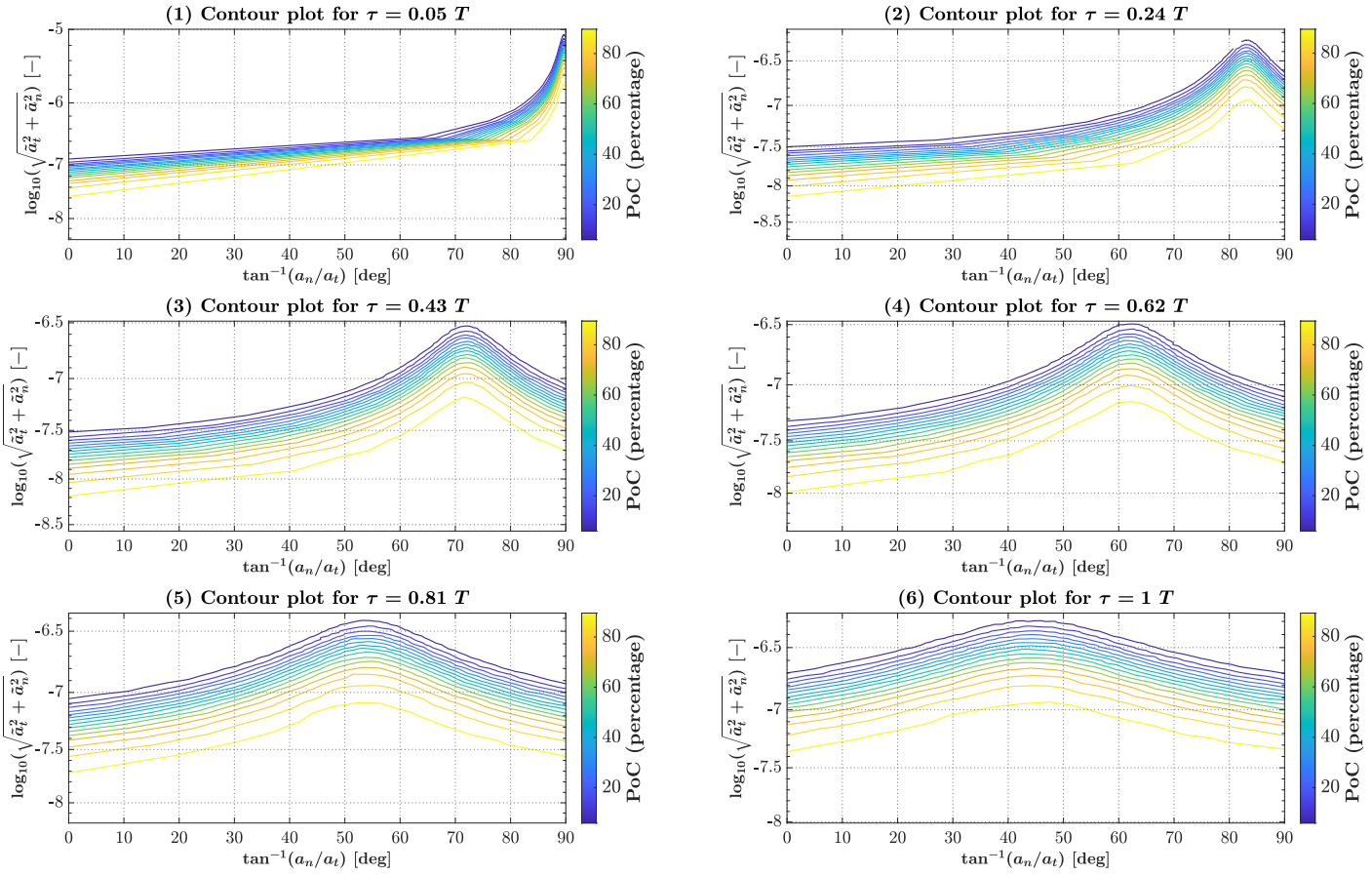

Figure 3.17: Level lines when the independent variables are switched to the norm of the thrust vector and the angle with respect to the tangential direction (for $k = 0.6$).

4 | Conclusions

In this work we developed a semi-analytical mathematical model for the 3D low thrust collision avoidance problem. The Gauss Planetary Equations are reduced to a simpler form by means of a Taylor expansion in the neighbourhood of the reference condition. Two different methods are developed: the first, denoted as *full model*, where the main functions are complicated non linear relations of the thrust accelerations and the second, denoted as *small thrust model*, which, on the contrary, has an explicit dependency from the small thrust parameters. All the integrations are performed by means of the Fourier Series tool and for the *small thrust model* the expressions of the Fourier Series coefficients are provided in closed form also involving the Gauss Hypergeometric function. Different simulations with various test cases to assess the effectiveness of the method are provided. By comparison with numerical outputs, both models are capable of reproducing accurately the solution of the Gauss Planetary Equations. In particular, for not too high eccentricity reference values, the solution provided by the *full model* has a by far greater accuracy for the semimajor axis and the true anomaly, specially if the first period is assumed as time span. On the contrary, the *small thrust model* even if less accurate, is nevertheless capable of granting an acceptable precision and a remarkable reduction of computational time. And this becomes even more evident considering higher eccentricities. In this case we would have a lower performance as it concerns accuracy: nevertheless knowing the closed form expressions of Fourier coefficients, the *small thrust model* succeeds to be more efficient in accuracy and elapsed time with respect to the *full model*. Then, the trade off chose the *small thrust model* as the winner. For both methods the greater computational expense occurs in time law inversion when solving a non linear root finding problem. One of the best computational qualities of these methods is that they allow to evaluate the orbital parameters (and then the state vector) at the wished instant of time without passing through the previous ones, what is convenient in PoC computing and in CAMs design. Two sample tests have been provided. In the first, only the tangential thrust is active; in the second there is also the normal component too. In both cases, beyond a good PoC evaluation, the *small thrust model* has been seen to provide a satisfactory approximation of orbital parameters.

Future developments

This thesis opens to a variety of future developments.
First, a possible technique to provide the time law inversion could be obtained following the procedure proposed by Bocci et. al [36] and [37]. This would lead to a remarkable gain in computational time because the non linear root finding problem would be substituted by a convergent series providing $\theta = \theta(t)$.
Moreover, some techniques for series manipulation could be used to deal with the problem of machine precision in the computation of the Fourier Series coefficients of the *small thrust model*. Both *full model* and *small thrust model* could be adopted for approximating a generic low thrust problem, not necessary a CAM one. For both models, some simulations show that there are regions where the error is slightly higher with relative low thrust action and higher length of the thrust arc. This is due to the first order approximation done for some of the orbital parameters. Indeed, referring for instance to Equation 2.4.11, if $\tilde{a}_t \to 0$ then $k_a \to 0$. Therefore substituting into Equation 2.3.15 it is easy to see that the function multiplying the exponential term diverges. This problem is solved merging those regions with the zero order solution Equation 2.3.8 which works perfectly for $\tilde{a}_t = 0$. Nevertheless the transition part from a sufficiently high thrust level and the null one is a little less accurate.
All these proposed refinements are the preamble for the biggest challenge as future development: optimize the method such that it could be implemented on-board. Finally, one of the most important assumptions we made is that no environmental perturbations are acting on the spacecraft. This is not true in reality. Typically, the satellite motion is perturbed by the solar radiation pressure, the drag due to Earth atmosphere and the effect of earth oblateness (i.e. the J_2 effect). These should be added to include non Keplerian orbits in the model.

Bibliography

[1] Union of Concerned Scientists, "UCS Satellite Database." https://www.ucsusa.org/resources/satellite-database.

[2] ESA, "The current state of space debris." https://www.esa.int/Safety_Security/Space_Debris/The_current_state_of_space_debris.

[3] IADC, "What's IADC." https://www.iadc-home.org/what_iadc.

[4] NASA, "Orbital Debris Program Office (ODPO)." https://orbitaldebris.jsc.nasa.gov.

[5] NASA, "NASA's efforts to mitigate the risks posed by orbital debris." https://oig.nasa.gov/docs/IG-21-011.pdf.

[6] ESA, "ESA's Space Environment Report 2022." https://www.esa.int/Safety_Security/Space_Debris/ESA_s_Space_Environment_Report_2022.

[7] ESA, "Space debris 2017 - a journey to Earth." https://www.esa.int/ESA_Multimedia/Videos/2017/04/Space_debris_2017_-_a_journey_to_Earth.

[8] B. Reihs, F. Mclean, S. Lemmens, K. Merz, and H. Krag, "Analysis of CDM covariance consistency in operational collision avoidance," in *Proceedings of the 7th European Conference on Space Debris, Darmstadt, Germany*, pp. 18–21, 2017.

[9] R. Book, "Conjunction data message." https://public.ccsds.org/Pubs/508x0b1e2s.pdf, 2013.

[10] T. Uriot, D. Izzo, J. Martinez-Heras, F. Letizia, J. Siminski, and K. Merz, "Collision Avoidance Challenge dataset." https://zenodo.org/record/4463683#.YptYgy0QOPF.

[11] ESA, "Dodging debris to keep satellites safe." https://www.esa.int/ESA_Multimedia/Videos/2021/04/Dodging_debris_to_keep_satellites_safe.

[12] S. Dural, U. Tugcular, and B. Daser, "General Collision Avoidance Maneuver Decision Algorithm." https://conference.sdo.esoc.esa.int/proceedings/sdc8/paper/156/SDC8-paper156.pdf.

[13] J. L. Gonzalo, C. Colombo, and P. Di Lizia, "Introducing miss, a new tool for collision avoidance analysis and design," *Journal of Space Safety Engineering*, vol. 7, no. 3, pp. 282–289, 2020.

[14] S. Aida, M. Kirschner, and R. Kiehling, "Collision avoidance operations for leo satellites controlled by gsoc," in *SpaceOps 2010 Conference Delivering on the Dream Hosted by NASA Marshall Space Flight Center and Organized by AIAA*, p. 2298, 2010.

[15] R. Abay, "Collision avoidance dynamics for optimal impulsive collision avoidance maneuvers," in *2017 8th International Conference on Recent Advances in Space Technologies (RAST)*, pp. 263–271, IEEE, 2017.

[16] L. Sánchez Fernández-Mellado and M. Vasile, "AI for autonomous CAM execution," in *71st International Astronautical Congress*, 2020.

[17] J. Crassidis, P. Singla, K. McConky, and M. Sudit, "Space collision avoidance," in *Proceedings of National Symposium on Sensor and Data Fusion*, 2011.

[18] J. A. Pulido Cobo, N. Sánchez Ortiz, I. Grande Olalla, and K. Merz, "CORAM: ESA's collision risk assessment and avoidance manoeuvres computation tool," in *Conference: Conference: 2nd IAA Conference on Dynamics and Control of Space Systems, At Rome*, 2014.

[19] J. Hernando-Ayuso, C. Bombardelli, and J. L. Gonzalo, "Occam: Optimal computation of collision avoidance maneuvers," in *6th International Conference on Astrodynamics Tools and Techniques (ICATT)*, 2016.

[20] J. L. Gonzalo and C. Colombo, "Collision avoidance algorithms for space traffic management applications," in *71st International Astronautical Congress (IAC 2020)*, pp. 1–8, 2020.

[21] C. Bombardelli, "Analytical formulation of impulsive collision avoidance dynamics," *Celestial Mechanics and Dynamical Astronomy*, vol. 118, no. 2, pp. 99–114, 2014.

[22] C. Bombardelli, J. Hernando-Ayuso, and R. García-Pelayo, "Collision avoidance maneuver optimization," *Advances in the Astronautical Sciences*, vol. 152, no. 7402, pp. 1857–1870, 2014.

[23] C. Bombardelli and J. Hernando-Ayuso, "Optimal impulsive collision avoidance in low earth orbit," *Journal of Guidance, Control, and Dynamics*, vol. 38, no. 2, pp. 217–225, 2015.

[24] B. A. Conway, "Near-optimal deflection of earth-approaching asteroids," *Journal of Guidance, Control, and Dynamics*, vol. 24, no. 5, pp. 1035–1037, 2001.

[25] J. L. Gonzalo, C. Colombo, and P. Di Lizia, "Analytical framework for space debris collision avoidance maneuver design," *Journal of Guidance, Control, and Dynamics*, vol. 44, no. 3, pp. 469–487, 2021.

[26] M. Vasile and C. Colombo, "Optimal impact strategies for asteroid deflection," *Journal of Guidance, Control, and Dynamics*, vol. 31, no. 4, pp. 858–872, 2008.

[27] K. Dharmarajan, G. Palmerini, and M. Sabatini, "Collision avoidance for satellites in formation flying," *Advances in Astronautical Sciences*, vol. 173, pp. 24–37, 2020.

[28] G. Slater, S. M. Byram, and T. Williams, "Collision avoidance for satellites in formation flight," *Journal of Guidance, Control, and Dynamics*, vol. 29, no. 5, pp. 1140–1146, 2006.

[29] J. A. Reiter and D. B. Spencer, "Solutions to rapid collision-avoidance maneuvers constrained by mission performance requirements," *Journal of Spacecraft and Rockets*, vol. 55, no. 4, pp. 1040–1048, 2018.

[30] C. Colombo, M. Vasile, and G. Radice, "Semi-analytical solution for the optimal low-thrust deflection of near-earth objects," *Journal of Guidance, Control, and Dynamics*, vol. 32, no. 3, pp. 796–809, 2009.

[31] J. L. Gonzalo, C. Colombo, and P. Di Lizia, "A semi-analytical approach to low-thrust collision avoidance manoeuvre design," in *70th International Astronautical Congress (IAC 2019)*, pp. 1–9, 2019.

[32] ERC and Politecnico di Milano, "Control for Orbit Manoeuvring through Perturbations for Application to Space Systems." https://www.compass.polimi.it.

[33] J. L. Gonzalo and C. Colombo, "Lightweight algorithms for collision avoidance applications," in *11th International ESA Conference on Guidance, Navigation & Control Systems, ESA GNC & ICATT 2021*, pp. 1–15, 2021.

[34] J. L. Gonzalo, C. Colombo, and P. Di Lizia, "Computationally efficient approaches for low-thrust collision avoidance activities," in *72nd International Astronautical Congress (IAC 2021)*, pp. 1–10, 2021.

[35] Y. Gao, "Near-optimal very low-thrust earth-orbit transfers and guidance schemes," *Journal of Guidance, Control, and Dynamics*, vol. 30, no. 2, pp. 529–539, 2007.

[36] A. Bocci and G. M. Scarpello, "Analytic inversion of closed form solutions of the satellite's J_2 problem," *Asian Research Journal of Mathematics*, vol. 17, no. 5, pp. 50–68, 2021.

[37] A. Bocci and G. M. Scarpello, "The Differential Equations of Gravity-free Double Pendulum: Lauricella Hypergeometric Solutions and Their Inversion," *Asian Research Journal of Mathematics*, vol. 18, no. 3, pp. 1–18, 2022.

[38] L. J. Slater, *Generalized hypergeometric functions*. Cambridge university press, 1966.

[39] I. Gradshteyn and I. Ryzhik, *Tables of Integrals, Series, and Products*. Academic Press, 2007.

[40] F. K. Chan *et al.*, *Spacecraft collision probability*. Aerospace Press El Segundo, CA, 2008.

[41] J. Dutka, "The early history of the hypergeometric function," *Archive for History of Exact Sciences*, pp. 15–34, 1984.

A | Appendix A

We recall here the basic ideas about the Gauss Hypergeometric function. The first hypergeometric series appeared in the Wallis's *Arithmetica infinitorum* (1656):

$$ {}_2F_1(a,b;c;x) = 1 + \frac{a\cdot b}{1\cdot c}x + \frac{a\cdot(a+1)\cdot b\cdot(b+1)}{1\cdot 2\cdot c\cdot(c+1)}x^2 + \cdots , $$

for $|x| < 1$ and real parameters a, b, c. The product of n factors:

$$ (\lambda)_n = \lambda\,(\lambda+1)\cdots(\lambda+n-1)\,, $$

called *Pochhammer symbol* (or *truncated factorial*TESIFINE) allows to write ${}_2F_1$ as:

$$ {}_2F_1(a,b;c;x) = \sum_{n=0}^{\infty} \frac{(a)_n\,(b)_n}{(c)_n}\frac{x^n}{n!}. $$

A meaningful contribution on various ${}_2F_1$ topics is ascribed to Euler[1]; but he does not seem Dutka [41] to have known the integral representation:

$$ {}_2F_1(a,b;c;x) = \frac{\Gamma(c)}{\Gamma(a)\Gamma(c-a)}\int_0^1 \frac{u^{a-1}(1-u)^{c-a-1}}{(1-xu)^b}\,\mathrm{d}u, $$

really due to A. M. Legendre[2]. The above integral relationship is true if $c > a > 0$ and for $|x| < 1$, even if this limitation can be discarded thanks to the analytic continuation.

[1] We quote three works: a) *De progressionibus transcendentibus*, Op. omnia, S.1, vol. 28; b) *De curva hypergeometrica* Op. omnia, S.1, vol. 16; c) *Institutiones Calculi integralis*, 1769, vol. II

[2] A. M. Legendre, *Exercices de calcul intégral*, II, quatriéme part, sect. 2, Paris 1811

B | Appendix B

Let us consider the following function of the variable x:

$$f(x) = \frac{g(x)}{h(x)} \tag{B.0.1}$$

where:

$$g(x) = \sqrt{1 + \alpha \cos(x)} \quad \text{and} \quad h(x) = [1 + \beta \cos(x)]^2 \tag{B.0.2}$$

clearly expanding in MacLaurin series $f(x)$ and obtaining a recurrence relation for the coefficients is impossible. Nevertheless, we could expand f in MacLaurin series considering as variable the $\cos(x)$, then the resulting expansion will be:

$$f[\cos(x)] = \sum_{k=0}^{+\infty} a_k \cos^k(x) \tag{B.0.3}$$

Let be for simplicity $\cos(x) = X$, referring to [39] formula 1.110 and formula 1.112-2 pag. 25 respectively, the MacLaurin expansion of f and $1/h$ are:

$$g(X) = \sqrt{1 + \alpha X} = \sum_{n=0}^{+\infty} \alpha^n \binom{1/2}{n} X^n \tag{B.0.4}$$

$$\frac{1}{h(X)} = (1 + \beta X)^{-2} = \sum_{n=0}^{+\infty} (-\beta)^n (1 + n) X^n \tag{B.0.5}$$

Where we denote with $\binom{p}{q}$ the binomial coefficient. The convolution is obtained by means of the Cauchy Product theorem for the power series:

Theorem B.0.1 (Convolution of two power series). Let:

$$\sum_{n=0}^{+\infty} a_n \quad \text{and} \quad \sum_{n=0}^{+\infty} b_n$$

be two infinite series with complex terms. The Cauchy product of these two infinite series is defined by a discrete convolution as follows:

$$\left(\sum_{n=0}^{+\infty} a_n\right) \cdot \left(\sum_{n=0}^{+\infty} b_n\right) = \sum_{n=0}^{+\infty} \sum_{k=0}^{n} a_k b_{n-k} \tag{B.0.6}$$

By applying Equation B.0.6 to the product of Equation B.0.4 and Equation B.0.5 we have:

$$\frac{g(X)}{h(X)} = \sum_{n=0}^{+\infty} \left[\sum_{k=0}^{n} (-1)^k (1+k) \binom{1/2}{n-k} \left(\frac{\beta}{\alpha}\right)^k \right] \alpha^n X^n \tag{B.0.7}$$

Now we recall some important properties:

Definition B.0.1. For the binomial coefficient it holds the following properties:

$$\binom{p}{q} = \frac{(p-q+1)_r}{(q-r+1)_r} \binom{p}{q-r} \tag{B.0.8}$$

$$\binom{p}{q} = \frac{p!}{q!(p-q)!} = \frac{\Gamma(p+1)}{\Gamma(q+1)\Gamma(p-q+1)} \tag{B.0.9}$$

Definition B.0.2. For the rising factorial it holds the following properties:

$$(p)_q = q! \binom{p+q-1}{q} \tag{B.0.10}$$

$$(p)_q = \frac{\Gamma(p+q)}{\Gamma(p)} \tag{B.0.11}$$

Where we denote with $(p)_q$ the rising factorial, with $p!$ the factorial and with Γ the Gamma function. Now by means of Equation B.0.8, setting $p = 1/2$, $q = n$ and $r = k$ we have:

$$\frac{(3/2-n)_k}{(n-k+1)_k} \binom{1/2}{n-k} = \binom{1/2}{n} \tag{B.0.12}$$

Then by means of Equation B.0.10, setting $p = n-k+1$ and $q = k$ we have:

$$(n-k+1)_k = k! \binom{n}{k} \tag{B.0.13}$$

Thus combining Equation B.0.12 and Equation B.0.13 we have:

$$\binom{1/2}{n-k} = \binom{1/2}{n} \frac{k!}{(3/2-n)_k} \binom{n}{k} \tag{B.0.14}$$

Plugging Equation B.0.14 into Equation B.0.7 we get:

$$\frac{g(X)}{h(X)} = \sum_{n=0}^{+\infty} \binom{1/2}{n} \left[\sum_{k=0}^{n} (-1)^k \frac{(1+k)k!}{(3/2-n)_k} \binom{n}{k} \left(\frac{\beta}{\alpha}\right)^k \right] \alpha^n X^n \tag{B.0.15}$$

And thanks to Equation B.0.11:

$$(1+k)k! = \Gamma(k+2) = \frac{\Gamma(k+2)}{\Gamma(2)} = (2)_k \tag{B.0.16}$$

It follows that the internal summation of Equation B.0.15 becomes:

$$S_n = \sum_{k=0}^{n} (-1)^k \frac{(2)_k}{(3/2-n)_k} \binom{n}{k} \left(\frac{\beta}{\alpha}\right)^k$$

which is case where the Gauss hypergeometric function ${}_2F_1(a,b;c)$ reduces to the hypergeometric polynomial: the series terminates if either a or b is a nonpositive integer. Then:

$$S_n = {}_2F_1 \left(\begin{matrix} 2 & -n \\ 3/2-n & \end{matrix} \middle| \frac{\beta}{\alpha} \right)$$

Thanks to Equation B.0.9 we have:

$$\binom{1/2}{n} = \frac{\Gamma(3/2)}{\Gamma(n+1)\Gamma(3/2-n)} = \frac{\pi^{1/2}/2}{\Gamma(n+1)\Gamma(3/2-n)}$$

Thus in conclusion:

$$\boxed{f(x) = \frac{\pi^{1/2}}{2} \sum_{n=0}^{+\infty} {}_2F_1 \left(\begin{matrix} 2 & -n \\ 3/2-n & \end{matrix} \middle| \frac{\beta}{\alpha} \right) \frac{\alpha^n \cos^n(x)}{\Gamma(n+1)\Gamma(3/2-n)}} \tag{B.0.17}$$

List of Figures

List of Tables

List of Acronyms

Acronym	Description
ESA	European Space Agency
CA	Close Approach
CAM	Collision Avoidance Manoeuvre
CDM	Conjunction Data Message
COMPASS	Control for Orbit Manoeuvring through Perturbations for Application to Space Systems
CSpOC	Combined Space Operations Center
GEO	Geostationary Orbit
GSOC	German Space Operation Center
IADC	Inter-Agency Space Debris Coordination Committee
ICS	Intelligent Classification System
LEO	Low Earth Orbit
MISS	Manoeuvre Intelligence for Space Safety
ML	Machine Learning
NASA	National Aeronautics and Space Administration
ODPO	Orbital Debris Program Office
ODEM	Orbit Determination for Extended Manoeuvre

OSMA	Office Safety and Mission Assurance
PDF	Probability Density Function
PoC	Probability of Collision
SGP4	Simplified General Perturbation 4
TCA	Time of Close Approach
TLE	Two Lines Elements
UCS	Union of Concerned Scientist
USSTRATCOM	US Strategic Command

List of Symbols

Variable	Description	Unit
a	Semimajor axis	km
a_h	Thrusters acceleration in the out of plane direction	km/s^2
a_n	Thrusters acceleration in the normal direction	km/s^2
a_t	Thrusters acceleration in the tangential direction	km/s^2
e	Eccentricity	–
G	Universal gravitational constant	$km^3/s^2/kg$
M	Mass of the celestial body	kg
h	Specific angular momentum	km^2/s
i	Inclination	deg
r	Norm of the position vector	km
T	Orbital Period	s
t	Generic time instant	s
t_A	Time of close encounter	s
v	Norm of the velocity vector	km/s
θ	True anomaly	deg
μ	Standard gravitational parameter of a celestial body	km^3/s^2
ω	Argument of perigee	deg
Ω	Right Ascension of the Ascending Node	deg

Acknowledgements

I wish to thank my thesis advisor Professor Juan Luis Gonzalo Gómez. You have helped me so much during this long work giving me always good advices both in terms of methodology and technical support.

I wish to thank my thesis co-advisor Professor Camilla Colombo for her support: mostly because thanks to her I discovered my passion for the Orbital Mechanics.

I wish to thank my parents Marzia Rodolfi and Nicola Bocci for supporting me during my studies and encouraging me in front of difficulties. You've helped me in all possible senses and supported me also in the worst moments.

I wish to thank Professor Giovanni Mingari Scarpello for all the effort put in helping me during this long journey. You have been, not only a technical guide, but also a friend whom I shared many nice moments with.

I wish to thank my friend Francesco Biral for all the time spent together here in Milan and of course for the great adventures in our lovely night clubs. I wish to thank also Georgiana Elena Stefan for the great moments spent together.

I wish to thank my university colleagues: Susanna Brisotto, Marco Gonella, Martina Stasi, Lorenzo Ambrosi and Alessio Cervellera. Thank you for all the great moments spent together.

I wish to thank all my friends from Ravenna: Dario Zanfini, Antonio Ferrara and Luca Bernabucci. Thank you for all the great moments together.

I wish to thank all my friends from Bologna: Anna Piombo and Federico Tosarelli. Thank you for all the great moments spent together.

I wish to thank my friends Andrea Brisotto and Yatma for all the great nights we spent together in Milano disco clubs. Very good friends for great and funny nights.